Contribution to the modelling of the viscoelastic behavior of elastomers with Payne effect

Adel Tayeb

Number order : 2017LYSEC62 Year : 2017

PhD Thesis
Submitted in partial fulfillment of the
requirements for the degree of

Doctor of Philosophy
of École Centrale de Lyon - France
& National Engineering school of Tunis - Tunisia

École doctorale MEGA (Mechanics, Energy, Civil Engineering, Acoustics)
École doctorale : Sciences et Techniques de l'ingénieur

Contribution to the modelling of the viscoelastic behavior of elastomers with Payne effect

Specialty : Mechanics

Presented and defended on December 9, 2017 at ENIT de Tunis

by

Adel TAYEB

The dissertation committee consists of :

President	:	Hatem	ZENZRI	- Professor, ENIT - Tunisia
Reviewers	:	Noureddine	BOUHADDI	- Professor, FEMTO-ST - France
	:	Adnane	BOUKAMEL	- Professor, RAILENIUM - France
Advisors	:	Mohamed	ICHCHOU	- Professor, ECL - France
	:	Jalel	BENABDALLAH	- Professor, ENIT - Tunisia
Co-advisors	:	Makrem	ARFAOUI	- Associate professor, ENIT - Tunisia
	:	Abdelmalek	ZINE	- Associate professor, ECL - France
	:	Adel	HAMDI	- Associate professor, ENIT - Tunisia
Examiners	:	Maher	MOAKHER	- Professor, LAMSIN - ENIT - Tunisia
	:	Olivier	BAREILLE	- Associate professor, ECL - France

Acknowledgment

Dedication

Abstract

It is well known that rubber-like materials exhibit nonlinear viscoelastic behavior over a wide range of strain and strain rates confronted in several engineering applications such as civil engineering, automotive and aerospace industries. This is due to their capacity to undergo high strain and strain rates without exceeding the elastic range of behavior. Further, the time dependent properties of these materials, such as shear relaxation modulus and creep compliance, are, in general, functions of the history of the strain or the stress. Therefore, in a wide range of strain, a linear viscoelasticity theory is no longer applicable for such material and new models are required to fully depict the behavior of rubber-like materials for quasi-static and dynamic configurations of huge interest in engineering applications. Despite the multitude of nonlinear viscoelastic models developed over the years, there is a lack of models capable of depicting the nonlinear behavior of rubber-like materials with ease of identification and implementation into commercial software.
In this work, a nonlinear viscoelastic model at finite strain is developed to describe nonfactorizable behavior of isotropic incompressible rubber-like materials. The model is developed within the framework of rational thermodynamics and internal state variable approach such that the second law of thermodynamics in the form of Clausius-Duhem inequality is satisfied. From experimental results on Bromobutyl (BIIR) a dependence of the shear relaxation modulus upon strain has been observed and introduced in the model via a strain dependent relaxation times which led to a reduced time similar to the thermorheologically simple material's formulation. Then, a systematic identification procedure have been developed to identify the model's parameters. A separation of the instantaneous elastic and viscoelastic contributions to the stress was employed which led to a separate identification of the characteristic functions of the model. This procedure was applied to experimental data and generated data from the Pipkin-Rogers model and a good capacity of the model to predict both static and dynamic behaviors of the material was observed.
Thereafter, the nonlinear viscoelastic model was implemented into Abaqus software using a Umat subroutine. To this end, the discrete form of the model was written and the tangent stiffness was calculated (required for the Umat) using the objective rate derivatives of Jaumann. The implementation was validated using homogeneous transformations of simple shear and simple extension for monotonic, sinusoidal and relaxation strain histories. The non vanishing components of the Cauchy stress tensor were calculated for the strain history considered and compared to the numerical results of the model. Finally, a non homogeneous transformation was considered. Namely, the problem of simple

torsion of a hollow viscoelastic cylinder for several strain histories. From the equilibrium equations, the indeterminate pressure arising from the incompressibility was computed and then the components of the Cauchy stress were calculated along the radius of the cylinder. The analytic results showed a total agreement with the simulations performed with the implemented model.

Résumé

TABLE OF CONTENTS

List of Figures

Figure **Page**

List of Tables

Table **Page**

NOTATIONS

Symbol	Designation
C_0	Reference configuration
C_t	Current configuration
Ω_0	Continuum body in the reference configuration
Ω_t	Continuum body in the current configuration
X	Point's coordinates in the reference configuration
x	Point's coordinates in the current configuration
$\phi(X,t)$	Mapping function between C_0 and C_t
$\boldsymbol{F}$	Deformation gradient tensor
$J = det[\boldsymbol{F}]$	Jacobian of the deformation
$\bar{\boldsymbol{F}}$	Isochoric part of the deformation gradient tensor
$\boldsymbol{F}_\tau$	Deformation gradient tensor with respect to time τ
x	point's coordinates in the current configuration
$\boldsymbol{C}$	Right Cauchy-Green strain tensor
$\bar{\boldsymbol{C}}$	Isochoric right Cauchy-Green strain tensor
$\boldsymbol{B}$	Left Cauchy-Green strain tensor
$\bar{\boldsymbol{B}}$	Isochoric left Cauchy-Green strain tensor
Ψ	Free energy density function
Ψ_0	Instantaneous elastic free energy density function
$\boldsymbol{\sigma}$	Cauchy stress tensor
$\boldsymbol{\tau}$	Kirchhoff stress tensor
$\boldsymbol{\pi}$	First Piola-Kirchhoff stress tensor
$\boldsymbol{S}$	Second Piola-Kirchhoff stress tensor
$\mathbb{C}$	Fourth order tensor of tangent stiffness
$\mathbb{C}^J$	Fourth order tensor of tangent stiffness of Jaumann
$\mathbb{C}^{Abaqus}$	Abaqus fourth order tensor of tangent stiffness
$G(t)$	Shear relaxation modulus
G'	Storage modulus
G''	Loss modulus
$g(t)$	Normalized shear relaxation modulus

Introduction

✧—☞ *Industrial and scientific context*

This thesis is a part of an international partnership between the laboratory of Applied Mechanics and Engineering of *École Nationale d'Ingénieurs de Tunis* and the laboratory of Tribology and Dynamics of Systems of *École Centrale de Lyon* as academics and *ArianeGroup* as an industrial counterpart. The aim of the thesis is the development of a nonlinear viscoelastic model able to describe the nonlinear viscoelastic behavior of rubber-like materials at finite strain and its implementation into finite elements software. The original industrial need is the design of the elastomeric device to be used in the inter-stage of the launcher which the role is to ensure the static and dynamic filtering and attenuate the vibrations caused by the boosters and transmitted to the stages of the launcher. However, thanks to the general framework in which the model was developed, it will fit this feature as well as other features needed in several engineering applications.
Nowadays, elastomers are frequently used in industrial applications, in particular in automotive, aeronautics, civil engineering applications and aerospace. The mechanical properties of these materials make them a class a part of materials. Their properties are used for several applications such as sealing, damping and isolation etc. In particular, they have high ability of deformability up to some hundred % associated with a quasi-reversible hyperelastic behavior. In addition, they have a dissipative properties shown when subjected to dynamic loading along with several softening phenomena. In general, these materials are subjected to severe mechanical and thermal loading in real world application.
In industry, the design of complex geometrical structures made of materials exhibiting nonlinear constitutive behavior, such as rubber-like materials, rely on the use of finite elements method. The performance of such tool is directly affected by the capacity of the model to depict the behavior of the used material. The possibility of accurately simulating the behavior of the material in the industrial application circumstances avoids the need of experimentation and therefore reducing the cost of the design process of such

structures.

Rubber-like materials have a very special behavior which could be described by the combination of elastic solid behavior and viscous fluid behavior. In addition, due to their peculiar micro-structure, theses materials are characterized by several nonlinear phenomena involving their response to static and dynamic loading. Therefore, the development of nonlinear viscoelastic models is crucial.

Research problematic and Objectives

The theory of viscoelasticity is crucial in describing materials, such as filled rubber, which exhibit time dependent stress-strain behavior. Over the years, several models have been developed to study the viscoelastic behavior of rubber-like materials from purely mathematical developments to applied studies where ease of application is for huge interest. In fact, the combination of the ease of identification of the model's parameters as well as the possibility to implement it in finite elements software plays a key role in the development of constitutive equations for these materials. Furthermore, several experimental investigation corroborated that the time-dependent properties of these materials such as relaxations function and creep compliance are in general strain dependent functions. The separability assumption used in linear viscoelasticity theory, *which states that the effect of time and strain are separable and hence the time-dependent properties are function of time only*, does not hold.

A review of the literature revealed significantly more well-established studies dealing with hyperelastic constitutive models, than those dealing with finite viscoelasticity. Furthermore, the task of identification of the material's parameters is well-studied and integrated in finite elements software such as Abaqus for the static (hyperelastic) case providing all the experimental techniques to identify the material constitutive parameters. However, for nonlinear viscoelastic materials such feature is lacking especially when dealing with nonlinear phenomena such as the dependence of the relaxation modulus upon strain.

On the other hand, in order to investigate the response of the material with the nonlinearities described above subjected to real industrial loading, the model describing this behavior should be implemented into finite elements software. Hence, all quantities involved in the model have to be defined carefully and therefore the simplicity of the model plays a key role in fulfilling this task.

Therefore, the objectives of this work are, on one hand: the development of a nonlinear viscoelastic model at finite strain taking into account the dependence of the time-dependent properties upon strain corroborated by experimental results done within this project on

a Bromobutyl rubber-like material, on the other hand, the development of a systematic identification procedure to identify all the model's parameters using experimental data and the implementation of the proposed model into one of the finite elements commercial software.

Methodology

In order to fulfill the objectives of this thesis the following methodology has been followed:

- The three dimensional viscoelastic model at finite strain to describe nonseparable behavior of rubber-like materials is developed within the framework of rational thermodynamics and internal state variable approach such that the second law of thermodynamics in the form of Clausius–Duhem inequality is satisfied. The model represents a generalization of the Simo model implemented in Abaqus software. Motivated by experimental results, the evolution law of the internal variables is set to be nonlinear. This non linearity was introduced via a strain dependent relaxation times which led to the use of the notion of reduced time via strain shift function similar to the thermorheologically simple material's behavior.

- The material's parameters are identified separately. In fact, the hyperelastic contribution to the total stress is identified from equilibrium data on simple extension and pure shear. The relaxation function was postulated by a Prony series and identified using relaxation experimental data in the linear range of the behavior with a strain relaxation level below 10%. The reduced time function is identified thanks to a minimization procedure over the error between the discrete stress of the model and the experimental stress.

- The implementation of the model was performed with Abaqus software via a subroutine Umat. To do so, first, the integration algorithm corresponding to the discrete of the model was implemented using Matlab software and validated with comparison with Abaqus software for one dimensional experiments of simple extension and pure shear for several strain histories. Then, the subroutine Umat was written: this requires the update formula for the stress using the objective rate equation of Jaumann required in Abaqus software and the update formula of the fourth order tangent stiffness tensor. The implementation of the model was then validated by the solution of initial boundary value problems for homogeneous transformations of simple shear and simple extension and non homogeneous one of simple torsion of a hollow cylinder.

Thesis outline

This thesis is decomposed in five chapters organized as follows:

- The first chapter summarizes the most important physical phenomena related to rubber-like materials and exposes the most known approaches and models to deal with these phenomena in the development of hyperelastic potentials for these materials. The last part of this chapter presents a literature survey for the approach followed in the development of nonlinear viscoelastic models at finite strain

- The second chapter presents the nonlinear viscoelastic model proposed within this work. First, a modification to the rheological model of Maxwell is carried out using experimental arguments. Then, an extension to the fully three dimensional domain is performed such that the second law of thermodynamics in terms of the Clausius-Duhem inequality is valid. For each case, constitutive equations of the stress, free energy density and intrinsic dissipation are obtained.

- The third chapter presents the systematic identification procedure of the model's parameters to experimental data. This identification procedure was applied to data generated from the Pipkin multi-integral model then applied to experimental data for Bromobutyl (BIIR)

- The fourth chapter deals with the numerical implementation of the nonlinear viscoelastic model developed in the previous chapters. First, the integration scheme of the one dimensional model is recalled. Then, the implementation of the three dimensional viscoelastic model into Abaqus software is performed using an implicit integration scheme in a Umat subroutine.

- The last chapter presents the validation of the implementation of the nonlinear viscoelastic model presented in the previous chapter via the solution of homogeneous and nonhomogeneous initial boundary problems numerically and analytically.

CHAPTER 1

PHYSICAL ASPECTS AND HYPERELASTIC BEHAVIOR OF RUBBER-LIKE MATERIALS

Contents

The first chapter aims to analyse the behavior of rubber-like materials from a phenomenological stand point. These materials are used in several engineering applications such as automotive, civil engineering and aerospace. These materials are capable of undergoing large deformation and recover to their original state. Due to their peculiar micro-structure composed by long chain molecules with presence of carbon black, their behavior is strongly nonlinear. This chapter is subdivided in three parts : the first part summarizes the most important physical phenomena related to rubber-like materials, the second one presents the mechanical framework of nonlinear elasticity and highlights the most known approaches and models to describe the hyperelastic behavior for these materials and the third part presents the framework of nonlinear viscoelasticity leading to the most known approaches and modeling procedures followed in the development of nonlinear viscoelastic models at finite strain and discusses the assumptions and limitations of each approach.

1.1 Phenomenology of rubber

1.1.1 Generalities and micro-structure

The term rubber is actually misleading: it is used both to indicate the material, technically referred to as natural rubber, and the broad class of synthetic elastomers which share with natural rubber some fundamental chemical properties. Indeed, the majority of rubber used for industrial applications are synthetically produced and derived from petroleum. These materials are characterized by their high deformability and dissipative properties which makes them widely used in several damping applications in many fields [29],[111],[97],[87]...

Rubber, or elastomer, has an internal structure which consists of flexible, long chain molecules that intertwine with each other and continually change contour due to thermal agitation. Elastomers are polymers with long chains [43]. The morphology of an elastomer can be described in terms of convolution, curls and kinks. Convolutions represent the long-range contour of an entire molecular chain, which forms entanglements (knots). Curls are shorter range molecular contours that develop between entanglements and crosslinks, and kinks are molecular bonds within a curl. Each molecular bond has rotational freedom that allows the direction of the chain molecule to change at every bond. Thus the entire molecular chain can twist, spiral and tangle with itself or with adjacent chains. This basic morphology is shared among all the fifty thousand compounds used in the market today and generically referred to by the term rubber. Despite this intricate internal structure, the random orientation of the molecular chains results in a material which is externally isotropic and homogeneous. Figure 1.1 illustrates the form of the molecular network of an elastomer

Before using, the elastomer is subjected to physical and chemical treatments to ameliorate its mechanical properties. One of these treatment is the vulcanization which consists of the addition of sulfur-based curatives which create crosslinks among the macromolecules chains through heating see [17].

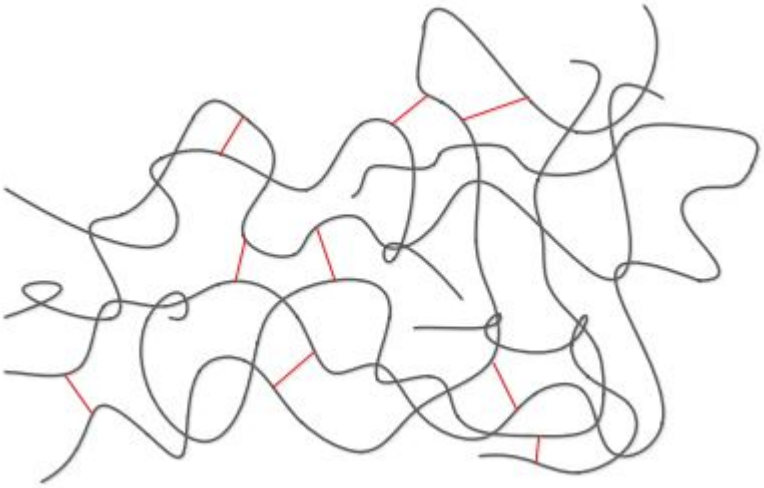

Figure 1.1: Molecular network of elastomers [78]

1.1.2 Quasi static response of rubber like materials

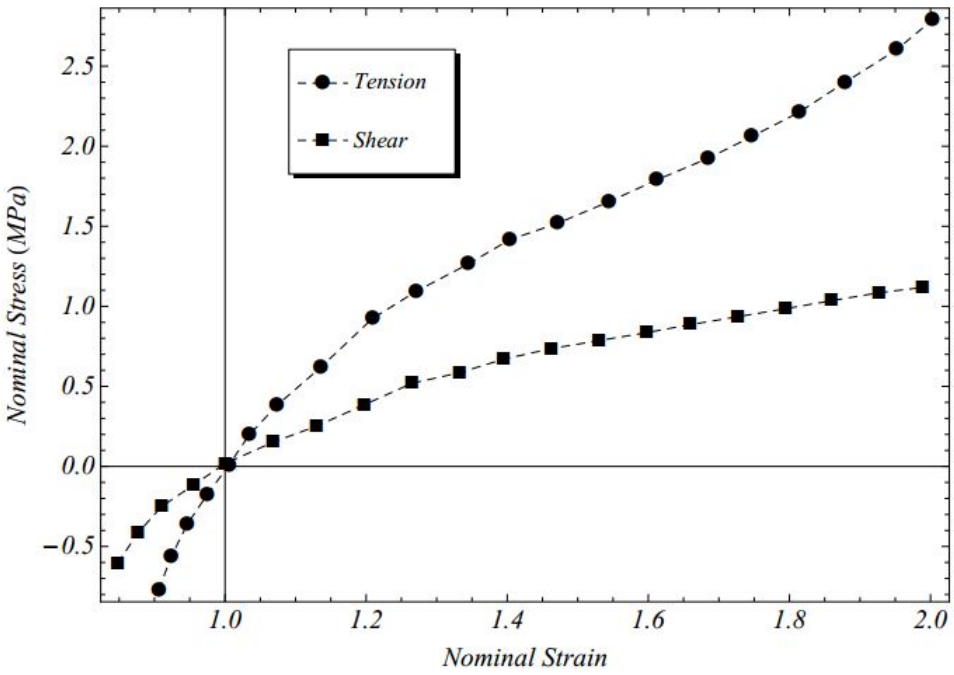

Figure 1.2: Stress strain curves for quasi-static loading [35]

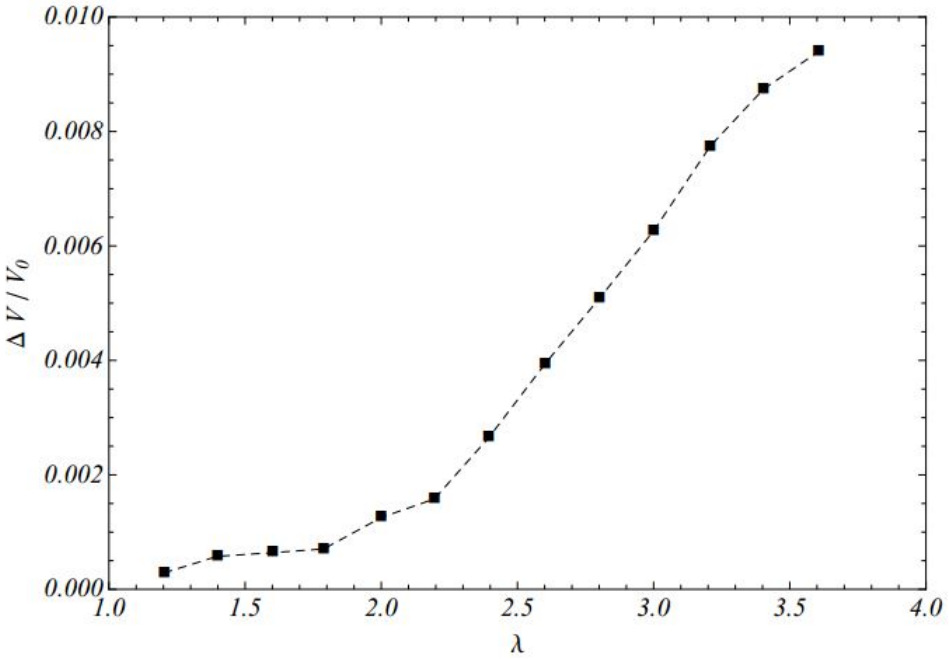

Figure 1.3: Volume dilatation for a rubber specimen undergoing a uniaxial tensile experiment[121]

The behavior of rubber-like materials can be described primarily as *hyperelastic* under static loading where time-dependent effects are negligible [123]. The response of rubber-like materials to quasi-static loading conditions of shear, compression/tension and equibiaxial tension have been widely studied in the literature [33],[82],[118] and [138] among others. It has been shown for all these experimental conditions that the stress-strain curves are strongly nonlinear.
The stress-strain curve response of a carbon black filled elastomer are shown in figure 1.2 [35]. The material is subjected to uniaxial tension/compression, and pure shear conditions. The constitutive nonlinearity of the material are evident, in fact as the breaking point approaches, the stiffness of the material increases significantly and as a result the slope of the stress strain curve rise. It is also noticed that the material have a non symmetric behavior between tensile and compression loads.

From figure 1.2 one could extract the value of the shear modulus G and the Young modulus E in the undeformed configuration. The ratio E/G is about 3 which means that the Poisson's ratio $\nu = 0.5$. Therefore, the material is incompressible in the underformed configuration.
Moreover, the incompressibility of rubber like materials have been studied in many works [8], [91], [106], [114], [121]. The experiments by [121] reported in figure 1.3 show a limited volume change $\Delta V/V_0 \cong= 0.01$ for a large stretch ($\lambda = 4$) confirms the incompressibility constraint used in several constitutive equations.

1.1.3 Dissipative phenomena of rubber like materials

In addition to phenomena described in the previous section, elastomers have a fluid-like or viscoelastic behavior when subjected to dynamic loading [44]. Two typical experiments that prove the viscoelastic behavior of rubber like materials are : the relaxation experiment for which a step-wise strain is applied to the specimen the stress response fall from the peak value when the strain was applied to an asymptotic value as it is shown in figure 4 from the experiment by [79] and the creep experiment when a sudden step force is applied to the specimen the strain increases slowly from the instantaneous value as shown in figure 1.5.

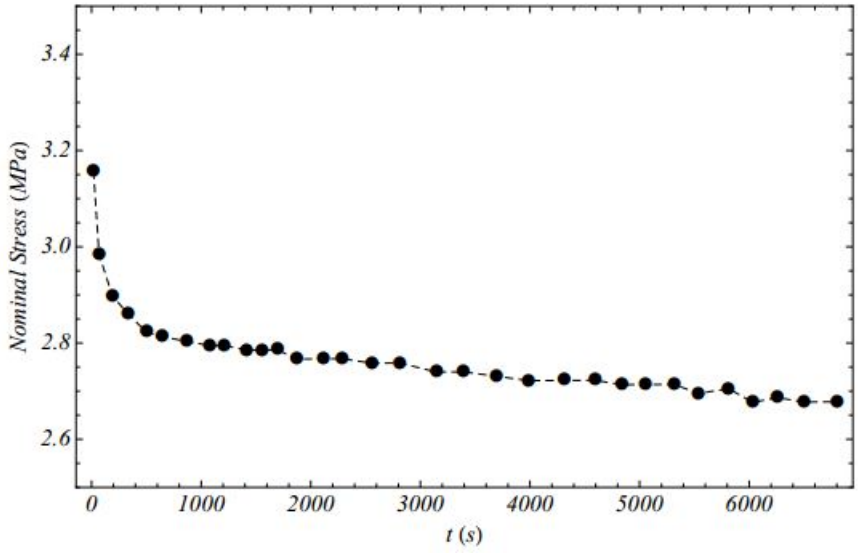

Figure 1.4: Nominal stress versus time for a relaxation experiment [79]

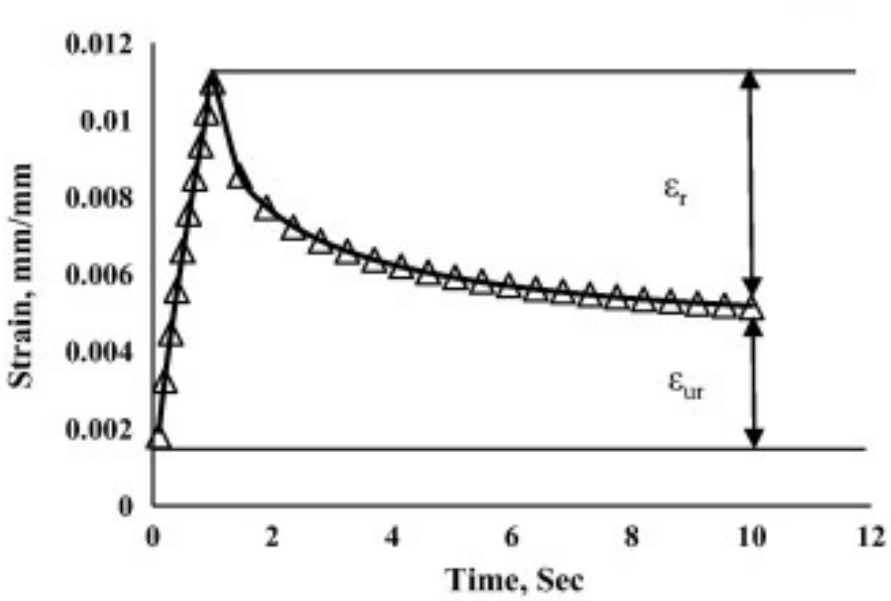

Figure 1.5: Nominal strain versus time for a creep experiment [138]

These two phenomena are caused by the complex geometrical entanglements between chains, which produce a local enhancement of the residual (Van der Walls) force. Under prolonged loading, such “entanglement-cohesion” will slowly breakdown, giving rise to the phenomena of stress-relaxation and creep presented above [138]. In the case of speed loading these phenomena are limited and the response of the material is elastic. These two phenomena emphasis the time dependent behavior of rubber like materials which

is still an active subject for research. Hence, the entire history of the strain must be incorporated in the constitutive equations for these materials.

1.1.4 Dynamic response of rubber like materials

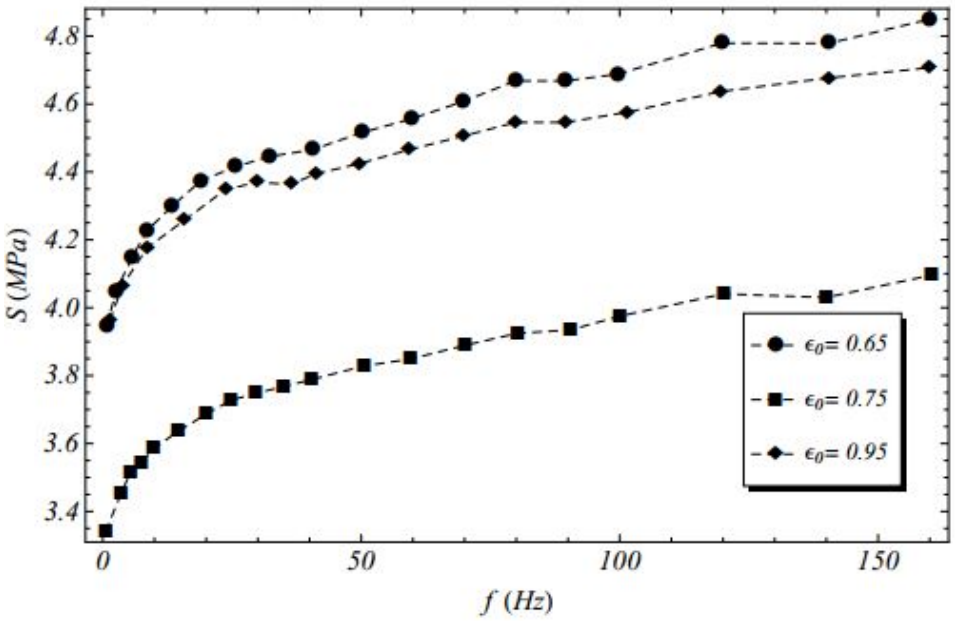

Figure 1.6: Storage modulus versus frequency [83]

From dissipative phenomena occurring for rubber like materials described in 1.1.3, it is needful to investigate the dynamic response of these materials. This is achieved by subjecting the material to a sinusoidal strain history of frequency ω of the form :

$$\varepsilon(t) = \varepsilon^a \sin(wt), \tag{1.1}$$

where ε^a is the dynamic amplitude. Under the dynamic loading the strain occur in the material with a certain delay due to the viscous frictions inside the material, this delay is observed for a harmonic deformation of equation (1.1) by a phase shift between the displacement and the loading [9]. The harmonic deformation of equation (1.1) lead to time-dependent stress of the form

$$\sigma = G^* \varepsilon^a, \tag{1.2}$$

where G^* is the complex modulus, its real part is denoted by G' and referred to as the *storage* modulus and its imaginary part is denoted by G'' and referred to as the *loss* modulus. These two moduli are dependent upon the dynamic amplitude especially for

large value of ε^a. In figures 1.6 and 1.7 is reported the dependence of the storage and loss moduli upon the frequency respectively using data from [83]. The storage modulus has a nonzero value as $w \to 0$ which corresponds to the equilibrium shear modulus since $t \to \infty$ as $w \to 0$.

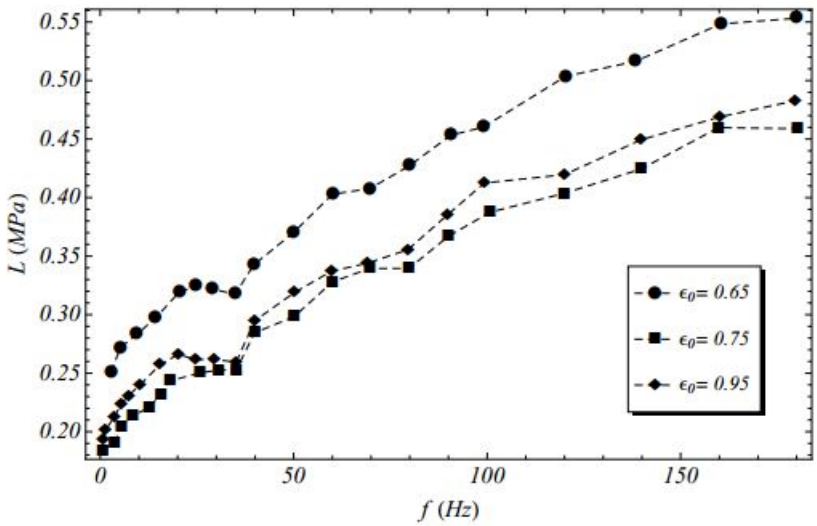

Figure 1.7: Loss modulus versus frequency [83]

1.1.5 Thermal response of rubber like materials

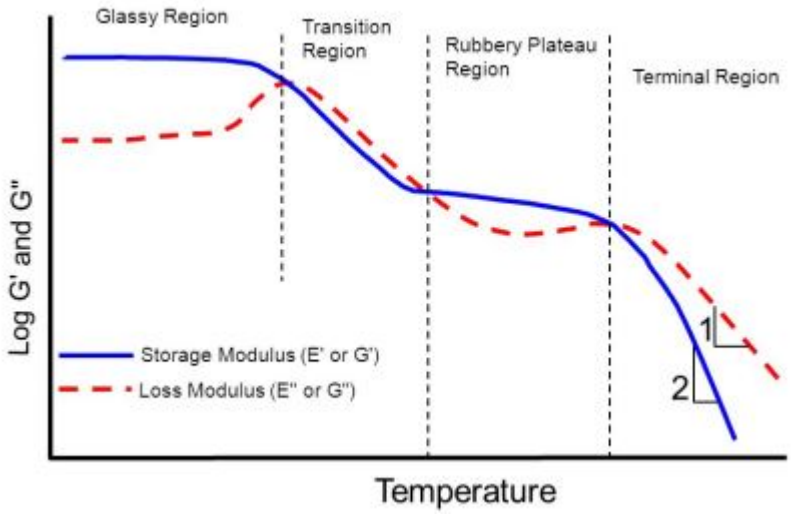

Figure 1.8: Evolution of dynamic moduli with temperature [135]

For both quasi-static and dynamic loading, the behavior of rubber like materials is strongly affected by temperature. The dynamic properties of the material exhibit big

changes with the temperature. In fact, at low temperatures the storage modulus is at its maximum whereas the loss modulus is at its minimum. This range of temperature is known as the glassy region. Increasing temperature from this region causes a brutal decrease of the storage modulus and an increase of the loss modulus in which it reaches its maximum. This range of temperature is called the transition region. A further increase in temperature, the material reach its *rubbery plateau* in which both dynamic moduli are stable. This range is the perfect range for applications using rubber like materials. This dependence of the dynamic moduli upon temperature is shown in figure 1.8.

On the other the hand the determination of the dynamic properties for wide range of frequency is not possible experimentally. Therefore, an assumption has been made in the modeling of rubber like materials which is the thermorehologically simple behavior. Within this context, the time-dependent properties of the material such as relaxation function, creep function and dynamic moduli when plotted versus the logarithm of time or frequency at several temperatures can be superimposed to form a single curve [116] and [146].

1.1.6 Other nonlinear phenomena

1.1.6.1 Mullins effect

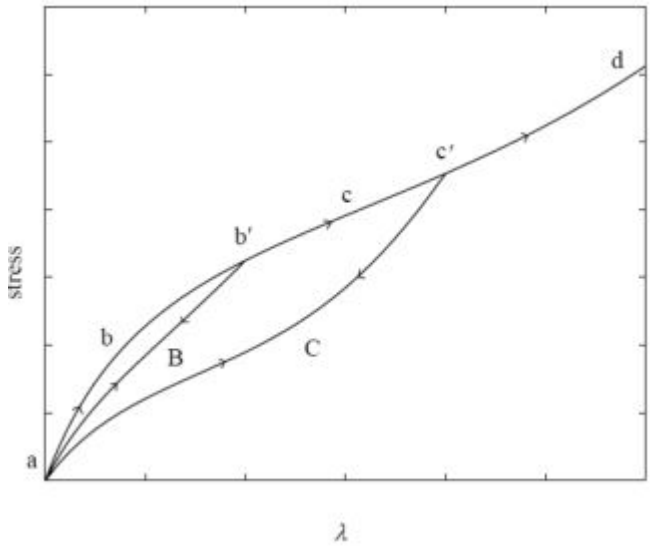

Figure 1.9: Mullins effect [93]

The Mullins effect is a strain induced softening phenomena. In fact the stress response of the material to a cyclic loading decreases significantly at a given level of strain during the unloading path compared to the stress reached in the loading path. This phenomena is observed in the first five or six loading-unloading paths. It was firstly discovered by [12] and then thoroughly studied by Mullins [100] and [101]. He suggested some physical interpretations explaining this phenomena. The Mullins effect is more pronounced for filled rubber than unfilled rubber.[15] and [16] explained this phenomena by a damage mechanism in the polymeric chains of the material. [55], [50], [96], [108] and [77] proposed several models to describe the Mullins effect. Figure 1.9 illustrates the Mullins effect for a three cyclic loading-unloading paths.

1.1.6.2 Payne effect

Another softening phenomena which manifests the dependence of the stress upon the entire history of deformation is the so-called Payne effect. Like the Mullins effect, this is a softening phenomena but it concerns the behavior of carbon black-filled rubber subjected to oscillatory displacement. Indeed, the dynamic part of the stress response presents a rather strong nonlinear amplitude dependence, which is actually the Payne effect [20], [73] and [112]. For a dynamic strain history, the storage and loss moduli are strongly nonlinear of the dynamic amplitude ε^a as shown in figure 1.10. Several models have been developed to explain the Payne effect. [20] made a classification to the Payne effect models: (i) filler-structure models, (ii) matrix filler bonding and debonding models and (iii) phenomenological or nonlinear network models. [112] suggested qualitatively that the amplitude dependence of the storage and loss moduli were due to a filler network in which the filler contacts depended on the strain amplitude. At lower amplitudes, he argued that the filler contacts are largely intact and contribute to the high value of the modulus. Conversely, at higher amplitudes the filler structure has broken down and does not have time to reform. In another work [81] suggested an empirical model based on the agglomeration/deagglomeration kinetics of filler aggregates, assuming a Van der Waals type interaction between the particles. [89] proposed a phenomenological model within the framework of continuum mechanics and nonlinear viscoelasticity. Experiments shown in figure 1.10 [124] were performed using the Bromobutyl rubber BIIR.

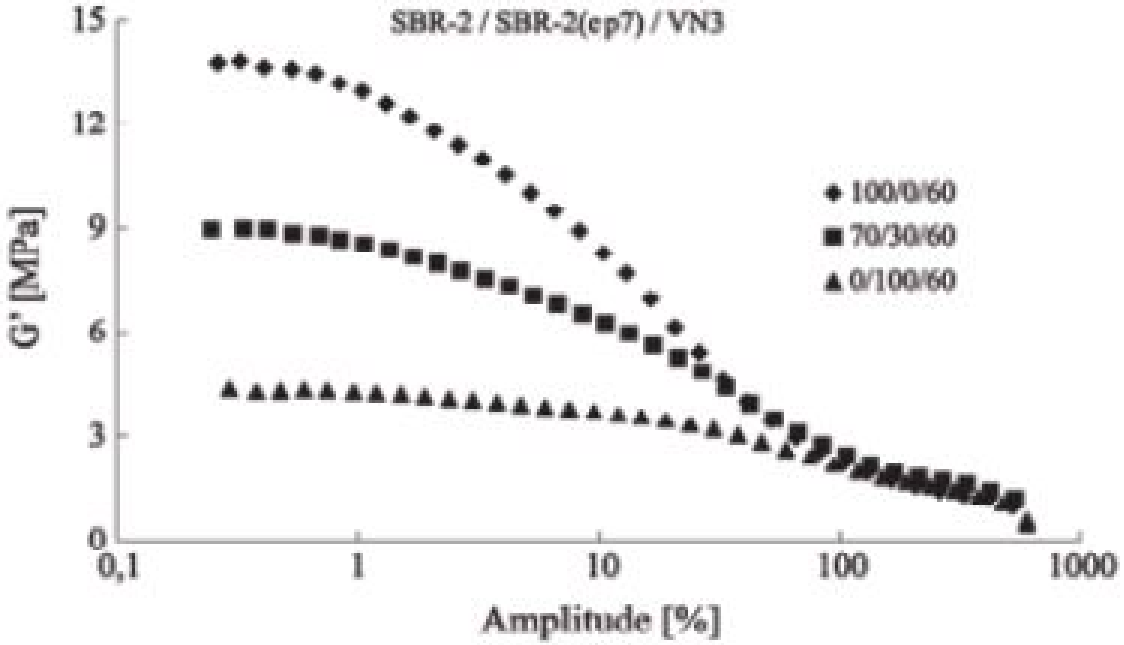

(a) Shear storage modulus

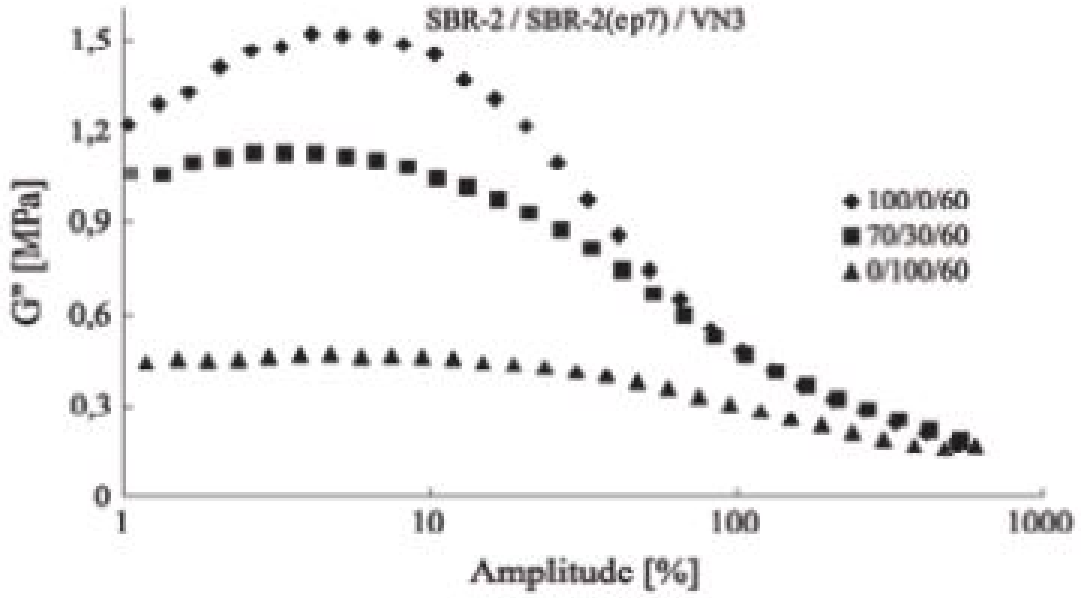

(b) Shear loss modulus

Figure 1.10: Payne effects on dynamic moduli [124]

1.2 Mechanical formulation in the high deformation

Consider an isotropic homogeneous elastic material which occupies the domain Ω_0 in the reference configuration or the unstressed one. Every material particle can be described by the cartesin coordinates (X_1, X_2, X_3) in the initial or the undeformed configuration and (x_1, x_2, x_3) in the current or deformed configuration which is illustrated in figure 1.11. The change of the mechanical state of the material particle moved from the initially position X to the actual position x can be described mathematically using a mapping function ϕ relating the reference and the current configuration as:

$$x = \phi(X,t) = X + u(X,t). \tag{1.3}$$

In the formulation of the continuum mechanics, it exists essentially two types of material description: Lagrangian and Eulerian descriptions. The first description uses the initial state of the material like a reference configuration and thus we can follow the material particle in its trajectory. Although, the Eulerian description considers the trajectory of the material particles passed by a chosen geometrical point in the space.

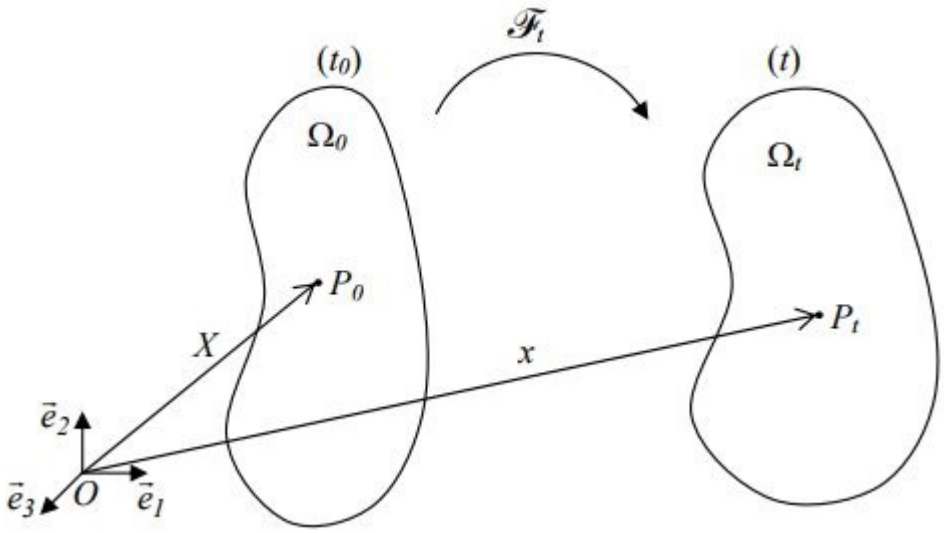

Figure 1.11: Transformation from undeformed to deformed configuration

1.2.1 The deformation gradient

In the continuum mechanics the deformation gradient plays an important role because it is involved in the different mechanical quantities. The deformation gradient relates

the infinitesimal vector dx in the current configuration to the infinitesimal vector dX in the undeformed configuration as the following:

$$dx = F \ \ dX. \tag{1.4}$$

In that sense, F is also a two-point tensor, i.e. it relates quantities in two different configurations. Now, tensor F can be defined as:

$$F = \frac{\partial x}{\partial X}, \tag{1.5}$$

where ∂ denoted the gradient operator with respect to the initial coordinates.

1.2.2 Polar decomposition of the deformation gradient

An advantageous use of the deformation gradient is its polar decomposition, that is decomposing the total deformation F into a tensor describing the rotation and another one describing the stretch. The polar decomposition is discovered by Cauchy using geometrical arguments. Mathematically, the polar decomposition, in the material configuration, is expressed as:

$$F = R \ \ U, \tag{1.6}$$

where R is the rotation tensor which is an orthogonal tensor, i.e. $RR^T = I$. While U is the material stretch tensor which is a symmetric tensor, i.e.
$U^T = U$.

Equivalently, in the spatial configuration, the polar decomposition is expressed as:

$$F = V \ \ R, \tag{1.7}$$

where V is the spatial stretch tensor that is also symmetric. It can be shown that both tensors U and V share the same principal values. As both tensors are symmetric, the spectral theorem can be applied. Thus, tensors V and U can be conveniently expressed as:

$$\begin{aligned} U &= \sum_{\alpha=1}^{3} \lambda_\alpha N_\alpha \otimes N_\alpha \\ V &= \sum_{\alpha=1}^{3} \lambda_\alpha n_\alpha \otimes n_\alpha, \end{aligned} \tag{1.8}$$

where λ_α are the principal stretches, N_α are the material principal directions of U, n_α are the spatial principal directions of V, and n is the number of dimensions involved.

1.2.3 Volume changes and isochoric/volumetric split

The deformation gradient is also used to obtain information about volume changes in the body studied. It can be shown that the determinant of F gives the ratio between differential volumes in the reference (dV) and current configurations (dv). This can be written as:

$$J = detF = \frac{dv}{dV}, \tag{1.9}$$

where J is the jacobian of the deformation gradient tensor. If $J = 1$, then no volumetric deformations are involved. It is crucial, when dealing with incompressible or nearly incompressible materials, to split the deformation into volumetric components and isochoric or distortional components. The aim of this split is to ensure that the isochoric component of the deformation, denoted by $\bar{F}$, does not contribute to any volume changes, that is:

$$det\bar{F} = 1. \tag{1.10}$$

Such a condition is satisfied for the following form $\bar{F}$ wich is defined as:

$$\bar{F} = J^{-\frac{1}{3}}F, \tag{1.11}$$

while the volumetric component F^v can be expressed as:

$$F^v = J^{\frac{1}{3}}I. \tag{1.12}$$

1.2.4 Strain

Several strain tensors are constructed from the deformation gradient tensor. Strain tensors are further categorized as material or spatial strain tensors based on the description they refer to. Some of the strain tensors in each category will be described in the following.

The right Cauchy-Green tensor is a material strain tensor that is expressed in terms of the deformation gradient tensor. It is defined as:

$$C = F^t \ F = U^2, \tag{1.13}$$

where the polar decomposition (1.6) is used. In view of the equation (1.8), this can be equivalently expressed as:

$$C = \sum_{\alpha=1}^{3} \lambda_\alpha^2 N_\alpha \otimes N_\alpha. \tag{1.14}$$

The strain tensor C is then used to define another material strain tensor, namely, the Green-Lagrange strain tensor defined as:

$$E = \frac{1}{2}(C - I). \tag{1.15}$$

Similarly, spatial strain tensors can be constructed. The left Cauchy-Green strain tensor is given by:

$$B = F \ F^t = V^2, \tag{1.16}$$

where equation (1.7) is used to obtain the last equality. Using equation (1.9), B can hence be expressed as:

$$B = \sum_{\alpha=1}^{3} \lambda_\alpha^2 n_\alpha \otimes n_\alpha. \tag{1.17}$$

Another measure of spatial strain tensors is the Almansi tensor, defined based on the left Cauchy-Green tensor as:

$$A = \frac{1}{2}(I - B^{-1}). \tag{1.18}$$

1.2.5 Stress

Consider an infinitesimal area Δa in the vicinity of a particle position x belonging to a deformable body in its current configuration Ω_t. If the resultant force acting on this area is denoted by Δf, the corresponding traction force is:

$$t(n) = \lim_{\Delta a \to 0} \frac{\Delta f}{\Delta a}, \tag{1.19}$$

where n is the outward normal to Δa at point x. The traction force satisfies Newton's third law, that is:

$$t(-n) = -t(n) \tag{1.20}$$

This traction force is then related to the normal vector via the Cauchy stress tensor σ as:

$$t = \sigma.n, \tag{1.21}$$

where

$$\sigma = \sum_{i,j=1}^{3} \sigma_{ij} e_i \otimes e_j, \tag{1.22}$$

in cartesian coordinates with basis unit vectors e in the current configuration. The Cauchy stress is a spatial tensor as it relates the current force vector to the deformed area. Other stress tensors can be constructed from the previously described measure of stress. Some of these stress tensors are provided in the following.

1.2.5.1 The First Piola-Kirchhoff Stress

The first Piola-Kirchhoff stress tensor, similar to F, is a two-point tensor that can be related to the Cauchy stress via the following relation:

$$\pi = J\sigma \ F^{-t}, \tag{1.23}$$

with

$$\pi = \sum_{i,j=1}^{3} \pi_{ij} e_i \otimes E_j, \tag{1.24}$$

where $(E_i)_{i=1,2,3}$ are the basis unit vectors in the reference configuration in cartesian coordinates. The first Piola-Kirchhoff stress, in that sense, relates the traction force in the current configuration to the corresponding differential area in the reference configuration. This implies that the traction force vector t in the deformed configuration can be mapped back to into the traction force T in the reference configuration. That is:

$$T = \pi \ N, \tag{1.25}$$

where N is unit outward normal vector to the particle point X (the initial position of x).

Remark: Traction force vector T defined in Equation 2.22 does not represent an actual traction force applied on point X, but it represents a co-linear vector to t in the reference configuration.

1.2.5.2 The Second Piola-Kirchhoff Stress

The second Piola-Kirchhoff stress tensor is completely defined in terms of quantities in the initial configuration. This tensor is expressed in terms of the Cauchy stress and the first Piola-Kirchhoff stress as:

$$S = JF^{-1} \ \sigma \ F^{-t} = F^{-1} \ \pi. \tag{1.26}$$

1.2.5.3 The Kirchhoff Stress

Another stress tensor that may be important for some constitutive laws is the Kirchhoff stress tensor that is expressed, in terms of the previously described stress tensors, as:

$$\tau = J\sigma = \pi \ F^t = F \ S \ F^t. \tag{1.27}$$

1.3 Hyperelasticity

1.3.1 Deformation energy

In the general theory of the elasticity, a material can be elastic with one condition, if the Cauchy stress tensor depends only on the state of the deformation which is characterized by any mesure of the strain. Thus, any measure of the stress is independent of the deformation path. The word of "hyperelasticty" can be divided essentially into two word "Hyper" and "Elasticity". In this scope, the first word denotes the range of large deformations and the second one is equivalent to the previous definition of the elasticity behaviour. To describe the non-linearity of the hyperelastic behavior, we need to postulate a form of energy potential, and by derivation of this potential the stress tensor can be obtained. This energy is also called deformation energy density or strain energy density and is often denoted as W or Ψ in the literature.

Now, consider A as a measure of the deformation state. The objectivity is one of the most important conditions to be verified by the energy potential which can be expressed mathematically as:

$$\Psi(QAQ^t) = \Psi(A). \tag{1.28}$$

where Q is an orthogonal tensor, i.e. $Q\ \ Q^t = I$. I is the second-order-unit tensor.

In other words, the objectivity of the deformation energy is nothing but its independence of any material reference. It's mentioned in [124], that to respect the objectivity principle, the strain energy density can be chosen as:

$$\Psi = \Psi(C). \tag{1.29}$$

In the case of an isotropic material, Ψ can be expressed in function of the invariants of C and B. But using that, Both of C and B have the same eigenvalues. So in consequence they have the same invariants.

$$\begin{aligned} I_1(C) &= I_1(B) \\ I_2(C) &= I_2(B). \\ I_3(C) &= I_3(B) \end{aligned} \tag{1.30}$$

These invariants can be expressed in this way:

$$\begin{aligned} I_1 &= trace(C) = \lambda_1^2 + \lambda_2^2 + \lambda_3^2 \\ I_2 &= \frac{1}{2}(I_1^2 - trace(C^2)) = \lambda_1^2\lambda_2^2 + \lambda_1^2\lambda_3^2 + \lambda_2^2\lambda_3^2, \\ I_3 &= det(C) = J^2 = \lambda_1^2\lambda_2^2\lambda_3^2 \end{aligned} \tag{1.31}$$

where λ_1, λ_2, λ_3 are the stretches in the principal direction of the two tensors C and B. Now to find the expressions of the different stress tensors we have to remind the couples of every strain measure and its ad-joint stress variable. We can present these couples in this way:

-(σ, B)

-(τ, F)

-(S, E)

By the definition of the couple of the ad-joint variables we deduce:

$$\sigma = \frac{1}{J}B\frac{\partial \Psi}{\partial B}\tau = \frac{\partial \Psi}{\partial F}S = \frac{\partial \Psi}{\partial E}. \tag{1.32}$$

The derivative of the different invariants compared to the tensor C may be expressed as:

$$\frac{\partial I_1}{\partial C} = I\frac{\partial I_2}{\partial C} = I_1 I - C\frac{\partial I_3}{\partial C} = I_3 C^{-1}. \tag{1.33}$$

From equations (1.32) and (1.33), it is deduced that:

$$S = 2\frac{\partial \Psi}{\partial C} = 2\sum_i \frac{\partial \Psi}{\partial I_i}\frac{\partial I_i}{\partial C}, \quad S = 2[(\frac{\partial \Psi}{\partial I_1} + I_1\frac{\partial \Psi}{\partial I_2})I - \frac{\partial \Psi}{\partial I_2}C + I_3\frac{\partial \Psi}{\partial I_3}C^{-1}]. \tag{1.34}$$

Having the equation (1.26) we can derive:

$$\begin{aligned} \sigma &= \frac{2}{J}[(\frac{\partial \Psi}{\partial I_1} + I_1\frac{\partial \Psi}{\partial I_2})B - \frac{\partial \Psi}{\partial I_2}B^2 + I_3\frac{\partial \Psi}{\partial I_3}I] \\ \tau &= 2[(\frac{\partial \Psi}{\partial I_1} + I_1\frac{\partial \Psi}{\partial I_2})F - \frac{\partial \Psi}{\partial I_2}B \;\; F + I_3\frac{\partial \Psi}{\partial I_3}F^{-t}]. \end{aligned} \tag{1.35}$$

1.3.2 The incompressibility condition

Almost of the rubber-like materials are characterized by an incompressible behavior. In fact, for this category of materials the compressibility module varies between 1000 and $2000MPa$, while the magnitude of the shear modulus is about $1MPa$. This difference signifies that the rubber hardly changes in volume, even under high stress. Its behavior is almost as incompressible. For most applications, modeling supposes a complete incompressiblity. So the incompressibility assumption is a good approximation for the modeling

of rubbery materials. The incompressibility condition can be shown mathematically through:

$$J = det(F) = 1. \tag{1.36}$$

Returning to the definition of the parameter J we can deduce that in an incompressible material, the volume is preserved and thus the transformation is isochoric. The incompressibility condition in the strain-stress relation can be introduced directly by the change of the formulation of the deformation energy which becomes:

$$\tilde{\Psi} = \Psi(I_1, I_2, I_3 = 1) - p(J-1), \tag{1.37}$$

where p denotes the Lagrange multiplier associated to the incompressibility condition. So the stress-strain relation in the Lagrangian configuration can be expressed in this way:

$$S = 2[(\frac{\partial \Psi}{\partial I_1} + I_1 \frac{\partial \Psi}{\partial I_2})I - \frac{\partial \Psi}{\partial I_2} C] - pC^{-1}. \tag{1.38}$$

And in the eulerian configuration, it becomes:

$$\sigma = \frac{2}{J}[(\frac{\partial \Psi}{\partial I_1} + I_1 \frac{\partial \Psi}{\partial I_2})B - \frac{\partial \Psi}{\partial I_2} B^2] - pI. \tag{1.39}$$

Using the relation (1.26) one can also deduce for the Kirchhoff stress:

$$\tau = 2[(\frac{\partial \Psi}{\partial I_1} + I_1 \frac{\partial \Psi}{\partial I_2})F - \frac{\partial \Psi}{\partial I_2} B \ \ F] - pF^{-T}. \tag{1.40}$$

Identifying the multiplier of Lagrange in the spheric part of the Cauchy stress tensor, p can be analyzed like a measure of the unknown hydrostatic pressure.

1.3.3 Examples of strain energy densities

Many forms of deformation energy densities have been proposed in the literature. Some are based on a statistical theory, others are purely phenomenological. in this part we will focus only on the deformation energy densities compatible with an incompressible material. There are several ways to classify the different energies of deformation. One way for example, it is to separate those expressed in terms of invariants, and those that are expressed in terms of the principal streches. In the first case the deformation energy depends linearly on the parameters of the constitutive law, and it is expressed in terms of the invariants I_1 and I_2. The coefficients of this type of laws behavior can be easily identified. They generally allow a good smoothing of the experimental results to a moderate level of deformation. For higher strain rate, will often increase the order of

the polynomial form. However, the fact of working with a large number of coefficients leads to numerical instabilities in the limits of the investigative deformation field range. For the models that are expressed as a power law as the model of Ogden, coefficients involved in non-linear form (exponent). These models usually have a good smoothing with few parameters for higher levels of deformation. However their identification is more difficult. We can find a more complete review of different energies deformation in this PHD thesis [124].

1.3.3.1 Developement in function of the invariants

The generalized model of Rivlin [123] implemented in most of finite element codes, is given by the following series expansion:

$$\Psi = \sum_{i+j=1}^{N} c_{ij}(I_1-3)^i(I_2-3)^j. \tag{1.41}$$

This type of behavior law is generally the most used. The strain energy is developed in order proportional to the desired deformation range (for N = 3, we have generally a good correlation with experimental measurements). In practice, most of the polynomial used laws correspond to a particular case of Rivlin development. For example, keeping only the first term of the expansion, we get the Neo-Hookean law:

$$\Psi = c_{10}(I_1-3), \tag{1.42}$$

which was first developed from statistical theory considering that the rubber vulcanized is a three-dimensional network of long molecular chains connected in some points. The Neo-Hookean model provides a good correlation to the degree of deformation moderate (up to 50 % [124]), but is not suitable for the incorporation of large deformations. The second special case of development corresponds to the phenomenological model of Mooney-Rivlin, widely used in the rubber industry. We then take the first 2 terms of Rivlin development, which allows writing:

$$\Psi = c_{10}(I_1-3)+C_{01}(I_2-3). \tag{1.43}$$

This time, a good correlation is obtained with the experimental results to levels deformation of the order of 150% [124].

1.3.3.2 Development in function of the principal streches

Ogden in [107] has proposed a strain energy in function of the principal stretches, which describes the change of these fields during the deformation.

$$\Psi = \Psi(\lambda_1, \lambda_2, \lambda_3) = \sum_{k=1}^{N} \frac{\mu_k}{\alpha_k}(\lambda_1^{\alpha_k} + \lambda_2^{\alpha_k} + \lambda_3^{\alpha_k} - 3), \tag{1.44}$$

where N is the chosen number of the terms in the series of the strain energy, while μ_k denotes the shearing coefficients and α_k are adimensional coefficients. Consider μ the slope in the origin of the stress-strain graph during a shearing test. Then with linearization we can obtain a relation between the Ogden shearing coefficient and μ:

$$\mu = \sum_{k=1}^{N} \alpha_k \mu_k, \tag{1.45}$$

under the following condition:

$$\alpha_k \mu_k > 0 \quad \forall k \in \{1, ..., N\}. \tag{1.46}$$

Using the Ogden model, it is possible to have good correlation with the experimental results. One of the advantages of this model, that we can fit well the experimental data even for a high level of deformation, giving the ability of having a more stable identification than the models expressed in function of the invariants. In the case of an incompressible transformation $\lambda_1\lambda_2\lambda_3 = 1$. So Using the previous incompressibility condition, and having $N = 2$, $\alpha_1 = 1$ and $\alpha_2 = -2$ we can identify the Mooney Rivlin model where $c_{10} = \frac{\mu}{2}$ and $c_{01} = -\frac{\mu}{2}$. With the same way, we can obtain the Neo-Hookean model with $c_{10} = \frac{\mu}{2}$ when $N = 1$ and $\alpha_1 = 2$. Another form of the strain energy density, also depending on the principal stretches, was proposed by Valanis and Landel [144]. The function of the strain energy density can be expressed as the sum of 3 separable functions, every one depending on only one principal stretch variable which is equivalent to:

$$\Psi(\lambda_1, \lambda_2, \lambda_3) = \psi_1(\lambda_1) + \psi_2(\lambda_2) + \psi_3(\lambda_3). \tag{1.47}$$

This form of the strain energy implies the absence of the interaction between the principal stretches variables. Using the strain energy density, we can express the stress tensors in the principal directions in the different configurations:

$$\sigma_\alpha = \lambda_\alpha \frac{\partial \Psi}{\partial \lambda_\alpha} P_\alpha = \frac{\partial \Psi}{\partial \lambda_\alpha} S_\alpha = \frac{1}{\lambda_\alpha} \frac{\partial \Psi}{\partial \lambda_\alpha} \tag{1.48}$$

1.4 Literature survey for nonlinear viscoelastic models

It is well known that rubber-like materials exhibit nonlinear viscoelastic behavior over a wide range of strain and strain rates confronted in several engineering applications such as civil engineering, automotive and aerospace industries. This is due to their capacity to undergo high strain and strain rates without exceeding the elastic range of behavior. Further, the time dependent properties of these materials, such as shear relaxation modulus and creep compliance, are, in general, functions of the history of the strain or the stress [45].

The study of viscoelastic behavior of solid materials has a long history and several models have been developed from purely mathematical approaches to applied studies where ease of application is for huge interest. The first, ever, models dedicated to the modeling of viscoelastic behavior have been established by Maxwell, Kelvin and Voigt who studied the one dimensional responses of these materials which led to the establishing of rheological models bearing their names which are still used to this day [92] (i.e. the Maxwell, Kelvin and Voigt rheological models). These rheoligical models were used by [10] to formulate the first three dimensional viscoelastic model for isotropic materials. This model is restricted to the linear viscoelasticity. However, due to the constitutive nonlinearities and the fact that these materials are able to undergo geometrical nonlinearities, in a wide range of strain, a linear viscoelasticity theory is no longer applicable for such material and new constitutive equations are required to fully depict the behavior of rubber-like materials for quasi-static and dynamic configurations of huge interest in engineering applications. In what follows, we present some of the most used modeling strategies in the literature.

1.4.1 Internal variables formulation

This approach was firstly introduced by [27] which consists on the formulation of the constitutive equation in terms of thermodynamic state variables : the internal energy is expressed as a function of the strain (or stress) and a set of internal state variables [24], [25], and [28]. These internal variables are related to their conjugate thermodynamic forces, which are the derivative of the internal energy with respect to the internal variables, via the evolution equations which could be linear or nonlinear.

One of the most known model following the internal state variable approach is the one

proposed by [131] which was the starting point for many contributions such as [51], [68], [66], [148] and our model proposed in [136] and presented in chapter 2 among others. The Simo's approach was based on the split of the internal energy density following a multiplicative decomposition of the deformation gradient tensor $\boldsymbol{F}$ into dilatational and volume preserving parts. Despite that this model may lead to non-physical results at finite strain [36], this model depict very well the behavior of rubber like materials for several applications and different load configurations. For this model, the internal energy is the sum of three different terms: a volumetric part depending on the jacobian of the deformation gradient tensor $J = det(\boldsymbol{F})$, an isochoric part depending upon the isochoric part of the deformation gradient tensor $\bar{\boldsymbol{F}} = J^{-1}\boldsymbol{F}$ and a part depending upon the internal variable noted $\boldsymbol{q}$ in the original paper which represents the non-equilibrium part of the stress. The evolution law of the internal variable $\boldsymbol{q}$ is postulated such that the generalized force is proportional to the derivative of the internal energy with respect to the isochoric strain. This assumption means that the behavior of the material is considered purely elastic for bulk, but it is viscoelastic for the shear. This formulation led to a single convolution integral representation of the constitutive equation of the stress. Similar formulations to the one used by [131] is due to the contribution by [51] where the internal variables were represented by a set of stress-like variables and the work by [68] where the internal variables were represented by a strain-like variables. The advantage of such formulation is the possibility to be used for modeling anisotropic behavior such as the work [66] in which the internal variables where dependent upon fiber orientation. The Simo's model is implemented in most of finite elements commercial software.

1.4.2 Additive decomposition of the free energy density

This approach relies on the decomposition of the deformation gradient tensor $\boldsymbol{F}$ as the sum of elastic deformation gradient tensor and an inelastic deformation gradient tensor. This decomposition was first proposed by [128] and followed by [90], [56], [41], [74] and [88] among many others.
Within this framework the deformation gradient tensor $\boldsymbol{F}$ is decomposed as follows:

$$\boldsymbol{F} = \boldsymbol{F}_e \boldsymbol{F}_i. \tag{1.49}$$

The inelastic part $\boldsymbol{F}_i$ characterizes an intermediate configuration between the reference and the actual configurations. This inelastic part of the deformation gradient tensor could be decomposed into several intermediate configurations. From (1.49) the free energy

density is also split as follows

$$\Psi = \Psi_e(\boldsymbol{C}) + \Psi_o(\boldsymbol{C}_e), \tag{1.50}$$

where $\boldsymbol{C}$ is the right Cauchy-Green strain tensor and $\boldsymbol{C}_e = \boldsymbol{F}_e{}^t \boldsymbol{F}_e$ is the elastic right Cauchy-Green strain tensor in the intermediate configuration. The free energy density of (1.50) have been used in several works such as [56], [41] and [88] among many others. [11] has proposed the following form for the free energy density

$$\Psi = \Psi_e(\boldsymbol{C}) + \Psi_o(\boldsymbol{C}, \boldsymbol{C}_i), \tag{1.51}$$

in which $\boldsymbol{C}_i = \boldsymbol{F}_i{}^t \boldsymbol{F}_i$ is the inelastic left Cauchy-Green strain tensor, the viscous component of the free energy density $\Psi_o(\boldsymbol{C}, \boldsymbol{C}_i)$ is assumed to be proportional to the elastic component $\Psi_e(\boldsymbol{C})$. The stress response in terms of the second Piola-Kirchhoff stress tensor $\boldsymbol{S}$ are obtained after applying the Coleman and Noll procedure [27] by verifying the Clausius-Duhem inequality for all admissible processes and is decomposed as

$$\boldsymbol{S} = \boldsymbol{S}_e + \boldsymbol{S}_i, \tag{1.52}$$

where $\boldsymbol{S}_e$ is the equilibrium stress whereas $\boldsymbol{S}_i$ is the over stress. Using an internal energy of the form of equation (1.50) these stresses are given by

$$\boldsymbol{S}_e = \frac{\partial \Psi_e}{\partial \boldsymbol{C}} \quad , \quad \boldsymbol{S}_i = \frac{\partial \Psi_i}{\partial \boldsymbol{C}_i} \tag{1.53}$$

In order to reach the expression of the stress, in addition to equation (1.53) one need to define the evolution law of the internal variable $\boldsymbol{F}_i$ or $\boldsymbol{F}_e$. A common choice for the flow rule is to apply a generalization of the one-dimensional linear Maxwell-model to the three-dimensional and nonlinear domain. In this case the evolution equations are assumed to be linear, and the overstress term arising from them is the generalization of the extra-stress arising in Maxwell element [66] and [73].Within this context and the framework of irreversible thermodynamics, [13] proposed a double decomposition of the deformation gradient tensor $\boldsymbol{F}$. First, the deformation gradient tensor is split into volumetric and isochoric parts, then the latter is split into elastic and inelastic parts :

$$\boldsymbol{F} = (J^{\frac{1}{3}} \boldsymbol{I}) \bar{\boldsymbol{F}} = (J^{\frac{1}{3}} \boldsymbol{I}) \bar{\boldsymbol{F}}_e \bar{\boldsymbol{F}}_i, \tag{1.54}$$

where $\bar{\boldsymbol{F}}$ is the incompressible deformation gradient tensor, $\bar{\boldsymbol{F}}_e$ is the elastic incompressible deformation gradient tensor and $\bar{\boldsymbol{F}}_i$ is the inelastic deformation gradient tensor. This

decomposition implies that the inelastic processes are isochoric. The free energy density, following (1.54), is decomposed as well into:

$$\Psi = \Psi_{eq} + \Psi_{neq} + \Psi_{vol}, \tag{1.55}$$

where the subscript eq, neq and vol stand for the equilibrium, non-equilibrium and volumetric parts of the free energy density respectively. The stress tensor is obtained after satisfying the second law of thermodynamics in terms of the Clausius-Duhem inequality and it is decomposed accordingly as

$$\boldsymbol{\sigma} = \boldsymbol{\sigma}_{eq} + \boldsymbol{\sigma}_{neq} + \boldsymbol{\sigma}_{vol}. \tag{1.56}$$

For the evolution law of the internal variables, three different rheoligical models were used [86]. The first model is the Zener model for which the evolution law takes the followingg form:

$$\dot{\bar{\boldsymbol{B}}}_e = \boldsymbol{L}\cdot\bar{\boldsymbol{B}}_e + \bar{\boldsymbol{B}}_e\cdot\boldsymbol{L}^t - \frac{2}{3}(\boldsymbol{I}:\boldsymbol{L})\bar{\boldsymbol{B}}_e - \frac{2}{\eta}\boldsymbol{\sigma}_{neq}\cdot\bar{\boldsymbol{B}}_e, \tag{1.57}$$

where $\bar{\boldsymbol{B}}_e = \bar{\boldsymbol{F}}_e\cdot\bar{\boldsymbol{F}}_e^t$ is the incompressible left Cauchy-Green strain tensor and it is considered the internal variable, $\boldsymbol{L}$ is the velocity gradient tensor and η is the viscosity coefficient. The second model is the Poynting–Thomson model for which the evolution law reads

$$\begin{aligned}\dot{\bar{\boldsymbol{B}}}_e =& \boldsymbol{L}\cdot\bar{\boldsymbol{B}}_e + \bar{\boldsymbol{B}}_e\cdot\boldsymbol{L}^t - \frac{2}{3}(\boldsymbol{I}:\boldsymbol{L})\bar{\boldsymbol{B}}_e - \frac{2}{\eta}\boldsymbol{\sigma}_{neq}\cdot\bar{\boldsymbol{B}}_e \\ &+ \frac{4}{J\eta}\Psi_{neq,1}\left(\bar{\boldsymbol{B}} - \frac{1}{3}\left(\bar{\boldsymbol{B}}:\bar{\boldsymbol{B}}^{-1}\right)\bar{\boldsymbol{B}}_e\right) \\ &+ \frac{4}{J\eta}\Psi_{neq,2}\left(\bar{\boldsymbol{B}}_e\cdot\bar{\boldsymbol{B}}^{-1}\cdot\bar{\boldsymbol{B}}_e - \frac{1}{3}\left(\bar{\boldsymbol{B}}^{-1}:\bar{\boldsymbol{B}}_e\right)\bar{\boldsymbol{B}}_e\right)\end{aligned} \tag{1.58}$$

where $\Psi_{neq,1}$ and $\Psi_{neq,2}$ are the derivative of the non equilibrium parts of the free energy density of equation (1.55) with respect to the first and second invariants of the inelastic left Cauchy-Green strain tensor $\bar{\boldsymbol{B}}_i$. The third model is the generalized Bingham viscoplastic model.

[88] proposed nonlinear evolution equations based on strain, time and temperature. [11] also used nonlinear evolution equations of rate type for the internal variables. These are based on a particular linear relaxation form of the Maxwell model which leads to a viscoelastic formulation that can be seen as a particular case of a large strain viscoplastic model. A variational formulation of Bonet's model has been developed in [40].

1.4.3 Integral based formulation

The integral-based formulation is an extension to the finite strain domain of the simple formulation of Boltzmann. Within this approach, the stress is decomposed into an instantaneous elastic response typically modeled by an hyperelastic response for rubber-like materials and an over-stress quantity which is expressed by a hereditary integral containing all the history of the strain up to the actual time t. The first contribution to this approach was the work by Green and Rivlin [52]. Inthis context, the internal energy Ψ was developed accordingly in agreement with the *fading memory* property i.e., strains which occurred in the distant past have less influence on the present value of Ψ than those which occurred in the more recent past. This work have been followed by several works who dealt with the definition of the internal energy accounting for deformation histories [31], [39] and [49]. One of the most known models to this approach is the multi-integral model proposed by Pipkin and Rogers [117] for which under incompressibility assumption the second Piola-Kirchhoff stress reads

$$\begin{aligned}\S(t) = &-p\boldsymbol{C}^{-1} + \int_0^t r_1\left(t-t'\right)\dot{\boldsymbol{E}}\left(t'\right)dt' + \\ &\int_0^t\int_0^t r_2(t-t',t-t'')\dot{\boldsymbol{E}}\left(t'\right)\dot{\boldsymbol{E}}\left(t''\right)dt'\,dt'' + \\ &\int_0^t\int_0^t\int_0^t r_3\left(t-t',t-t'',t-t'''\right)tr\left[\dot{\boldsymbol{E}}\left(t'\right)\dot{\boldsymbol{E}}\left(t''\right)\right]\dot{\boldsymbol{E}}\left(t'''\right)dt'dt''dt''' + \\ &\int_0^t\int_0^t\int_0^t r_4\left(t-t',t-t'',t-t'''\right)\dot{\boldsymbol{E}}\left(t'\right)\dot{\boldsymbol{E}}\left(t''\right)\dot{\boldsymbol{E}}\left(t'''\right)dt'dt''dt''',\end{aligned} \tag{1.59}$$

$r_k\,(k = 1..4)$ are the relaxation kernels expressed by a decaying exponential functions and $\dot{\boldsymbol{E}}(t)$ is the time derivative of the Green-Lagrange deformation tensor. Equation (1.59)will be used later in chapter 3 to generate data which will be used in the identification procedure presented therein. This work was followed by several contributions such as the pseudo-linear model proposed by [57] in which a the stress is expressed as Boltzmann integral over the history of a nonlinear measure of strain.
Thanks to their simplicity for engineering applications, several models using this approach have been thoroughly investigated [4], [58] and [23] among others. In the latter, a comparative study have been made to investigate seven single-integral viscoelastic models response using data in compression for a filled rubber for relaxation and loading/unloading/creep cycles at different strain rates, namely the models due to [47], [48], [54], [147], [63], [89] and [127]. These models could be written in the same form in terms

of the first Piola-Kirchhoff stress as

$$\begin{aligned}\boldsymbol{\pi}(t) &= \boldsymbol{\pi}^{(e)} + \boldsymbol{F}(t)\boldsymbol{\Lambda}(t)\int_0^t \frac{\partial k(t-s)}{\partial(t-s)}\boldsymbol{\Psi}(t-s)\,ds \\ \boldsymbol{\pi}^{(e)} &= \phi_1(t)\boldsymbol{F}(t) + \phi_2(t)\boldsymbol{F}(t)\boldsymbol{C}(t),\end{aligned} \tag{1.60}$$

where $\boldsymbol{\pi}^e$ is the hyperelastic contribution to the stress and the functions ϕ_1 and ϕ_2 are functions of the first two invariants of the left Cauchy-Green strain tensor $\boldsymbol{C}$. A suitable choice for $\boldsymbol{\Lambda}$, $\boldsymbol{\Psi}$ as well as the viscoelastic kernel k allows all the models under consideration to be encompassed.

Another contributions in this context are the quasi-linear viscoelastic models which was first proposed by [48] to describe the behavior of biological tissues. This model, which is a special case of a more general Pipkin–Rogers constitutive model [117], predicts that at any time a stress that is equal to the instantaneous elastic stress response decreased by an amount depending on the past history, assuming that a Boltzmann superposition principle holds. This work was followed by [99] and [98] where the linearized strain is expressed in terms of a nonlinear measure of the stress.

1.4.4 Differential viscoelasticity

Finally, another approach to describe viscoelastic behavior of rubber-like materials is the differential nonlinear viscoelasticity [7], [126] and [143]. Within this context, the stress and strain tensors are related through differential equations. It is the generalization to the three-dimensional nonlinear case of the linear rheological elementary models, namely the Hook spring for which the stress is expressed by the following

$$\sigma = G\varepsilon, \tag{1.61}$$

for the linear case and

$$\sigma = \phi_e(\varepsilon), \tag{1.62}$$

for the nonlinear case and the viscous dashpot for which the stress is expressed as

$$\sigma = \eta\dot{\varepsilon}, \tag{1.63}$$

for the linear case and

$$\sigma = \phi_v(\dot{\varepsilon}), \tag{1.64}$$

for the nonlinear case. In general, the stress-strain differential relation arising from any combination of these elementary models reads

$$\sum_{m=0}^{M} a_m \frac{\partial^m \sigma}{\partial t^m} = \sum_{n=0}^{N} b_n \frac{\partial^n \varepsilon}{\partial t^n}, \tag{1.65}$$

where a_m and b_m are functions of the rheological characteristics of the elementary models associated. In the case when $m = n$, the stress-strain relation arising from (1.65) is equivalent to the one obtained from the generalized Maxwell model. The generalization of these rheological models to the three-dimensional domain is done by replacing the one dimensional stress σ and strain ε by their three-dimensional counterparts $\boldsymbol{\sigma}$ and $\boldsymbol{\varepsilon}$ respectively. The Rivlin-Ericksen model is a simplified form of relation (1.65) which does not include time derivative of the stress

$$\sigma = \sum_{n=1}^{N} b_n \frac{\partial^n \varepsilon}{\partial t^n}. \tag{1.66}$$

In relation (1.66) σ is replaced by the Cauchy stress tensor $\boldsymbol{\sigma}$ and the derivative $\frac{\partial^n \varepsilon}{\partial t^n}$ by the nth Rivlin-Ericksen tensor $\boldsymbol{A}_n$ [34].Therefore the Cauchy stress tensor is given by

$$\boldsymbol{\sigma} = \sum_{n=1}^{N} b_n \boldsymbol{A}_n. \tag{1.67}$$

In particular, the second order model obeys the equation

$$\boldsymbol{\sigma} = \eta \boldsymbol{A}_1 + b_{12} \boldsymbol{A}_1^2 + b_{21} \boldsymbol{A}_2, \tag{1.68}$$

where η, b_{12} and b_{21} are adjustable parameters. The model of equation (1.68) was employed by [2], [3], [26] and [122] to study laminar flow of viscoelastic fluids.
Another model arising from (1.66) is the White-Metzner model for which $\frac{\partial^n \varepsilon}{\partial t^n}$ is replaced by the nth White-Metzner tensor $\boldsymbol{B}_n$. The model reads

$$\boldsymbol{\sigma} = \sum_{n=1}^{N} b_n \boldsymbol{B}_n, \tag{1.69}$$

which was used by [2], [76] and [145].
Other contributions to this approach is the extension to finite strain domain of the so-called Maxwell rheological model composed by a spring in series with a dashpot, the Kelvin-Voigt model composed by a spring parallel to a dashpot or the standard viscoelastic solid model composed by two springs and a dashpot with two configuration as it is shown in figure 1.12. Version A was extended to large deformation by [59] in which the linear dashpot was replaced by a nonlinear one and linear spring with Young's modulus E_2 was replaced by an hyperelastic spring where the strain energy density was taken in the Langevin form. This model was used to describe the effect of strain rate of the yield stress in cellulose derivatives and poly(vinyl chloride). Version B was extended to finite strains by [14]. In that model, the linear spring with Youn's modulus E_1 was

replaced by a hyperelastic spring and the Maxwell element in parallel was replaced by a nonlinear Maxwell element of Leonov's type. Numerical simulation demonstrates that this model provides qualitative agreement with experimental data for polymeric materials [34].

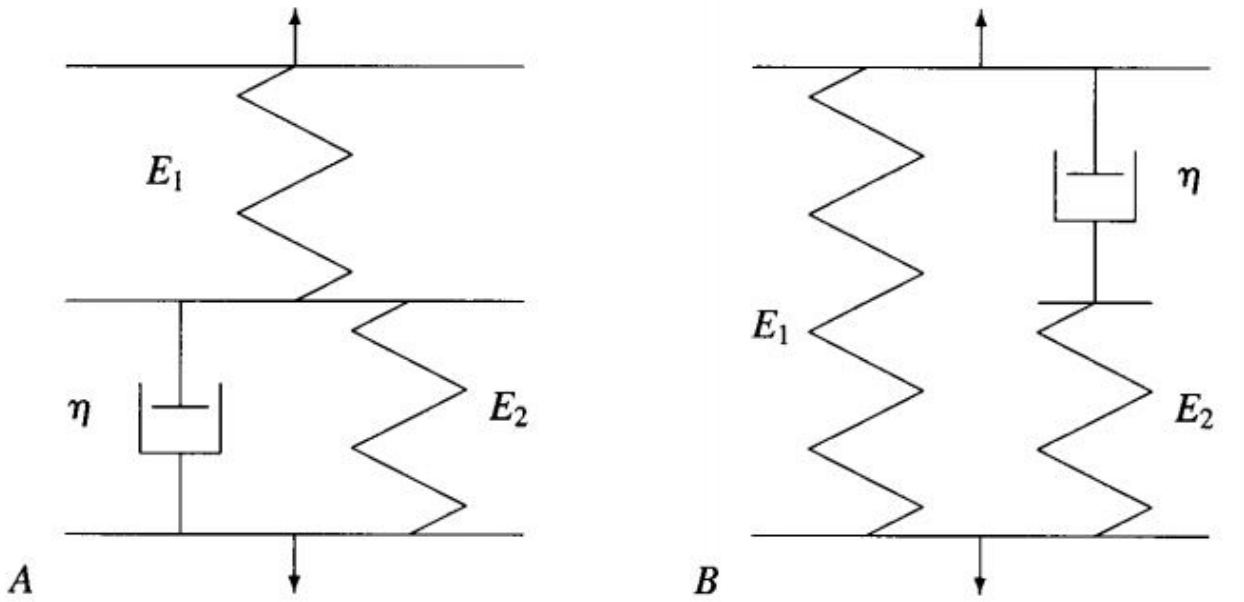

Figure 1.12: Two versions of the standard viscoelastic solid

Thus in the simplest case, the stress depends upon the current values of strain and strain rate only. In this sense, it can account for the nonlinear short-term response and the creep behavior, but it fails to reproduce the long-term material response (e.g., relaxation tests)

1.5 Conclusion

Within this chapter, we tried to present a review of the behavior of rubber-like materials from a phenomenological point of view. In the first part, we recalled the most known physical aspect related to these materials evolving high deformability and damping properties corroborated with several experiments found in literature. In the second part, we recalled the basis mechanics for the nonlinear elasticity framework needed in the development of nonlinear viscoelasticity models. In the third part, we tried to classify the different approaches and modeling procedures followed in the development of nonlinear viscoelatic models for rubber-like. The common thing about all these approaches is

that the constitutive equation of the stress is represented by a hereditary integral over the history of the strain or equivalent quantities. In the next chapter, we present the nonlinear viscoelastic model proposed within this work.

CHAPTER 2

PROPOSED NONLINEAR VISCOELASTIC MODEL

Contents

N this chapter we shall develop a nonlinear viscoelastic model at finite strain within the framework of rational thermodynamics and the approach of internal state variables, the model is derived through a modification to approaches

in [131], [65] and [120] taking into account the dependence of the time dependent functions upon the state of the strain.
In section 2.1, a one dimensional nonlinear viscoelastic model is developed using a modified Maxwell rheological model. Section 2.2 is devoted to the extension of the model to the three-dimensional domain under the assumption of linear kinematics. In section 2.3, this model is extended to the fully nonlinear formulation using a nonlinear set of evolution equation of the internal state variables within the rational thermodynamic framework. The shear relaxation modulus is set to be a function upon the invariants of the right Cauchy-Green strain tensor via a strain shift function analogous to the temperature shift function for the thermorheologically simple materials, this choice is motivated experimentally following the experimental characterization of BIIR from [103]. The constitutive equation for the stress is then obtained by resolving the set of nonlinear evolution equations.

2.1 Experimental and rheological motivations

In this section, we develop the rheological and experimental arguments leading to the proposed finite strain viscoelastic model. To motivate the three dimensional model developed below, we first highlight some experimental results leading to this model and then we consider a suitable modification to the generalized Maxwell rheological model to build the one dimensional nonlinear viscoelastic model.

2.1.1 Experimental motivation

A significant class of rubbers shows nonfactorizable behavior at low and average range of strain. This phenomenon consists on the dependence of the shear relaxation modulus upon strain level. Several works were dedicated to deal with this class of behavior especially the series of papers by [134] and [104]. In a recent work [103], an experimental characterization was carried out with three rubber-like materials: the natural rubber (NR), the Bromobutyl (BIIR)and a mixture of these materials (NR-BIIR). Samples of the three materials were subjected to monotonic experiments of simple extension and pure shear with a relaxation of 10 minutes every 50% of strain in order to depict the equilibrium behavior of the materials. Moreover, a dynamic characterization was carried out in simple shear for a wide window of frequency at several temperatures and predeformations in order to construct the master curve of the material. This material

showed a dependence of the shear relaxation modulus upon strain. In figure 2.1 it is plotted the logarithm of the shear relaxation modulus $G(t)$ versus the logarithm of time for two different level of strain 10% and 50% for BIIR material. The shear relaxation modulus shows a dependence upon the strain level which leads according to [141] to a shift in the time with a strain dependent function since the shear relaxation modulus at any level could be obtained through a combination of a vertical and horizontal translation from the reference curve at a strain level of 10%. Therefore, a one dimensional viscoelastic model, taking in consideration these results, is developed in the next section through a generalization of the Maxwell rheological model.

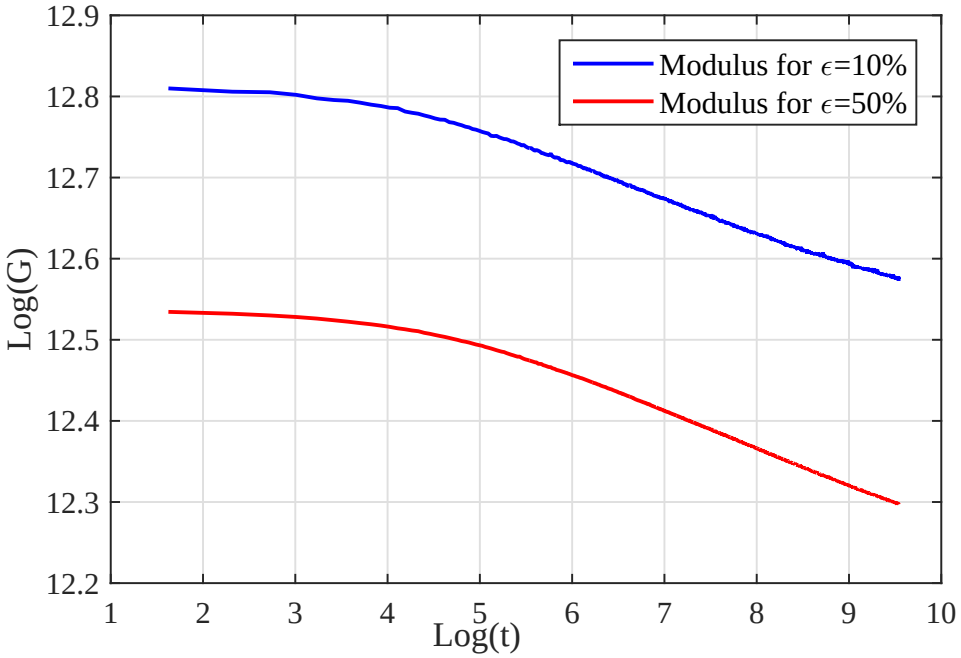

Figure 2.1: Dependence of the shear relaxation modulus upon strain for BIIR rubber

2.1.2 Rheological motivation

Before we develop the three-dimensional viscoelastic model, we shall investigate the following formulation for a standard linear solid. In this model, which is a modification to the rheological Maxwell model reported in figure 2.2, σ denotes the total stress, ε denotes the total strain, G_i and τ_i are the parameters of the Maxwell model. Unlike the rheological model used in [129], the relaxation times τ_i are, due to the experimental result outlined above, functions of the total strain ε . Furthermore, let α_i be the deformation of

the dashpot of each Maxwell branch and $Q_i = G_i \alpha_i$ an internal variable stress measure characterizing the model. The internal deformation variables variables α_i, according to the rheological model of figure 2.2, are governed by the following evolution equations.

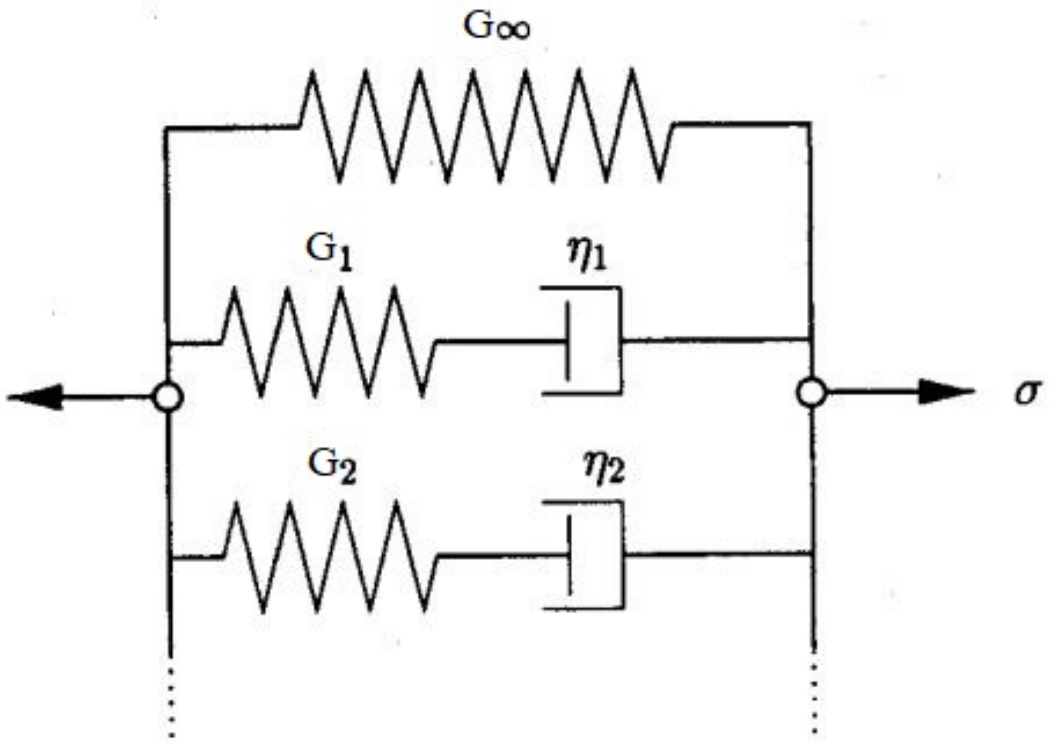

Figure 2.2: Generalized Maxwell model

$$\dot{\alpha}_i + \frac{1}{\tau_i(\varepsilon)}\alpha_i = \frac{1}{\tau_i(\varepsilon)}\varepsilon, \quad \alpha_i|_{t=0} = 0. \tag{2.1}$$

Which can be written in terms of the stress internal variables Q_i as follow:

$$\dot{Q}_i + \frac{1}{\tau_i(\varepsilon)}Q_i = \frac{1}{\tau_i(\varepsilon)}G_i\varepsilon, \quad Q_i|_{t=0} = 0. \tag{2.2}$$

The total stress σ derive directly from the rheological model as the difference between the elastic instantaneous stress and the non-equilibrium stresses Q_i.

$$\sigma = G_o\varepsilon - \sum_i Q_i, \tag{2.3}$$

where $G_o = G_\infty + \sum_i G_i$ is the instantaneous shear modulus. The time parameters of the Maxwell model are set to be a strain dependent function; this idea follows from

the description of thermorheologically simple materials' behavior see [141] and [140], for which all parameters are temperature dependent via a single variable function called *'temperature shift-function'*. [95, 125] and [104] among others generalized this notion to describe thermorheologically complex materials' behavior where the shift function depend upon temperature and stress or strain. Other contributions modeled this phenomena by a strain-rate dependent relaxation times , see [21] and references therein. In our work, since the study was carried out using relaxation data, the time parameters take the following form.

$$\tau_i(\varepsilon) = a(\varepsilon)\tau_i, \tag{2.4}$$

$a(\varepsilon)$ is a positive strain function, following the dissipation inequality, called strain shift function. Therefore, the law of evolution of the equation (2.1) became a linear differential equation over the reduced time ξ

$$\frac{d\alpha_i}{d\xi} + \frac{1}{\tau_i}\alpha_i = \frac{1}{\tau_i}\,\varepsilon \;\text{ with }\; \xi(t) = \int_0^t \frac{dt'}{a(\varepsilon)}, \tag{2.5}$$

where $\xi(t)$ is an increasing function of time. Considering the form of the time parameters of equation (2.4), the integration of the differential equations in (2.5) lead to the following expression of α_i:

$$\alpha_i(t) = \frac{1}{\tau_i}\int_0^t \exp\left[-\left(\xi-\xi'\right)/\tau_i\right]\varepsilon\left(t'\right)d\xi', \tag{2.6}$$

which can be integrated by parts to lead to

$$\alpha_i(t) = \varepsilon(t) - \int_0^t \exp\left[-\left(\xi-\xi'\right)/\tau_i\right]\dot{\varepsilon}\left(t'\right)d\xi'. \tag{2.7}$$

Substituting of α by its expression into (2.3) with $Q_i = G_i\alpha_i$ yield the expression of the total stress σ as a Boltzmann convolution integral of the strain as follow :

$$\sigma(t) = \int_0^{\xi} G\left(\xi-\xi'\right)\dot{\varepsilon}\left(t'\right)d\xi', \tag{2.8}$$

where $G(t)$ is the shear relaxation modulus expressed by a Prony series as follows:

$$G(t) = G_\infty + \sum_i G_i \exp\left(-\frac{t}{\tau_i}\right) = G_o - \sum_i G_i\left(1-\exp\left(-\frac{t}{\tau_i}\right)\right). \tag{2.9}$$

2.1.3 Thermodynamic considerations

Another way to motivate the evolution equations (2.1), is to consider the thermodynamic arguments following from the modified Maxwell rheological model. Considering the set

of variables governing the model, namely the total strain ε and the set of internal strains α_i, the total free energy density reads:

$$\psi(\varepsilon,\boldsymbol{\alpha}) = \frac{1}{2}G_\infty\varepsilon^2 + \sum_i \frac{1}{2}(\varepsilon-\alpha_i)^2, \tag{2.10}$$

where $\boldsymbol{\alpha}$ is the vector of strain internal variables α_i. The forces in the dashpots of the Maxwell model are given by

$$\sigma_i^v = G_i(\varepsilon-\alpha_i) = \eta_i\dot{\alpha}_i, \tag{2.11}$$

where $\eta_i = \tau_i G_i$ are the viscosity coefficients characterizing the dashpots in the Maxwell model which are functions of the total deformation ε following from the dependence of the relaxation times τ_i upon ε due to equation (2.4). Equation (2.11) implies the evolution law of equation (2.1) and thus the dissipation function $D[\varepsilon,\boldsymbol{\alpha},\dot{\boldsymbol{\alpha}}]$ is given by

$$D[\varepsilon,\boldsymbol{\alpha},\dot{\boldsymbol{\alpha}}] = \sum_i \sigma_i^v\dot{\alpha}_i = \sum_i \eta_i(\dot{\alpha}_i)^2 \geq 0. \tag{2.12}$$

These thermodynamic quantities could be be expressed as a convolution integrals in terms of the history of the deformation ε by substituting the internal variables α_i by their expressions in equations (2.10) and (2.12) to lead to the following

$$D[\varepsilon,\boldsymbol{\alpha},\dot{\boldsymbol{\alpha}}] = -\frac{1}{a(\varepsilon)}\frac{1}{2}\int_0^\xi\int_0^\xi \frac{\partial G\left(2\xi-\xi'-\xi''\right)}{\partial\xi}\frac{\partial\varepsilon}{\partial t'}\frac{\partial\varepsilon}{\partial t''}d\xi'd\xi'', \tag{2.13}$$

for the dissipation function, and

$$\psi = \frac{1}{2}\int_0^\xi\int_0^\xi G\left(2\xi+\xi'+\xi''\right)\dot{\varepsilon}\left(t'\right)\dot{\varepsilon}\left(t''\right)d\xi'd\xi'', \tag{2.14}$$

for the free energy density. Note that the positivity of the deformation shift function $a(\varepsilon)$ is a sufficient condition to the positivity of the dissipation function $D[\varepsilon,\boldsymbol{\alpha},\dot{\boldsymbol{\alpha}}]$ in equation (2.13).

2.2 Formulation restricted to linear kinematics

In this section, we extend the simple nonlinear models discussed in the preceding section to three-dimensional physically nonlinear elasticity. This extension is patterned after the model presented in section 2.1. First, we discuss the formulation of the general three–dimensional constitutive model within the linear kinematics framework (i.e. small strain domain). Next, we examine the thermodynamic aspects within the framework of irreversible thermodynamics with internal state variables.

2.2.1 Formulation of the model

Viscoelastic constitutive equations arise when modeling the behavior of rubber-like materials. The bulk response of these materials is elastic and much stiffer than the deviatoric response. Further, for most engineering applications using these materials the assumption of incompressibility holds with high degree of approximation. Considering these assumptions, we introduce an additive split of the strain tensor into volumetric and deviatoric parts as

$$\varepsilon = e + \frac{1}{3}\mathbf{\Theta} \boldsymbol{I}, \tag{2.15}$$

where e is the deviatoric strain given by

$$e = \varepsilon - \frac{1}{3} tr[\varepsilon] \boldsymbol{I}, \tag{2.16}$$

and $\mathbf{\Theta}$ is the deviatoric strain defined by

$$\mathbf{\Theta} = tr[\varepsilon]. \tag{2.17}$$

Following the additive split of the strain of equation (2.15) the initial stored elastic energy density is split as well

$$\Psi^0(\varepsilon) = \bar{\Psi}^0(e) + U^0(\mathbf{\Theta}). \tag{2.18}$$

Both $\bar{\Psi}^0(e)$ and $U^0(\mathbf{\Theta})$ are positive functions of their arguments. The initial elastic stress is given by

$$\boldsymbol{\sigma}^o = \frac{\partial \Psi^0(\varepsilon)}{\partial \varepsilon}, \tag{2.19}$$

which can be expressed using equations (2.16) and (2.17) and the chain rule as follows:

$$\boldsymbol{\sigma}^o = \boldsymbol{dev}[\frac{\partial \bar{\Psi}^0(e)}{\partial e}] + U^{0\prime}(\mathbf{\Theta}) \boldsymbol{I}. \tag{2.20}$$

Now, in accordance with the one dimensional model of 2.1 the total stress is given by

$$\boldsymbol{\sigma}(t) = \boldsymbol{\sigma}^o - \sum_i \boldsymbol{Q}_i(t), \tag{2.21}$$

where $\boldsymbol{Q}_i, i = 1..N$ is a set of over-stress internal variables with the evolution law, motivated by the one dimensional model of 2.1, defined by

$$\dot{\boldsymbol{Q}}_i + \frac{1}{\tau_i(\varepsilon)} \boldsymbol{Q}_i = \frac{\gamma_i}{\tau_i(\varepsilon)} \boldsymbol{dev}\left[\frac{\partial \bar{\Psi}^0(e)}{\partial e}\right]. \tag{2.22}$$

Note that the set of relaxation times τ_i are dependent of the total strain ε as it was postulated for the one dimensional model in equation (2.4)

$$\tau_i(\varepsilon) = a(\varepsilon)\tau_i, \tag{2.23}$$

where $a(\varepsilon)$ is the strain shift function. The solution of the set of linear differential equations of (2.22) yields the convolution representation of the internal variables

$$\boldsymbol{Q}(t) = \frac{\gamma_i}{\tau_i}\int_0^{\xi} \exp\left[-\left(t-t'\right)/\tau_i\right] \boldsymbol{dev}\left[\frac{\partial \bar{\Psi}^0(\boldsymbol{e})}{\partial \boldsymbol{e}}\right] dt'. \tag{2.24}$$

In equation (2.24), ξ is the reduced time. Substituting of (2.24) into (2.21), integration by parts and use of the fact that the internal variables vanish for $t<0$ gives the constitutive equation of the stress tensor as the convolution integral

$$\boldsymbol{\sigma}(t) = \int_0^{\xi} g\left(\xi-\xi'\right)\frac{d}{dt'}\left(\boldsymbol{dev}\left[\frac{\partial \bar{\Psi}^0\left(\boldsymbol{e}\left(t'\right)\right)}{\partial \boldsymbol{e}}\right]\right)dt' + U^{0'}(\boldsymbol{\Theta})\boldsymbol{I}, \tag{2.25}$$

where $g(t)$ is the normalized relaxation function, in this case it is expressed by the following

$$g(t) = \gamma_\infty + \sum_i \gamma_i \exp\left[-t/\tau_i\right]. \tag{2.26}$$

Note that in equation (2.25) $U^{0'}(\boldsymbol{\Theta})\boldsymbol{I} \rightarrow -p\boldsymbol{I}$ for incompressible materials, where p is the hydraustatic pressure [30]. This completes the development of the three-dimensional viscoelastic model in small strain domain.

2.2.2 Thermodynamic considerations

Once again motivated by the rheological arguments of the previous section, now we proceed to investigate the thermodynamic foundation of this model within the framework of irreversible thermodynamic and the internal state variables. It should be noted, however, that this development is carried out under isothermal conditions. Therefore, attention is restricted to purely mechanical theory. Our starting point is the form of the free energy function which is postulated by the following:

$$\Psi(\boldsymbol{Q}_i, \varepsilon) = \Psi^0(\varepsilon) - \sum_i \boldsymbol{Q}_i \cdot \boldsymbol{e} + \Xi\left(\sum_i \boldsymbol{Q}_i\right). \tag{2.27}$$

Note that the function Ξ is a positive function of the set of internal variables $\boldsymbol{Q}_i$ and may be expressed by a Taylor series especially in the case of small strains. The second law

of thermodynamics in terms of the Clausius-Duhem inequality for a purely mechanical theory leads to the inequality

$$-\dot{\Psi}(\boldsymbol{Q}_i,\varepsilon)+\boldsymbol{\sigma}:\dot{\varepsilon}\geq 0. \tag{2.28}$$

This inequality is regarded as a constitutive restriction to be satisfied by all admissible states defined $\varepsilon,\boldsymbol{Q}_i$ and for all strain rates $\dot{\varepsilon}$ for all admissible processes. From (2.28) and using the chain rule it follows

$$\dot{\Psi}=\left(\frac{\partial\Psi^0}{\partial\varepsilon}-\sum_i dev\left[\boldsymbol{Q}_i\right]\right):\dot{\varepsilon}-\boldsymbol{D}\left[\varepsilon,\boldsymbol{Q}_i,\dot{\boldsymbol{Q}}_i\right], \tag{2.29}$$

where

$$\boldsymbol{D}\left[\varepsilon,\boldsymbol{Q}_i,\dot{\boldsymbol{Q}}_i\right]=\sum_i\left[\boldsymbol{e}-\frac{\partial\Xi}{\partial\boldsymbol{Q}_i}\right]:\dot{\boldsymbol{Q}}_i \tag{2.30}$$

is the dissipation function. Substitution of equations (2.29)and (2.30) in (2.28) yields the following inequality

$$\left(\boldsymbol{\sigma}-\frac{\partial\Psi^0}{\partial\varepsilon}+\sum_i dev\left[\boldsymbol{Q}_i\right]\right):\dot{\varepsilon}+\boldsymbol{D}\left[\varepsilon,\boldsymbol{Q}_i,\dot{\boldsymbol{Q}}_i\right]\geq 0. \tag{2.31}$$

Inequality (2.31) must hold for all rates $\dot{\varepsilon},\dot{\boldsymbol{Q}}_i$, then standard arguments leads to

$$\begin{aligned}\boldsymbol{\sigma}&=\frac{\partial\Psi^0}{\partial\varepsilon}-\sum_i dev\left[\boldsymbol{Q}_i\right]\\ \boldsymbol{D}\left[\varepsilon,\boldsymbol{Q}_i,\dot{\boldsymbol{Q}}_i\right]&=\sum_i\left[\boldsymbol{e}-\frac{\partial\Xi}{\partial\boldsymbol{Q}_i}\right]:\dot{\boldsymbol{Q}}_i.\end{aligned} \tag{2.32}$$

The first relation of equation (2.32) is the generalization to the three-dimensional domain of the stress expression for the rheological model of section 2.1 and the second one is the three-dimensional counterpart of the dissipation of (2.12).

2.3 Fully nonlinear viscoelastic model

In this section, we extend the formulation outlined above to the fully nonlinear range. Hence, the mechanical framework and the thermodynamic assumptions leading to the model are outlined. It should be noted, however, that this model is derived through an isothermal conditions.

2.3.1 Mechanical framework and form of the Helmholtz free energy density

Consider a viscoelastic material with reference placement Ω_0 in the reference configuration C_0. It occupies at the time t the placement Ω in the deformed configuration C_t. Let φ denote a macroscopic motion between the two configurations, which maps any point X in the reference configuration C_0 to the point x in the deformed configuration. Let $\boldsymbol{F}(X,t) = \partial x/\partial X$ be the deformation gradient tensor. Likewise, let $J = \det(\boldsymbol{F})$ be the jacobian of the deformation gradient tensor. From the deformation gradient $\boldsymbol{F}(X,t)$ the deformation tensor of Green Lagrange $\boldsymbol{E} = 1/2(\boldsymbol{C} - \boldsymbol{I})$, the right and left Cauchy-Green strain tensors $\boldsymbol{C} = \boldsymbol{F}^t\boldsymbol{F}$ and $\boldsymbol{B} = \boldsymbol{F}\boldsymbol{F}^t$ are obtained, together with their principal invariants.

$$I_1 = tr\boldsymbol{C},\ \ I_2 = \frac{1}{2}\left[(tr\boldsymbol{C})^2 - tr\boldsymbol{C}^2\right] \ \text{ and } \ I_3 = \det(\boldsymbol{C}) = J^2, \tag{2.33}$$

which, otherwise, can be expressed in terms of principal stretches by

$$I_1 = \lambda_1^2 + \lambda_2^2 + \lambda_3^2,\ \ I_2 = \lambda_1^2\lambda_2^2 + \lambda_2^2\lambda_3^2 + \lambda_1^2\lambda_3^2 \ \text{ and } \ I_3 = \lambda_1^2\lambda_2^2\lambda_3^2. \tag{2.34}$$

The formulation in the nonlinear range is based on the decomposition of the gradient $\boldsymbol{F}(X,t)$ into a volume-preserving and pure dilatational part as it is originally proposed by [46] and used in several works such as [131] and [67] among others as follow:

$$\boldsymbol{F} = \bar{\boldsymbol{F}}\det(\boldsymbol{F})^{1/3}\boldsymbol{I} \ \text{ where } \ \det\left(\bar{\boldsymbol{F}}\right) = 1, \tag{2.35}$$

$\bar{\boldsymbol{F}}$ is the volume-preserving gradient tensor. The Cauchy-Green strain tensor associated and the Lagrangian strain tensor associated with the volume-preserving gradient are expressed as

$$\bar{\boldsymbol{C}} = \bar{\boldsymbol{F}}^t\bar{\boldsymbol{F}} = J^{-2/3}\boldsymbol{C},\ \ \bar{\boldsymbol{E}} = \frac{1}{2}\left(\bar{\boldsymbol{C}} - \boldsymbol{I}\right), \tag{2.36}$$

$\boldsymbol{I}$ is the metric tensor in the reference configuration. Furthermore, several applications of the chain rule lead to the following

$$\frac{\partial\bar{\boldsymbol{E}}}{\partial\boldsymbol{E}} = \frac{\partial\bar{\boldsymbol{C}}}{\partial\boldsymbol{C}} = J^{-2/3}\left[\boldsymbol{I} - \frac{1}{3}\boldsymbol{C}\otimes\boldsymbol{C}^{-1}\right], \tag{2.37}$$

$\boldsymbol{I}$ is the fourth order unit tensor and the sign $\otimes$ designates the tensorial product. Hence, we postulated an uncoupled free energy density as it is expressed in [131] by a Taylor series in which terms higher than the second order are omitted. Moreover the behavior in bulk is considered purely elastic.

$$\Psi(\boldsymbol{C},\boldsymbol{Q}) = U^0(J) + \bar{\Psi}^0\left(\bar{\boldsymbol{C}}\right) - \frac{1}{2}\boldsymbol{Q}:\bar{\boldsymbol{C}} + \Psi_I(\boldsymbol{Q}), \tag{2.38}$$

$\boldsymbol{Q}$ is a second order overstress tensor internal variable akin to the second Piola-Kirchhoff stress tensor $\boldsymbol{S}$. The first two terms of the free energy density of equation (2.10) are the dilatational and volume-preserving parts of the instantaneous elastic stored energy density. The third and fourth terms are responsible for the time-dependent behavior of the material. Note that $\Psi_I(\boldsymbol{Q})$ is a convex function of the internal variable $\boldsymbol{Q}$. This decomposition of the free energy density leads to a decomposition in the stress into a deviatoric (shear) and hydrostatic (bulk) parts.

2.3.2 Rate and constitutive equations

The rate equation of the internal variable $\boldsymbol{Q}$ is motivated by the rate equation (2.4) of the rheological model in which the elastic stress is replaced by the deviatoric part of the hyperelastic Second Piola-Kirchhoff stress tensor as it's expressed in [131].

$$\frac{\partial \boldsymbol{Q}}{\partial \xi} + \frac{1}{\tau}\boldsymbol{Q} = \frac{\gamma}{\tau} DEV\left[2\frac{\partial \bar{\Psi}^0(\bar{\boldsymbol{C}})}{\partial \bar{\boldsymbol{C}}}\right] \quad \text{with} \quad \xi(t) = \int_0^t \frac{dt'}{a(\bar{\boldsymbol{C}})}, \tag{2.39}$$

in which $DEV(\bullet) = (\bullet) - \frac{1}{3}[\boldsymbol{C} : (\bullet)]\boldsymbol{C}^{-1}$ denotes the deviator operator in the reference configuration and $\gamma \leq 1$ is the stiffness ratio. As in the previous section, $a(\bar{\boldsymbol{C}})$ is a function of the invariants of the volume-preserving right Cauchy-Green strain tensor $\bar{\boldsymbol{C}}$ and ξ is referred to as the reduced time and it is an increasing function of time. The second law of thermodynamic is expressed in terms of the Clausius-Duhem inequality in the reference configuration C_0.

$$-\dot{\Psi} + \frac{1}{2}\boldsymbol{S} : \dot{\boldsymbol{C}} \geq 0. \tag{2.40}$$

Standard arguments [25] and [139] using inequality (2.12) lead to the expression of intrinsic dissipation and the second Piola-Kirchhoff stress tensor.

$$-\frac{\partial \Psi(\boldsymbol{C},\boldsymbol{Q})}{\partial \boldsymbol{Q}} : \dot{\boldsymbol{Q}} \geq 0 \quad \text{and} \quad \boldsymbol{S} = \frac{1}{2}\frac{\partial \Psi(\boldsymbol{C},\boldsymbol{Q})}{\partial \boldsymbol{C}}. \tag{2.41}$$

Let $\boldsymbol{\Pi} = J\boldsymbol{\sigma}\boldsymbol{F}^{-t} = \boldsymbol{F}\boldsymbol{S}$ be the first Piola-Kirchhoff stress tensor which is the quotient of the actual force by the indeformed area, where $\boldsymbol{\sigma}$ is the Cauchy stress tensor and $\boldsymbol{S}$ is the second Piola-Kirchhoff stress tensor. Considering relations (2.9), (2.11) and (2.13) one could simply lead to the convolution representation of the second Piola-Kirchhoff stress tensor.

$$\boldsymbol{S} = J^{-2/3}\int_0^{\xi} g(\xi - \xi')\frac{\partial}{\partial \xi'} DEV\left(2\frac{\partial \bar{\Psi}^0(\bar{\boldsymbol{C}})}{\partial \bar{\boldsymbol{C}}}\right) d\xi' + Jp\boldsymbol{C}^{-1}, \tag{2.42}$$

$p = \partial U^0(J)/\partial J$ is the hydrostatic part of the stress, for an incompressible material, p is an undetermined pressure to be obtained by the boundary conditions. g is the normalized shear relaxation modulus and it is a decaying function of time [22], it is often expressed by a power law function or a decaying exponential function. For computational reasons it is more efficient to consider the Cauchy stress tensor rather than the second Piola-Kirchhoff stress tensor. Application of an integration by parts to the expression of the second piola-Kirchhoff stress tensor of relation (2.14) and considering the relative distortional deformation gradient tensor
$\bar{\boldsymbol{F}}_t(t') = J^{-1/3}\partial\varphi(X,t')/\partial\varphi(X,t)$ the Cauchy stress tensor reads

$$\boldsymbol{\sigma} = \boldsymbol{\sigma}_o^d + dev\int_0^{\xi}\frac{\partial g(\xi')}{\partial\xi'}\left(\bar{\boldsymbol{F}}_{\xi}^{-1}(\xi-\xi')\,\boldsymbol{\sigma}_o^d(\xi-\xi')\,\bar{\boldsymbol{F}}_{\xi}^{-t}(\xi-\xi')\right)d\xi' + p\boldsymbol{I}, \tag{2.43}$$

in which $dev(\bullet) = (\bullet) - \frac{1}{3}[\boldsymbol{I}:(\bullet)]\boldsymbol{I}$ denotes the deviator operator in the current configuration. $\boldsymbol{\sigma}_o^d = dev(\boldsymbol{\sigma}_o)$ is the deviatoric part of the instantaneous elastic Cauchy stress tensor $\boldsymbol{\sigma}_o$ which may be written [139]

$$\boldsymbol{\sigma}_o = \beta_0\boldsymbol{I} + \beta_1\boldsymbol{B} + \beta_{-1}\boldsymbol{B}^{-1}, \tag{2.44}$$

where $\beta_j = \beta_j(I_1,I_2,I_3)$ are the elastic response functions. In terms of the instantaneous elastic stored energy density they are given by

$$\begin{aligned}\beta_0(I_1,I_2,I_3) &= \tfrac{2}{J}\left[I_2\Psi_1^0 + I_3\Psi_3^0\right]\\ \beta_1(I_1,I_2,I_3) &= \tfrac{2}{J}\Psi_1^0\\ \beta_{-1}(I_1,I_2,I_3) &= -2J\Psi_2^0,\end{aligned} \tag{2.45}$$

where

$$\Psi^0 = U^0(J) + \bar{\Psi}^0(\bar{C}) \;\text{ and }\; \Psi_k^0 = \frac{\partial\Psi^0}{\partial I_k}, \quad k = 1,2,3. \tag{2.46}$$

The instantaneous stored elastic energy density has an alternative form in terms of the principle stretches given by

$$\tilde{\Psi}^o(\lambda_1,\lambda_2,\lambda_3) = \Psi^o(I_1,I_2,I_3). \tag{2.47}$$

From (2.35) and (2.36) the deviatoric part of the instantaneous elastic Cauchy stress is expressed by

$$\boldsymbol{\sigma}^d = \frac{2}{J}\left[\frac{1}{3}\left(I_2\Psi_2^0 - I_1\Psi_1^0\right)\boldsymbol{I} + \Psi_1^0\boldsymbol{B} - I_3\Psi_2^0\boldsymbol{B}^{-1}\right], \tag{2.48}$$

or using $\tilde{\Psi}_i^o$ and the principle stretches by

$$\boldsymbol{\sigma}_{oi}^d = \lambda_i\tilde{\Psi}_i^o - \frac{1}{3}\sum_{j=1}^{3}\lambda_j\tilde{\Psi}_j^o, \tag{2.49}$$

where $\tilde{\Psi}^o_i$ refers to the derivative $\tilde{\Psi}^o$ with respect to λ_i. The first term of the right hand side of (2.33) designates the instantaneous elastic response of the material, the second one denotes the time dependent part of the material whereas the third one is the hydrostatic pressure. For an incompressible material relation (2.33) holds with $J=1$ and $\bar{\boldsymbol{F}}_t(t') = \boldsymbol{F}_t(t') = \partial\varphi(X,t')/\partial\varphi(X,t)$. Henceforth, the material is considered incompressible.

2.3.3 Functional formulation and thermodynamic considerations

The formulation described in the previous sections can be obtained in a similar way as in 2.1 for the three dimensional behaviour. Our starting point is the form of the instantaneous stored elastic energy density of equation (2.38) and the evolution law of the internal variable of equation (2.39). The resolution of the differential equation in (2.39) lead to the following convolution representation of the internal variable $\boldsymbol{Q}$

$$\boldsymbol{Q}(t) = \frac{\gamma}{\tau}\int_0^{\xi} \exp\left[-(\xi-\xi')/\tau\right] DEV\left[2\frac{\partial\bar{\Psi}^0\left(\overline{C}\right)}{\partial\overline{C}}\right] d\xi', \tag{2.50}$$

From this expression of the internal variable one could lead to the functional formulation of the model by substituting equation (2.50) in the expression of the instantaneous stored elastic energy density of equation (2.38). Hence, (2.38) is expressed as

$$\begin{aligned}\Psi(\boldsymbol{C},\boldsymbol{Q}) &= U^0(J) + \bar{\Psi}^0\left(\overline{C}\right) - \frac{\gamma}{2\tau}\int_0^{\xi}\exp\left[-(\xi-\xi')/\tau\right] DEV\left(2\frac{\partial\Psi^0(\bar{C})}{\partial\bar{C}}\right) d\xi' : \overline{C} \\ &+ \frac{1}{4\mu_o\tau}\int_0^{\xi}\int_0^{\xi}\exp\left[-(2\xi-\xi'-\xi'')/\tau\right] DEV\left(2\frac{\partial\Psi^0(\bar{C})}{\partial\bar{C}}\right) DEV\left(2\frac{\partial\Psi^0(\bar{C})}{\partial\bar{C}}\right) d\xi' d\xi''\end{aligned} \tag{2.51}$$

these convolution representations of the instantaneous stored elastic energy density Ψ and the internal variable $\boldsymbol{Q}$ are obtained using a Taylor expansion of the energy function $\Psi_I(\boldsymbol{Q})$ as follow

$$\Psi_I(\boldsymbol{Q}) = \frac{1}{4\mu_o\gamma}\boldsymbol{Q}:\boldsymbol{Q}, \tag{2.52}$$

where μ_o is the initial shear modulus. The Clausius-Duhem inequality of equation (2.40) is rewritten in terms of the functional representation by the following:

$$\left(\boldsymbol{S}-2\frac{\partial\Psi^0}{\partial\boldsymbol{C}}+\boldsymbol{Q}\right):\dot{\boldsymbol{C}}-$$
$$\frac{\gamma}{2\tau^2 a\left(\bar{\boldsymbol{C}}\right)}\left(\boldsymbol{C}:\int_0^{\xi}\exp\left[-\left(\xi-\xi'\right)/\tau\right]DEV\left(2\frac{\partial\bar{\Psi}^0\left(\bar{\boldsymbol{C}}\right)}{\partial\bar{\boldsymbol{C}}}\right)d\xi'\right)-$$
$$\frac{\gamma}{2\mu_o\left(\tau^2 a\left(\bar{\boldsymbol{C}}\right)\right)^2}\int_0^{\xi}\int_0^{\xi}\exp\left[-\left(2\xi-\xi'-\xi''\right)/\tau\right]DEV\left(2\frac{\partial\bar{\Psi}^0\left(\bar{\boldsymbol{C}}\right)}{\partial\bar{\boldsymbol{C}}}\right)DEV\left(2\frac{\partial\bar{\Psi}^0\left(\bar{\boldsymbol{C}}\right)}{\partial\bar{\boldsymbol{C}}}\right)d\xi'd\xi''\geq 0. \tag{2.53}$$

The first terms of the equation (2.53) lead to the expression of the second Piola-Kirchhoff stress tensor $\boldsymbol{S}$ of equation (2.42). The second and third terms of the inequality represent the functional form of the dissipation function D for which a sufficient condition to ensure the admissibility of any process is to consider a positive deformation shift function $a\left(\bar{\boldsymbol{C}}\right)$.

2.4 Conclusion

In this chapter, we presented the nonlinear viscoelastic model at finite strain proposed by [136] that incorporates a strain dependent relaxation times to describe nonseparable behavior of rubber-like materials. Before presenting the model, an experimental and rheological arguments leading to the model were recalled and a one-dimensional nonlinear viscoelastic model was developed. Then, this model was extended to the three-dimensional domain under the assumption of small strain. Finally, the fully nonlinear viscoelastic model was presented. The model is based upon the internal state variables approach and the framework of rational thermodynamics and experimental arguments. The free energy density is decomposed into a volumetric and deviatoric parts. Furthermore, thermodynamic restrictions are fulfilled via a sufficient condition on the model's parameters resulting from the application of the Clausius-Duhem inequality for an arbitrary process. For each model presented here (the one-dimensional model, the three-dimensional model under small strain assumption and the fully three-dimensional nonlinear viscoelastic model) the constitutive equations for the stress and the dissipation were exposed. In the next chapter we present a systematic identification procedure of the proposed model to experimental data.

CHAPTER 3

IDENTIFICATION OF THE NONLINEAR VISCOELASTIC MODEL

Contents

This chapter presents the systematic identification procedure of the model's parameters to experimental data. The material's parameters are identified

separately. In fact, the hyperelastic contribution to the total stress is identified equilibrium data on simple extension and pure shear. The relaxation function was postulated by a Prony series and identified using relaxation experimental data in the linear range of the behavior with a strain relaxation level below 10%. The reduced time function is identified thanks to a minimization procedure over the error between the discrete stress of the model and the experimental stress. This identification procedure was applied to data generated from the Pipkin multi-integral model [115] then applied to experimental data for Bromobutyl (BIIR) from [103]. The capacity of the model to reproduce the behavior of the material is then highlighted with comparison to experiments.

3.1 Model identification

In this section, a systematic identification of the material parameters for an incompressible nonfactorizable viscoelastic constitutive equation at finite strain is highlighted. This procedure relies on the separate identification of hyperelastic potential, viscoelastic kernel and the reduced time function. Considering the form of the constitutive equation (2.43), each characteristic function identification reduces to the solution of a nonlinear optimization problem. The identification procedure is carried out considering homogenous (in space) uniaxial transformations of simple extension and pure shear. For such transformation, assuming incompressibility, in the material basis the deformation gradient tensor may be specified as

$$\boldsymbol{F}(t) = diag(\lambda_1(t), \lambda_2(t), \lambda_3(t)). \tag{3.1}$$

The condition of incompressibility $J = 1$ leads to the following expression of the deformation gradient tensor

$$\boldsymbol{F}(t) = diag\left(\lambda(t), \lambda^{-1/2}(t), \lambda^{-1/2}(t)\right), \tag{3.2}$$

for simple extension and

$$\boldsymbol{F}(t) = diag\left(\lambda(t), \lambda^{-1}(t), 1\right), \tag{3.3}$$

for pure shear. In both cases only one component of the stress remains and the indeterminate hydrostatic pressure is eliminated

$$\sigma_2 = \sigma_3 = 0 \quad \text{and} \quad \sigma_1 = \sigma_1 - \sigma_2. \tag{3.4}$$

From (2.43) and (3.4) the expression of the stress in theses cases is given by

$$\sigma = \sigma_{01}^d - \sigma_{02}^d + \int_0^\xi \frac{\partial g\left(\xi'\right)}{\partial \xi'} \left(\frac{\lambda^2(\xi)}{\lambda^2(\xi - \xi')} \sigma_{01}^d - \frac{\lambda\left(\xi - \xi'\right)}{\lambda(\xi)} \sigma_{02}^d \right) d\xi', \tag{3.5}$$

for the simple extension and

$$\sigma = \sigma_{01}^{d} - \sigma_{02}^{d} + \int_0^{\xi} \frac{\partial g(\xi')}{\partial \xi'} \left(\frac{\lambda^2(\xi)}{\lambda^2(\xi - \xi')} \sigma_{01}^{d} - \frac{\lambda^2(\xi - \xi')}{\lambda^2(\xi)} \sigma_{02}^{d} \right) d\xi', \tag{3.6}$$

for pure shear. The first two terms of relations (3.5) and (3.6) refer to the principle components of the deviatoric instantaneous elastic part of the stress which can be obtained from the equilibrium deviatoric elastic stress via:

$$\sigma_{0i}^{d} = \frac{G_0}{G_\infty} \sigma_{\infty i}^{d}, \tag{3.7}$$

in which G_0 and G_∞ refer to the instantaneous and equilibrium shear relaxation modulus, whereas the integral term depicts the dissipative or the time dependent part of the stress. A general identification procedure could be applied separately to each component of the stress. Hence, let
$\Lambda = (\Lambda_1, \Lambda_2, ..., \Lambda_m)^t$ be the vector of experimental input data and
$\Theta = (\Theta_1, \Theta_2, ...\Theta_m,)^t$ be the vector of corresponding experimental response. For each component of the stress the response function is written $F(\Lambda, p) : \mathbb{R} \times \mathbb{R}^n \rightarrow \mathbb{R}$ in which $p = (p_1, p_2, ..., p_n)^t$ is a vector of material parameters. The objective function is defined through the Least square norm as follow

$$S_F(p) : \|F(\Lambda, p) - \Theta\|_2^2 = \sum_{i=1}^{m} (F(\Lambda_i, p) - \Theta_i)^2. \tag{3.8}$$

The identification procedure turns out into a minimization problem which reads as follow

$$\min_p \; S_F(p). \tag{3.9}$$

3.1.1 Identification of the hyperelastic potential

The instantaneous elastic stored energy density Ψ^o is a function of, either, the invariants of the right Cauchy-Green strain tensor or the principles stretches. The condition of incompressibility reads

$$\lambda_1 \lambda_2 \lambda_3 = 1 \text{ or } \quad I_3 = J^2 = 1 \tag{3.10}$$

The general form of Mooney-Rivlin [123] instantaneous elastic stored energy density is considered which reads for an incompressible hyperelastic material as follow

$$\Psi^o(I_1, I_2) = \sum_{i,j} c_{ij} (I_1 - 3)^i (I_2 - 3)^j \tag{3.11}$$

c_{ij} are the material parameters of the instantaneous stored elastic energy density which usually should satisfy the stability conditions to ensure an admissible response of the model for any process see [119]. Note that the instantaneous stored elastic energy density Ψ^o vanishes in the reference configuration so that $c_{00} = 0$. The conditions of stability are expressed as follow:

$$\frac{\partial \Psi^o}{\partial I_1} > 0 \quad \text{and} \quad \frac{\partial \Psi^o}{\partial I_2} \geq 0. \tag{3.12}$$

In the case of uniaxial experiment, the nominal stress which is the measured quantity, actual force over reference area, and the principle stretch are related through the instantaneous elastic stored energy density Ψ^o by the relation

$$\Pi^o = \frac{\partial \Psi^o}{\partial \lambda} = \sum_{i,j} c_{ij}\, \phi(i,j,\lambda), \tag{3.13}$$

where $\phi(i,j,\lambda)$ is a nonlinear function of i,j and λ, given by

$$\begin{aligned} \phi(i,j,\lambda) = \; & 2i\left(\lambda - \frac{1}{\lambda^2}\right)\left(\lambda^2 + \frac{2}{\lambda} - 3\right)^{i-1}\left(2\lambda + \frac{1}{\lambda^2} - 3\right)^{j} + \\ & 2j\left(1 - \frac{1}{\lambda^3}\right)\left(\lambda^2 + \frac{2}{\lambda} - 3\right)^{i}\left(2\lambda + \frac{1}{\lambda^2} - 3\right)^{j-1}, \end{aligned} \tag{3.14}$$

for the simple extension and

$$\phi(i,j,\lambda) = 2(i+j)\left(\lambda - \frac{1}{\lambda^3}\right)\left(\lambda^2 + \frac{1}{\lambda^2} - 2\right)^{i+j-1}, \tag{3.15}$$

for pure shear. An alternative useful representation of equation (3.13) with respect to the identification procedure is used.

Let $c^t = \left(c_{01}, ..., c_{0j}, c_{10}, ..., c_{1j}, ..., c_{i0}, ..., c_{ij}\right)$ be the vector of material parameters, Φ be a matrix representation of the function $\phi(i,j,\lambda)$ and Π^o the discrete vector of nominal stress. Equation (3.13) became

$$\Pi^o = \Phi\, c, \tag{3.16}$$

The identification of the material parameters c_{ij} is performed using data for simple extension and pure shear simultaneously. Therefore, a modification of the objective function (3.8) is adopted see [109]. The new objective function reads as follow

$$\min_{c \in \mathbb{R}^{i \times j}} \left(\left\| \Phi^{se}\, c - \tilde{\Pi}^{se} \right\|_2^2 + \left\| \Phi^{ps}\, c - \tilde{\Pi}^{ps} \right\|_2^2 \right). \tag{3.17}$$

The superscript se and ps refers to the simple extension and pure shear respectively. $\tilde{\Pi}$ denotes the recorded experimental nominal stress vector. A least square minimization procedure is then employed under conditions (3.12) using Matlab software to reach the numerical values of c_{ij}. The results of this identification and its efficiency are discussed in sections 3.2 and 3.3 of this work.

3.1.2 Identification of the viscoelastic kernel

The time dependent part of the stress is characterized by the shear relaxation function $G(\xi)$ which is a decaying positive function of the reduced time ξ . It is often expressed by, either, a sum of decaying exponential functions called Prony series function or a power law functions. This identification is performed using experimental results from relaxation tests and dynamic tests in the linear range of behavior so that the reduced time is equal to the real time $\xi = t$ and the behavior of the material is described by the single Boltzmann convolution integral:

$$\sigma(t) = \int_0^t G\left(t - t'\right) \dot{\varepsilon}\left(t'\right) dt', \tag{3.18}$$

ε is the linearized strain tensor.

3.1.2.1 Identification from relaxation test

The relaxation test is performed in shear deformation. The strain is suddenly increased to a value ε_o and kept constant

$$\varepsilon(t) = H(t)\varepsilon_o \text{ with } H(t) = \begin{cases} 0, & t < 0 \\ 1, & t > 0 \end{cases}. \tag{3.19}$$

From equations (3.18) and (3.19) the shear relaxation modulus follows

$$G(t) = \frac{\sigma(t)}{\varepsilon_o}. \tag{3.20}$$

In this work we adopted the Prony series form of the shear relaxation modulus

$$G(t) = G_\infty + \sum_{i=1}^{N} G_i \exp\left(-\frac{t}{\tau_i}\right), \tag{3.21}$$

G_∞ denotes the long term shear relaxation modulus, G_i $(i = 1,..,N)$ are the coefficients of the Prony series and τ_i $(i = 1,..,N)$ are the relaxation time constants. Furthermore, in order to avoid the ill-conditioning of the optimization problem the set of the relaxation times τ_i are a-priori fixed as one time constant per decade in the logarithmic time scale for the experimental time window see [142] and [80]. The optimization problem arising from the identification of the N-terms Prony coefficients is

$$\min_{\{G\}\in\mathbb{R}^N} \left\| \Gamma\{G\} - \hat{G} \right\|_2^2, \tag{3.22}$$

where $\Gamma \in \mathbb{R}^{M\times N}$ is the matrix representation of relation (3.21) with M experimental points taking the following form

$$\Gamma = \begin{bmatrix} 1 & \exp\left(-t_1/\tau_1\right) & \dots & \exp\left(-t_1/\tau_N\right) \\ 1 & \exp\left(-t_2/\tau_1\right) & \dots & \exp\left(-t_2/\tau_N\right) \\ \dots & \dots & \dots & \dots \\ 1 & \exp\left(-t_M/\tau_1\right) & \dots & \exp\left(-t_M/\tau_N\right) \end{bmatrix}, \tag{3.23}$$

$t = (t_1,\dots,t_M)$ are the discrete time instants and $\hat{G} = \left(\hat{G}_1,\dots,\hat{G}_M\right)$ are the corresponding experimental values of the shear relaxation modulus using relation (3.20). A linear least square algorithm is used to solve the optimization problem (3.22) using Matlab software.

3.1.2.2 Identification from dynamic tests

The dynamic tests are performed using a cylindrical shear sheet loaded by a sinusoidal deformation without a predeformation and with small amplitude

$$\varepsilon(t) = \varepsilon^a \exp(\mathrm{j}\omega t) \quad \text{with} \quad \varepsilon^a << 1, \tag{3.24}$$

ω is the circular frequency and j is the unit imaginary number. Hence, from equations (3.18) and (3.24) the stress-strain relation follows

$$\sigma = G^* \varepsilon^a, \tag{3.25}$$

G^* is the complex dynamic shear modulus, its real and imaginary parts are denoted G' and G'' are called storage and loss modulus respectively and may be obtained by a Fourier transform of equation (3.21) and given by :

$$\begin{aligned} G' &= G_\infty + \sum_{i=1}^{N} G_i \frac{(\tau_i\omega)^2}{1+(\tau_i\omega)^2} \\ G'' &= \sum_{i=1}^{N} G_i \frac{\tau_i\omega}{1+(\tau_i\omega)^2} \end{aligned} . \tag{3.26}$$

As mentioned in the previous section, the relaxation times τ_i are a-priori fixed as one time constant per decade in the logarithmic scale of time. Thereby, both storage and loss modulus are linear with respect to the N-terms Prony coefficients. The arising optimization problem from this identification procedure reads

$$\min_{\{G\}\in\mathbb{R}^N} \left(\left\| \Gamma'\{G\} - \hat{G}' - G_\infty \right\|_2^2 + \left\| \Gamma''\{G\} - \hat{G}'' \right\|_2^2 \right), \tag{3.27}$$

G_∞ is directly identified from the storage modulus curve as $\omega \to 0$. $\hat{G}'$ and $\hat{G}''$ are the experimental vectors of storage and loss modulus, as recorded by the DMA machine,

respectively. Γ' and Γ'' are two M by N matrices representing equation (3.26) and can be expressed through the relaxation time constants and the discrete frequency vector by

$$\Gamma' = \begin{bmatrix} \frac{(\tau_1\omega_1)^2}{1+(\tau_1\omega_1)^2} & \dots & \frac{(\tau_N\omega_1)^2}{1+(\tau_N\omega_1)^2} \\ \dots & \dots & \dots \\ \frac{(\tau_1\omega_M)^2}{1+(\tau_1\omega_M)^2} & \dots & \frac{(\tau_N\omega_M)^2}{1+(\tau_N\omega_M)^2} \end{bmatrix}, \Gamma'' = \begin{bmatrix} \frac{\tau_1\omega_1}{1+(\tau_1\omega_1)^2} & \dots & \frac{\tau_N\omega_1}{1+(\tau_N\omega_1)^2} \\ \dots & \dots & \dots \\ \frac{\tau_1\omega_M}{1+(\tau_1\omega_M)^2} & \dots & \frac{\tau_N\omega_M}{1+(\tau_N\omega_M)^2} \end{bmatrix}. \tag{3.28}$$

The optimization problem (3.27) is an ill-posed problem [37]. Therefore, a Tikhonov [102] regularization method was employed to solve this system. The results of this identification using randomly perturbed simulated and real experimental data are shown in sections 3.2 and 3.3 of this chapter.

3.1.3 Identification of the reduced time function

Once the hyperelastic potential and the viscoelastic kernel are identified, the problem of determining the reduced time function can be addressed. This identification relies on the discretization of the stress-strain relation (2.43) with respect to the time. let $t = (t_1, ..., t_M)$ be the discrete experimental time vector and $\xi = (\xi_1, ..., \xi_M)$ be the corresponding reduced time vector, Δt is the experimental time increment and $\Delta\xi$ is the reduced time increment. The general form of this discretization formula for a nonlinear viscoelastic behavior as it is described in [63] and [129] is reported in equation (3.29). The identification of the reduced time vector ξ is performed thanks to a recursive dichotomy algorithm applied to the error between the discretized stress (3.29) and the experimental stress $\tilde{\sigma} = (\tilde{\sigma}_1, ..., \tilde{\sigma}_M)$.

$$\begin{aligned} &\boldsymbol{\sigma}(t_{n+1}) = \boldsymbol{\sigma}_o^d(t_{n+1}) - \sum_{i=1}^{N} \boldsymbol{\sigma}_i^d(t_{n+1}) + p\boldsymbol{I} \\ &\boldsymbol{\sigma}_i^d(t_n) = \frac{g_i}{\tau_i} \int_0^{\xi} \bar{\boldsymbol{F}}_{\xi}^{-1}(\xi - \xi')\, \boldsymbol{\sigma}_o^d(\xi - \xi')\, \bar{\boldsymbol{F}}_{\xi}^{-t}(\xi - \xi') \exp\left(-\frac{\xi'}{\tau_i}\right) d\xi' \\ &\boldsymbol{\sigma}_i^d(t_{n+1}) = \alpha_i g_i \boldsymbol{\sigma}_o^d(t_{n+1}) + \beta_i g_i \hat{\boldsymbol{\sigma}}_o^d(t_n) + \gamma_i \hat{\boldsymbol{\sigma}}_i^d(t_n) \\ &\text{with} \\ &\gamma_i = \exp\left(-\frac{\Delta\xi}{\tau_i}\right);\ \alpha_i = 1 - \frac{\tau_i}{\Delta\xi}(1-\gamma_i);\ \beta_i = \frac{\tau_i}{\Delta\xi}(1-\gamma_i) - \gamma_i \\ &\hat{\boldsymbol{\sigma}}_j^d(t) = \bar{\boldsymbol{F}}_t(t+\Delta t)\, \boldsymbol{\sigma}_j^d(t)\, \bar{\boldsymbol{F}}^t(t+\Delta t)\ ;\ j = 0, 1, ...N. \end{aligned} \tag{3.29}$$

Once the reduced time vector ξ is obtained the identification of the reduced time function $a(\boldsymbol{C})$ can be addressed since it is the inverse of the derivative of the reduced time with respect to real time:

$$\frac{1}{a} = \frac{d\xi}{dt}. \tag{3.30}$$

The derivative in equation (3.30) is obtained numerically since the reduced time and the real time are two discrete vectors. Hence, one leads to the numerical vector of function $a(\boldsymbol{C}) : a = (a_1, ..., a_M)$. Furthermore, a sufficient condition on this function with respect to the second principle of thermodynamics in terms of Clausius-Duhem inequality is to adopt a positive function of the invariants of the right Cauchy-Green strain tensor.

$$a(\boldsymbol{C}) = f(I_1, I_2) > 0. \tag{3.31}$$

3.2 Identification of the model using data from the Pipkin isotropic model

In this section, the capacity of the proposed model to depict the response of other complicated viscoelastic models is presented. The main concern is to reformulate a complicated model namely the isotropic viscoelastic model by Pipkin [115] in the form of our simple model presented herein. To this end the identification procedure outlined above is applied using data generated from the isotropic viscoelastic model proposed by Pipkin [115] see equations (3.32) and (3.33). Data were generated from the stress-strain relation in the case of simple extension and pure shear experiments. Several strain histories were considered to provide a complete description of the behavior. The hyperelastic potential was identified using data of simple extension and pure shear at equilibrium, the relaxation function was obtained using a relaxation test performed in simple extension and the reduced time was calculated using monotonic test in simple extension for different strain rates. The identification procedure is validated by predicting the behavior in pure shear monotonic tests for different strain rates.

3.2.1 Pipkin isotropic model

Pipkin [115] proposed a third order development of the tensorial response function $\boldsymbol{Y}$ for an isotropic incompressible material. The principle of material indifference requires that the Cauchy stress tensor takes the following form:

$$\boldsymbol{\sigma} = \boldsymbol{R}\boldsymbol{Y}\boldsymbol{R}^t + p\boldsymbol{I}, \tag{3.32}$$

$\boldsymbol{R}$ is the rotation tensor obtained from the polar decomposition of the transformation gradient tensor $\boldsymbol{F}$ and p is the indeterminate parameter due to incompressibility. The

third functional development of $\boldsymbol{Y}$ reads

$$\begin{aligned}\boldsymbol{Y}(t) = &\int_0^t r_1(t-t')\dot{\boldsymbol{E}}(t')\,dt' + \\ &\int_0^t\int_0^t r_2(t-t',t-t'')\dot{\boldsymbol{E}}(t')\,\dot{\boldsymbol{E}}(t'')\,dt'\,dt'' + \\ &\int_0^t\int_0^t\int_0^t r_3(t-t',t-t'',t-t''')\,tr\left[\dot{\boldsymbol{E}}(t')\,\dot{\boldsymbol{E}}(t'')\right]\dot{\boldsymbol{E}}(t''')\,dt'dt''dt''' + \\ &\int_0^t\int_0^t\int_0^t r_4(t-t',t-t'',t-t''')\,\dot{\boldsymbol{E}}(t')\,\dot{\boldsymbol{E}}(t'')\,\dot{\boldsymbol{E}}(t''')\,dt'dt''dt''',\end{aligned} \tag{3.33}$$

$r_k\,(k=1..4)$ are the relaxation kernels expressed by a decaying exponential functions and $\dot{\boldsymbol{E}}(t)$ is the time derivative of the Green-Lagrange deformation tensor. Expression of r_i according to [57] is reported in equation (3.34), the choice of $r_2(t_1,t_2)=0$ is motivated by thermodynamic arguments to ensure the positivity of the free energy density. Further arguments could be found in [57] and references therein.

$$\begin{cases} r_1(t) = a_1 + b_1\exp(c_1 t) \\ r_2(t_1,t_2) = 0 \\ r_3(t_1,t_2,t_3) = a_3 + b_3\exp(c_3(t_1+t_2+t_3)) \\ r_4(t_1,t_2,t_3) = b_4\exp(c_4(t_1+t_2+t_3)). \end{cases} \tag{3.34}$$

A crucial choice of the parameters a_k, b_k and c_k enables us to describe the behavior of the material for any given strain history.

3.2.2 Identification results

3.2.2.1 Hyperelastic potential

The identification of the instantaneous elastic stored energy density requires data at equilibrium in the case of simple extension and pure shear experiments. Hence, data were generated by omitting the time-dependent part of the stress. Considering the incompressibility of the behavior of equations (3.2) and (3.3) it is straightforward to obtain from (3.33) the relations for the equilibrium stress

$$\sigma = \left(\lambda^2 - \frac{1}{\lambda}\right)\left[\frac{a_1}{2} + \frac{a_3}{8}\left(\lambda^4 - 2\lambda^2 - \frac{4}{\lambda} + \frac{2}{\lambda^2} + 3\right)\right], \tag{3.35}$$

in the case of simple extension and

$$\sigma = \left(\lambda^2 - \frac{1}{\lambda^2}\right)\left[\frac{a_1}{2} + \frac{a_3}{8}\left(\lambda^4 - 2\lambda^2 - \frac{2}{\lambda^2} + \frac{1}{\lambda^4} + 2\right)\right], \tag{3.36}$$

for the simple shear. Results of the identification using the generalized Mooney-Rivlin model in terms of the first Piola-Kirchhoff stress are reported in figure 3.1 for simple extension and pure shear experiments. A second order generalized Mooney-Rivlin potential, in relation (3.11), was satisfactory to describe the hyperelastic part of the Pipkin model.

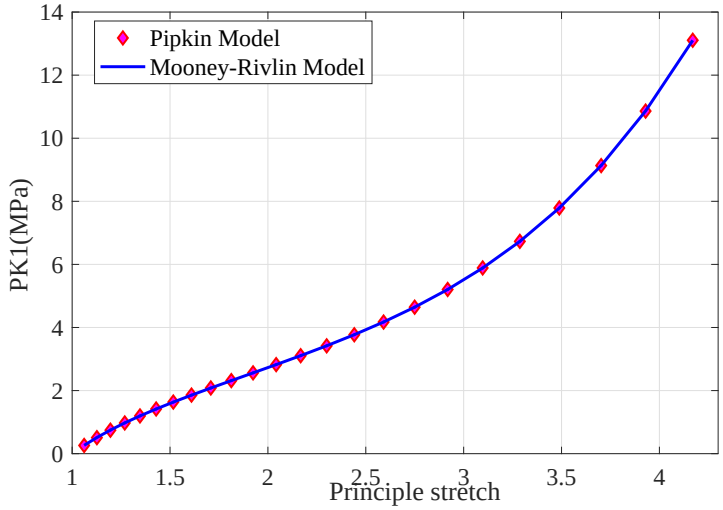

(a) Equilibrium stress for simple extension

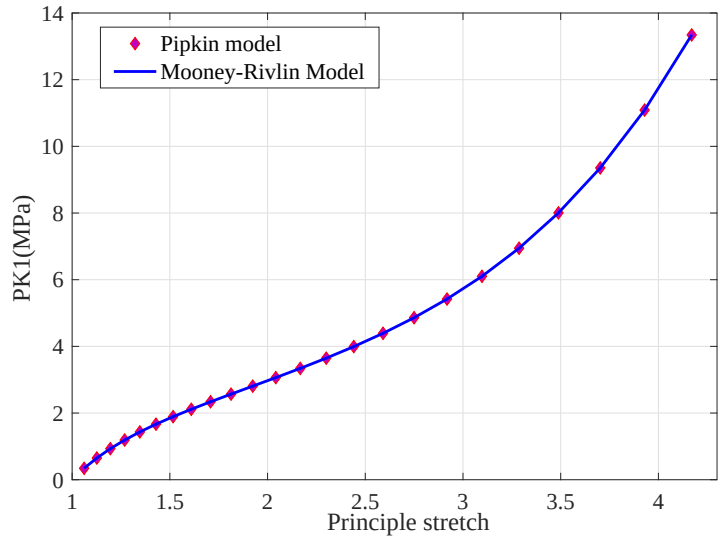

(b) Equilibrium stress for pure shear

Figure 3.1: Equilibrium stresses versus principle stretch for the Pipkin model (diamond) and the Mooney-Rivlin model (solid curve)

g_i	$\tau_i(s)$
$6.25\ 10^{-2}$	2.003
$2.84\ 10^{-5}$	14.06
$1.12\ 10^{-4}$	82.76

Table 3.1: Prony series parameters

3.2.2.2 Viscoelastic kernel

The identification of the Prony series requires shear relaxation data at low level of strain. To this end, a Heaviside strain history of relation (3.19) is considered. Introduction of this strain history into (3.32) and (3.33) yields the relaxation stress-strain relationship.

$$\begin{aligned}\sigma(t) = &\frac{r_1(t)}{2}\left(\lambda^2-\frac{1}{\lambda^2}\right)+\\ &\frac{r_3(3t)}{8}\left(\lambda^2-\frac{1}{\lambda^2}\right)\left(\lambda^4-2\lambda^2-\frac{2}{\lambda^2}+\frac{1}{\lambda^4}+2\right)+\\ &\frac{r_4(3t)}{8}\left(\lambda^2-\frac{1}{\lambda^2}\right)\left(\lambda^4-3\lambda^2-\frac{3}{\lambda^2}+\frac{1}{\lambda^4}+4\right).\end{aligned} \tag{3.37}$$

In figure 3.2 are reported curves of the normalized shear relaxation modulus versus time for four different levels of strain. It is well shown that the hypothesis of separability doesn't hold for the Pipkin model since the normalized shear relaxation modulus depends upon strain level. But for small value of the strain the normalized shear relaxation modulus is independent of the strain level. Hence, the identification procedure is performed using results of the 5% level of strain. Prony series parameters are reported in Table 3.1.

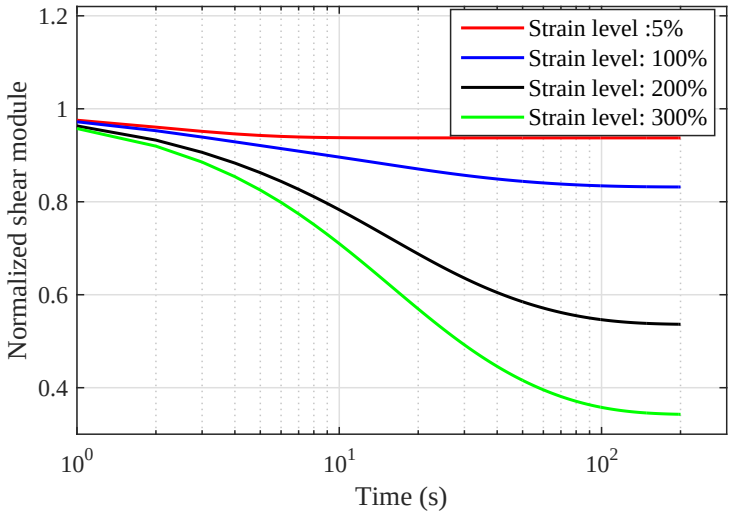

Figure 3.2: Normalized shear relaxation modulus of Pipkin model versus time for four different strain levels.

3.2.2.3 Reduced time function

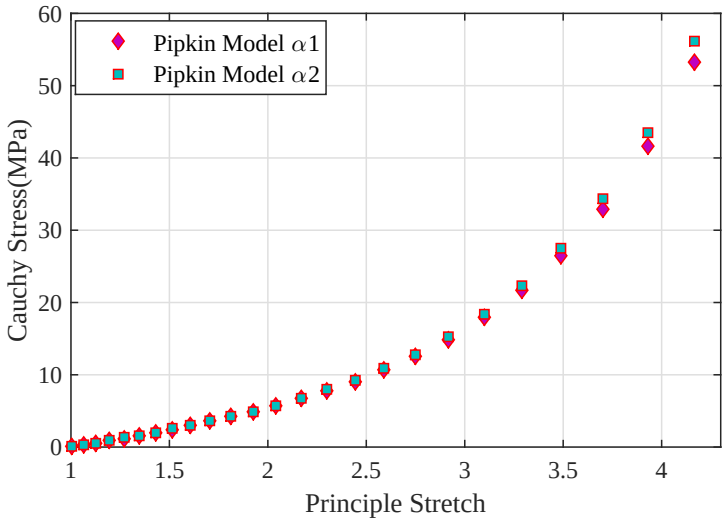

Figure 3.3: Simple extension Cauchy stress versus principle stretch for two different strain rates $\alpha_1 = 1.19\,10^{-2}s^{-1}$ and $\alpha_2 = 6\,10^{-3}s^{-1}$

In this part, monotonic tests of simple extension and pure shear were generated from the Pipkin model. Simple extension test was used in the identification of the reduced time function whereas pure shear test was used in the validation of the results. For computational convenience with respect to the multi-integral form involved in (3.33),

the principle stretch corresponding to a monotonic test was set to be an increasing exponential function of time of the form:

$$\lambda(t) = \exp(\alpha t), \tag{3.38}$$

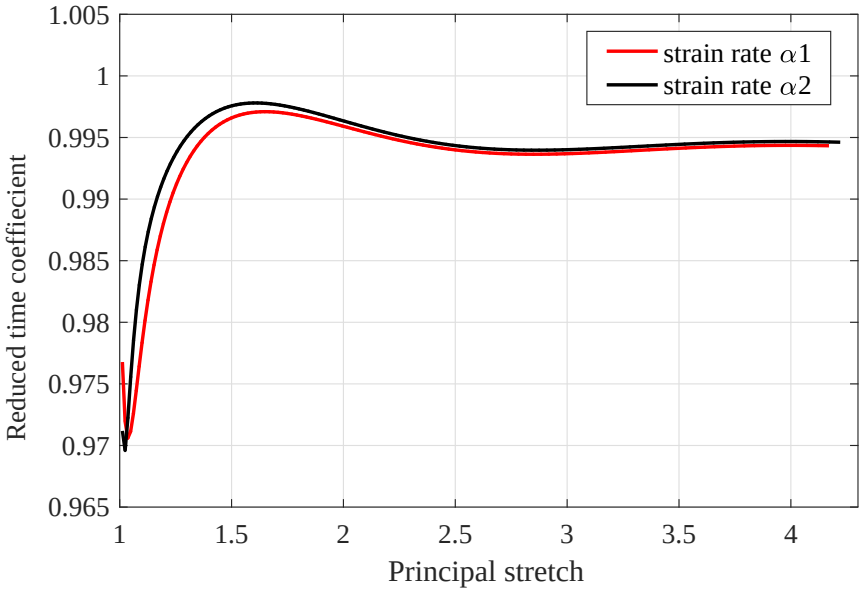

(a) Reduced time ratio versus principle stretch

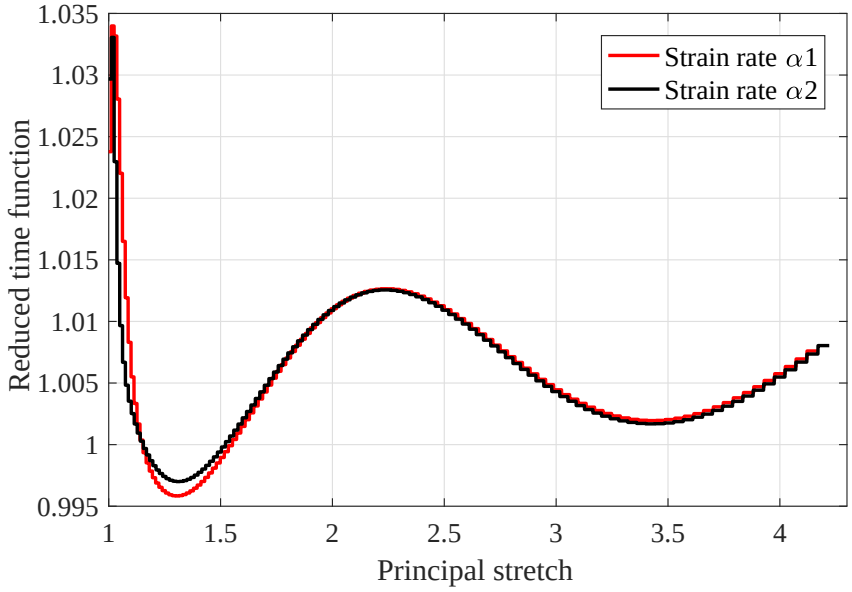

(b) Reduced time function versus principle stretch

Figure 3.4: Reduced time function and reduced time ratio versus principle stretch for two strain rates $\alpha_1 = 1.19\ 10^{-2} s^{-1}$ and $\alpha_2 = 6\ 10^{-3} s^{-1}$

where α is a positive constant that could be interpreted as a strain rate. Replacing the principle stretch in (3.33) by its expression yields the expression of the Cauchy stress. For each test, two different strain rates were considered $\alpha_1 = 1.19\ 10^{-2} s^{-1}$ and $\alpha_2 = 6\ 10^{-3} s^{-1}$. Data for simple extension Cauchy stress versus principle stretch are plotted in figure 3.3. Hence, the identification procedure highlighted above was applied to identify the reduced time function. Results are reported in figure 3.4 by means of the reduced time ratio $\xi(t)/t$ and the reduced time function $a(C)$ for the two considered strain rates. The reduced time function is obtained numerically via a numerical derivation of the reduced time with respect to time. It shows a significant dependence upon strain level which is consistent with the results shown in Figure 3.2. Furthermore, this function is independent of the strain rate which motivate the choice of the form of the reduced time function of equation (3.31). The capacity of the nonlinear viscoelastic model developed herein is evaluated by predicting the behavior of the Pipkin model using the parameters identified in this section. In order to avoid a division by small value of the force when the principle stretch is near to one, a modified relative error formula was used as proposed in [105]

$$err_i = \frac{\left|\sigma_i - {\sigma_i}^P\right|}{\max\left\{0.5, {\sigma_i}^P\right\}}, \tag{3.39}$$

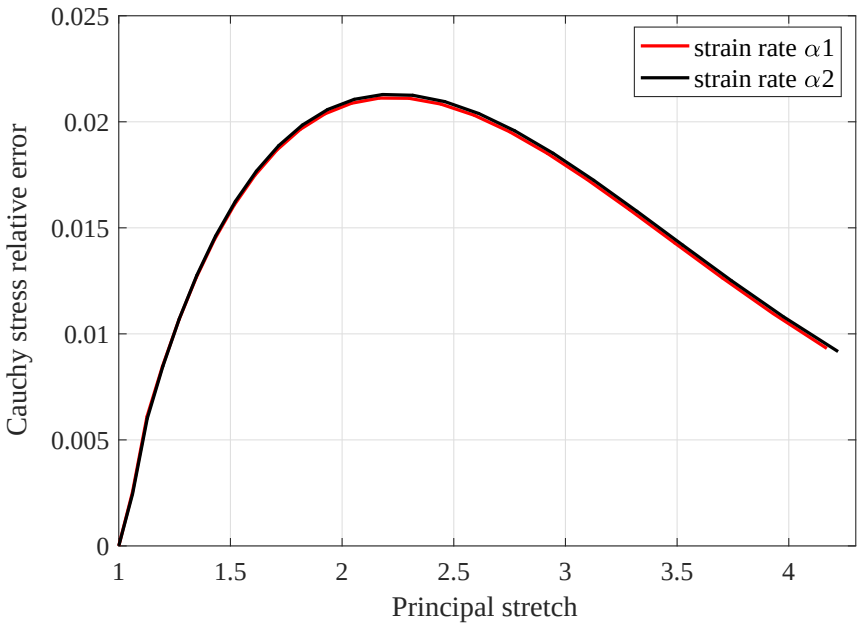

Figure 3.5: Relative error of the predicted Cauchy stress of the Pipkin model for pure shear experiment

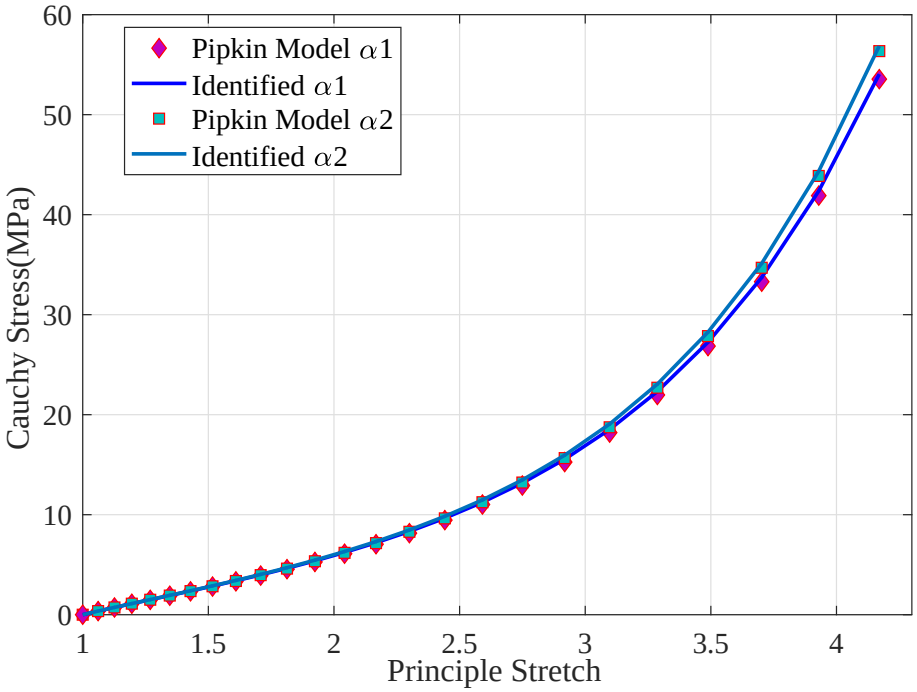

Figure 3.6: Pure shear Cauchy stress for the model (solid curve) and the Pipkin model (diamond and square)

in which σ_i is the Cauchy stress computed using (2.43) and ${\sigma_i}^P$ is the Pipkin Cauchy stress computed using (3.32) and (3.33). This function is plotted versus the principle stretch in figure 3.5 in the case of pure shear experiment. For the two strain rates considered, the relative error remains under 2.5%. In figure 3.6 is plotted the Cauchy stress versus principle stretch for the Pipkin model and the proposed model.

3.3 Application of the identification procedure to experimental data

In this section, the identification procedure outlined in section 3.1 is used to identify the parameters of the proposed model using experimental data for a bromobutyl (BIIR) rubber material. Experimental data used here are those from [103], in which a complete experimental characterization was performed to obtain the response of the material for several strain history configuration and several temperatures. In what follows, results of the identification of the model's parameters are highlighted and discussed.

3.3.1 Hyperelastic potential

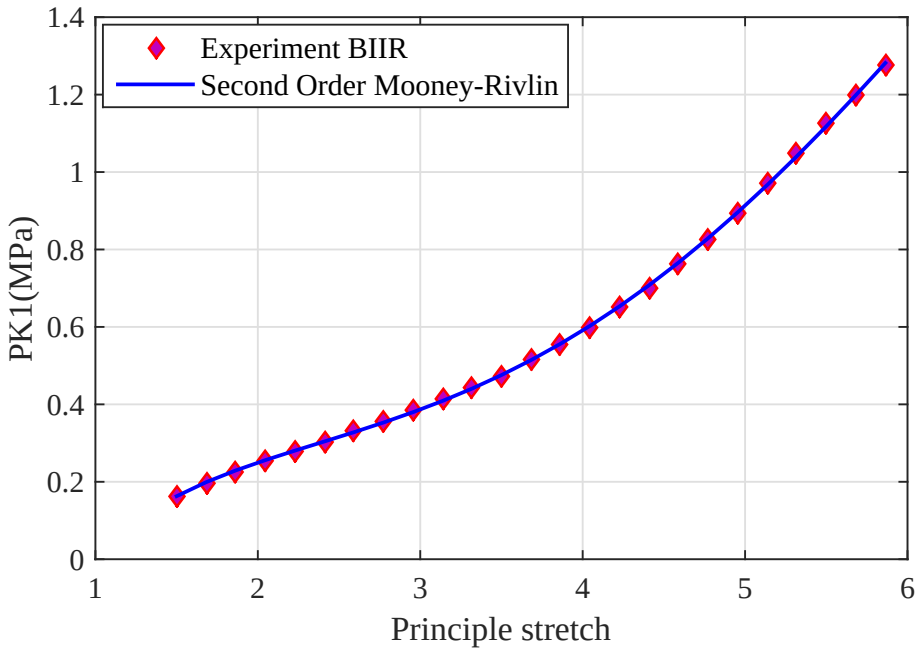

(a) Equilibrium stress for simple extension

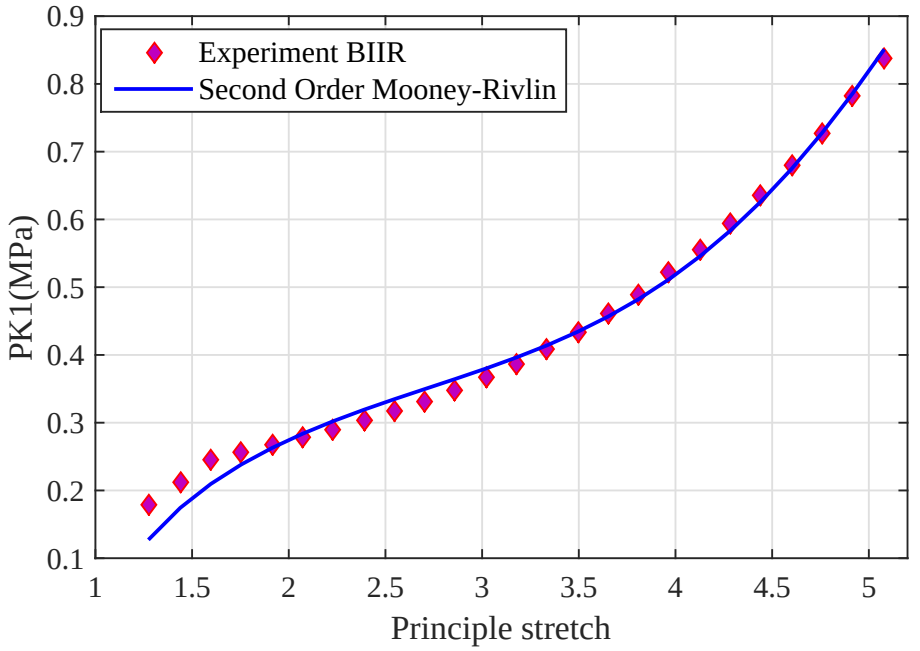

(b) Equilibrium stress for pure shear

Figure 3.7: Equilibrium stresses versus principle stretch: Experimental (diamond) and the identified Mooney-Rivlin model (solid curve)

g_i	$\tau_i(s)$
$4.46\ 10^{-3}$	14.79
$3.77\ 10^{-2}$	125.71
$5.69\ 10^{-2}$	460.7
$5.84\ 10^{-2}$	1761.6
$8.76\ 10^{-2}$	9598.5

Table 3.2: Prony series parameters for BIIR rubber

The identification of the instantaneous elastic stored energy density coefficients of relation (3.17) is performed under stability conditions of the relation (3.12) using Matlab software. A second order Mooney-Rivlin potential was able to describe the hyperelastic behavior of the material for simple extension and pure shear experiments. In figure 3.7 are plotted experimental and identified Piola-Kirchhoff stresses versus principle stretch at equilibrium for simple extension and pure shear. The relative error of the relation (3.39) was calculated for both experiments, its average value is $0,5$ % for simple extension and $2,3$ % for pure shear which are very satisfactory considering the non-linearity of the material.

3.3.2 Viscoelastic kernel

The identification of the viscoelastic kernel, as it is described in section 3.1, is performed using two different experimental data: shear relaxation experiment in the linear range of the behavior and dynamic tests for low level of dynamic amplitude and without pre-strain. In what follows, results of this identification procedure are discussed.

3.3.2.1 From shear relaxation experiment

The shear relaxation experiment is performed in simple shear deformation at a strain level of 10 %. it is considered, however, in the linear range of the behavior since the material is highly deformable. From figure 2.1 data for shear relaxation experiment at 10 % are extracted and used in the identification of the Prony series parameters. These parameters are reported in table 3.2. The average relative error between the experimental and the identified viscoelastic kernel is in the order of 0.1 %. The identified and the experimental normalized shear relaxation modulus are plotted versus time in figure 3.8.

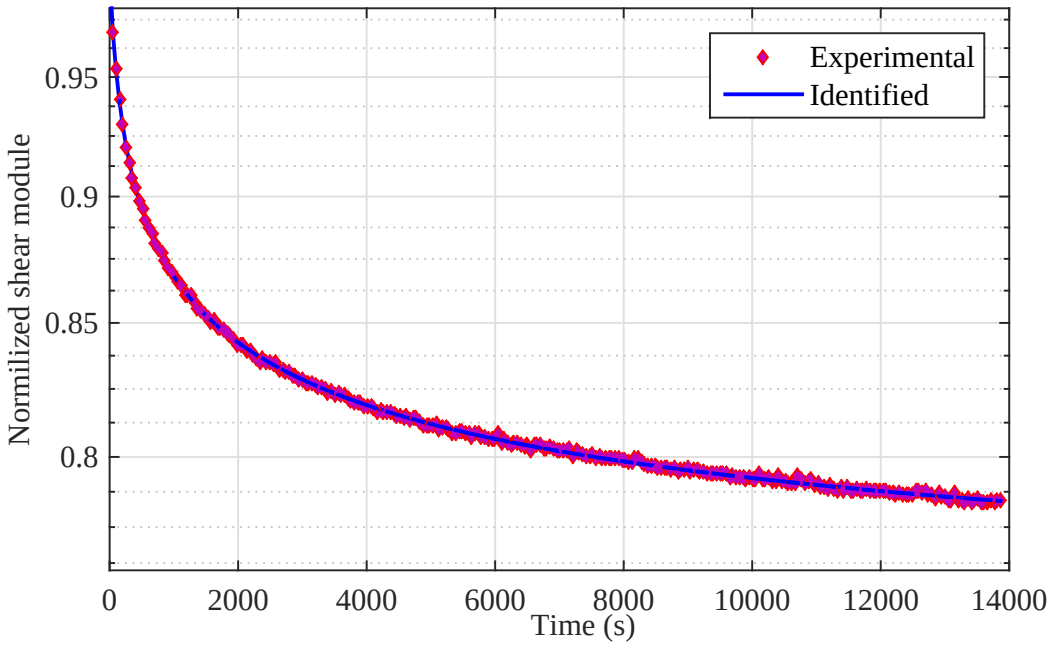

Figure 3.8: Normalized shear relaxation modulus of BIIR rubber versus time.

3.3.2.2 From dynamic experiments

The dynamic experiments are performed in simple shear deformation with a small dynamic amplitude and without a pre-strain of the form of equation (3.24). It is recalled that the problem of the identification of the viscoelastic parameters from dynamic data (3.27) is an ill-posed problem. Hence, a regularization procedure of Tikhonov is used. In what follows, this method is recalled and applied to theoretical dynamic data using parameters from [110] and then applied to dynamic data for BIIR material from [103].

- Tikhonov regularization method:
  The linear system arising from the identification of the Prony series parameters from dynamic data is an ill-posed problem [37]. From the original system of equation (3.27) the following system arise:

$$Ax = b, \tag{3.40}$$

  in which A is the global matrix of the system to be calculated from (3.28), b is the vector of experimental storage modulus and loss modulus vectors $\hat{G}'$ and $\hat{G}''$ and x is the vector of the Prony series parameters $G_i, (i = 1..N)$. Tikhonov regularization

method replaces system (3.40) by:

$$\left(A^t A + \mu I\right) x = A^t b, \tag{3.41}$$

in which $\mu > 0$ is the regularization parameter and I is the identity matrix. The regularization parameter is determined via an L-curve technique using Matlab software. It is well established that the solution of system (3.41) noted x_μ gives the minimum residual for the minimization problem arising from system (3.40) which means:

$$\begin{gathered} \forall\, x \in \mathbb{R}^N \\ \left\|A\,x_\mu - b\right\|^2 \leqslant \|A\,x - b\|^2, \text{ such that } \|x\|^2 \leqslant \left\|x_\mu\right\|^2. \end{gathered} \tag{3.42}$$

The proof of (3.42) and further development of the convergence of the regularized Tikhonov problem are well studied in [18].

- Application of the Tikhonov method to simulated dynamic data:

The Tikhonov regularization procedure described above was applied to a simulated dynamic data generated using Prony series parameters from [110] and relations in (3.26). Moreover, in order to test the ability of the method to deal with noisy experimental data, the second member of system (3.41) was perturbed randomly as follow:

$$\tilde{b} = (1 \pm \epsilon)\, b, \tag{3.43}$$

in which ϵ takes three different values: 10%, 15% and 20%. The Prony series parameters from [110] are reported in table 3.3 with an equilibrium modulus $G_\infty = 2.24\ 10^6\ Pa$. The results of this identification are reported in figure 3.9 in terms of the dynamic moduli versus frequency for the perturbed and original simulated data. The mean relative error for the three perturbed data remains under 10% and hence this procedure shows a huge capacity to predict the dynamic response functions despite the perturbation of the second member of the system (3.42).

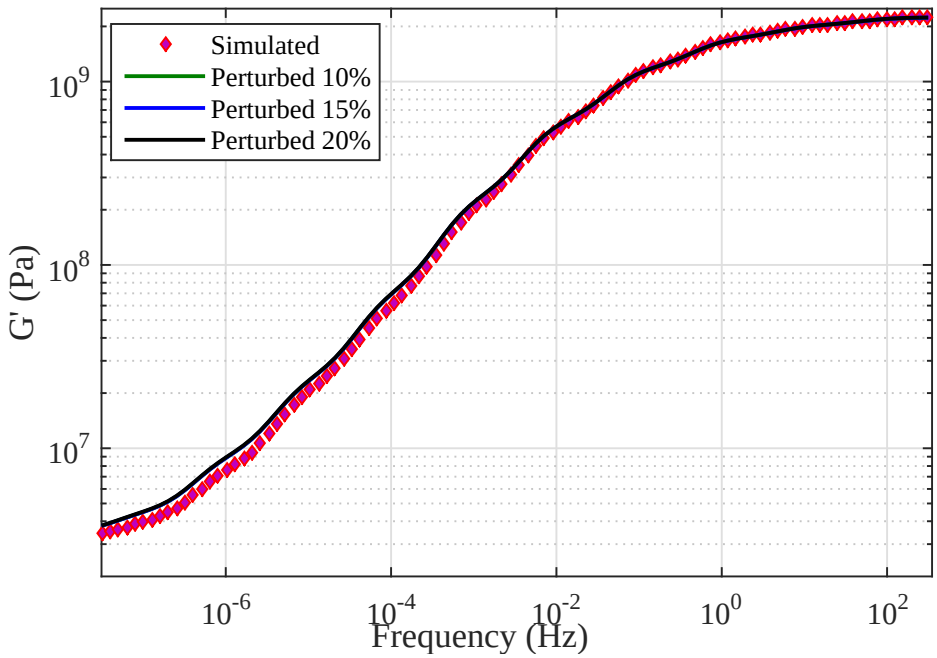

(a) Storage modulus versus frequency for simulated and perturbed data

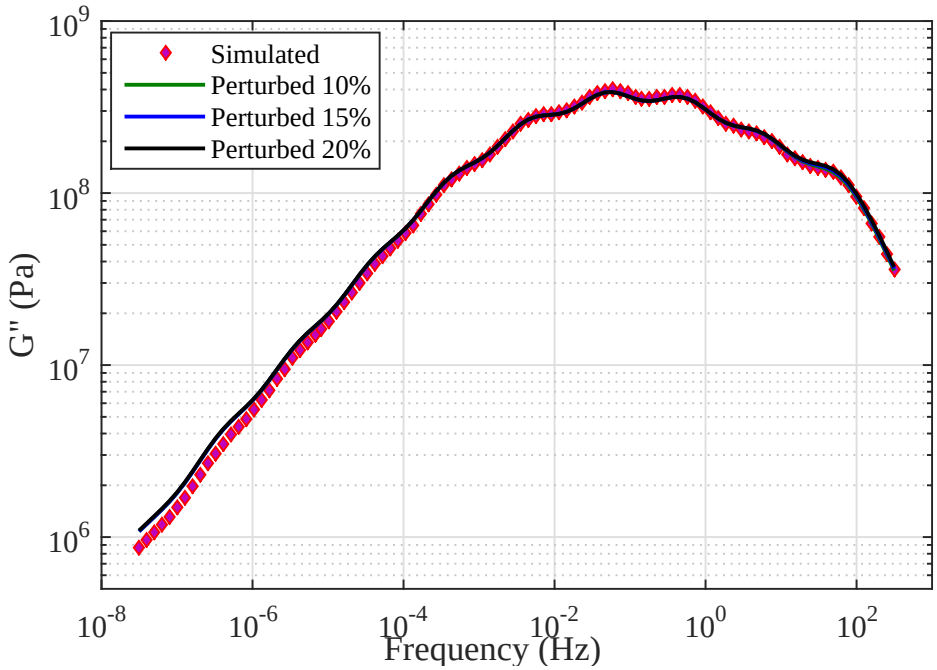

(b) Loss modulus versus frequency for simulated and perturbed data

Figure 3.9: Storage and loss moduli versus frequency for simulated and perturbed data

- Application of the Tikhonov method to experimental dynamic data from [103]

$G_i(Pa)$	$\tau_i(s)$
$1.94\ 10^8$	$2\ 10^{-2}$
$2.83\ 10^8$	$2\ 10^{-1}$
$5.54\ 10^8$	$2\ 10^0$
$6.02\ 10^8$	$2\ 10^1$
$3.88\ 10^8$	$2\ 10^2$
$1.56\ 10^8$	$2\ 10^3$
$4.1\ 10^7$	$2\ 10^4$
$1.38\ 10^7$	$2\ 10^5$
$3.68\ 10^6$	$2\ 10^6$
$7.9\ 10^5$	$2\ 10^7$
$9.6\ 10^5$	$2\ 10^8$

Table 3.3: Prony series parameters from [110]

$G_i(Pa)$	$\tau_i(s)$
$3.13\ 10^8$	$7.1\ 10^{-8}$
$2.61\ 10^7$	$1\ 10^{-6}$
$9.86\ 10^6$	$1.4\ 10^{-5}$
$1.94\ 10^6$	$1.98\ 10^{-4}$
$9.42\ 10^5$	$2.8\ 10^{-3}$
$3.03\ 10^5$	$3.92\ 10^{-2}$
$1.4\ 10^5$	$5.52\ 10^{-1}$
$8.53\ 10^4$	$7.77\ 10^0$
$8.45\ 10^4$	$1.09\ 10^2$
$7.72\ 10^4$	$1.53\ 10^3$
$7.71\ 10^4$	$2.16\ 10^4$
$2.06\ 10^4$	$3.05\ 10^5$

Table 3.4: Prony series parameters from experimental dynamic data

The dynamic experiment are represented by the storage and loss moduli G' and G'' as functions of the frequency for the experimental frequency window of $[10^{-5},\ 10^7\ Hz]$. The tikhonov regularization is applied and a regularization parameter μ is obtained for a 12 parameters Prony series reported in table 3.4. The mean relative error is about 20%.

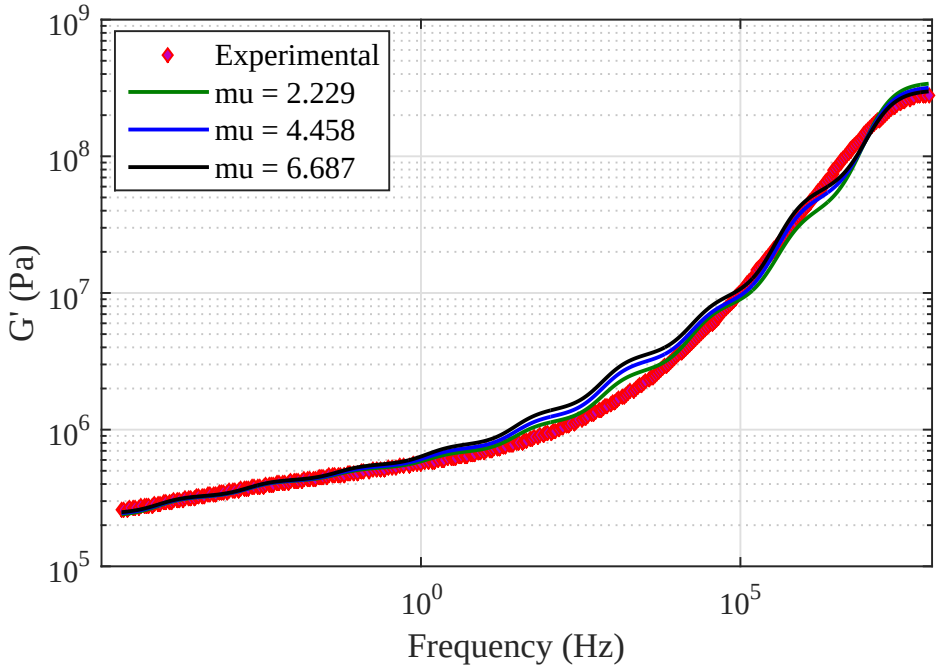

(a) Storage modulus versus frequency for dynamic experimental data

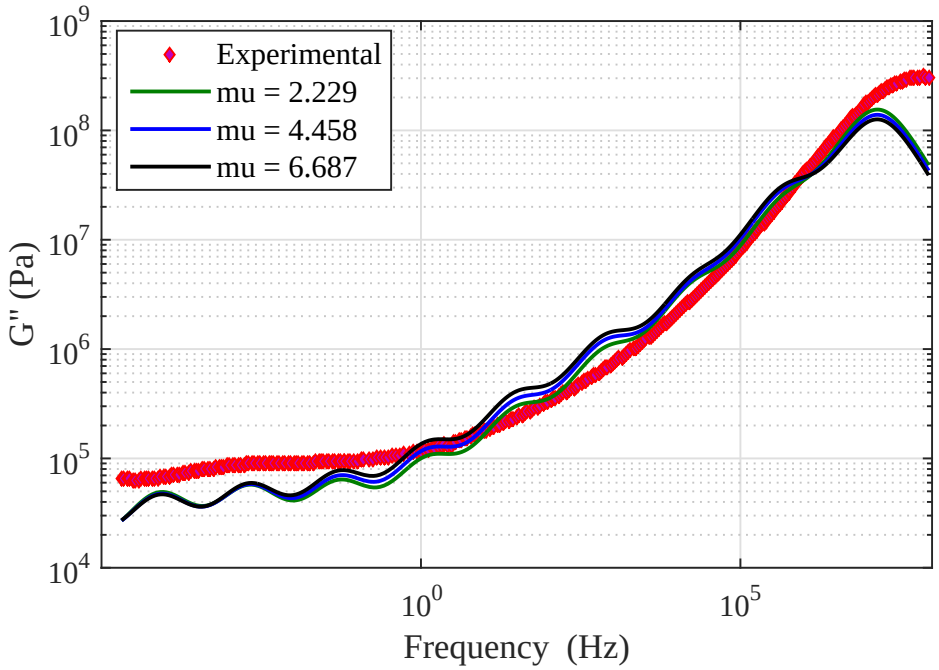

(b) Loss modulus versus frequency for dynamic experimental data

Figure 3.10: Storage and loss moduli versus frequency for dynamic experimental data for different values of the regularization parameter μ

3.3.3 Reduced time function

The reduced time is identified using the discretization formula (3.29) and monotonic experiments of simple extension for two strain rates: 100% s^{-1} and 200% s^{-1}. Cauchy stress versus principle stretch are plotted in figure 3.11. Results of the identification are reported in figure 3.12 in terms of the reduced time coefficient which is a nonlinear function of time for the strain rates considered. The pure shear experiment was predicted using the reduced time, the predicted and experimental data for this experiment are plotted in figure 3.13 against the principle stretch. From this result the relative error of the Cauchy stress is calculated using relation (3.39), its mean value remains under 2.5%. Hence, the proposed model is suitable to describe the material's behavior at low and moderate strains.

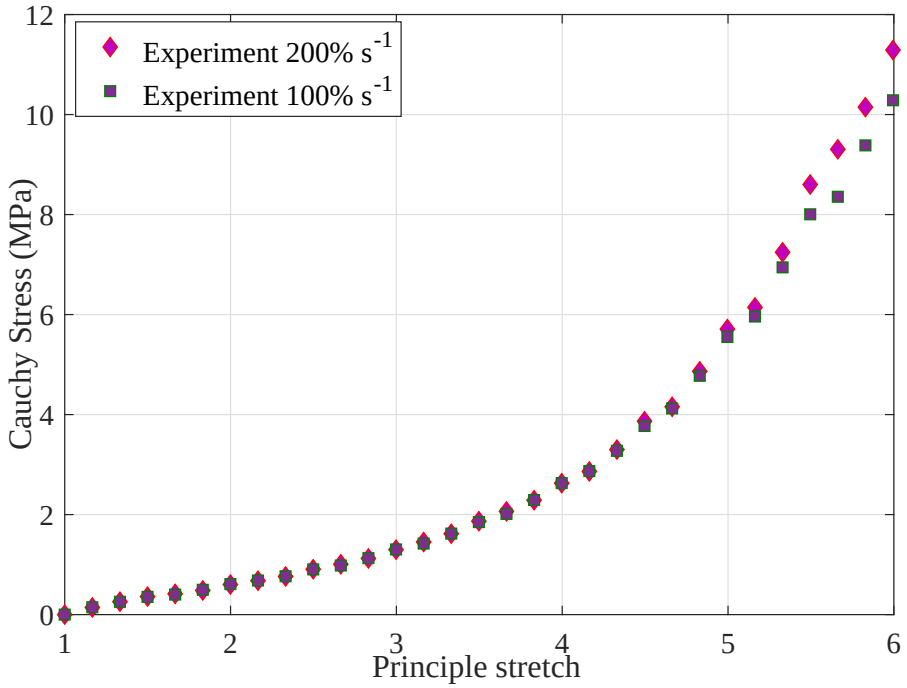

Figure 3.11: Cauchy stress versus principle stretch for simple extension experiment

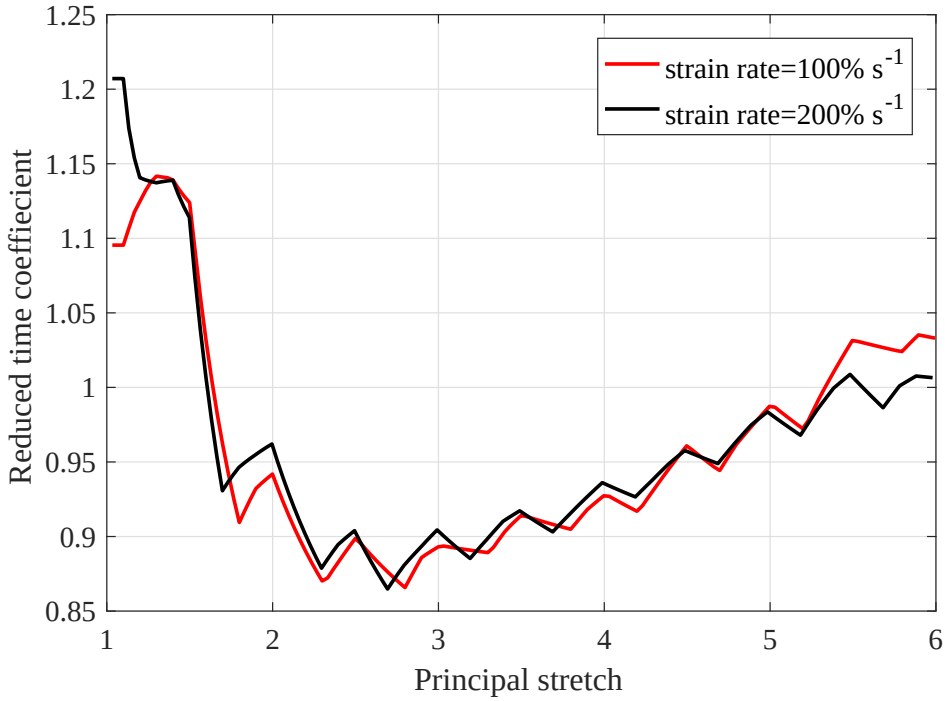

Figure 3.12: Reduced time coefficient for two strain rates 100% s^{-1} and 200% s^{-1}

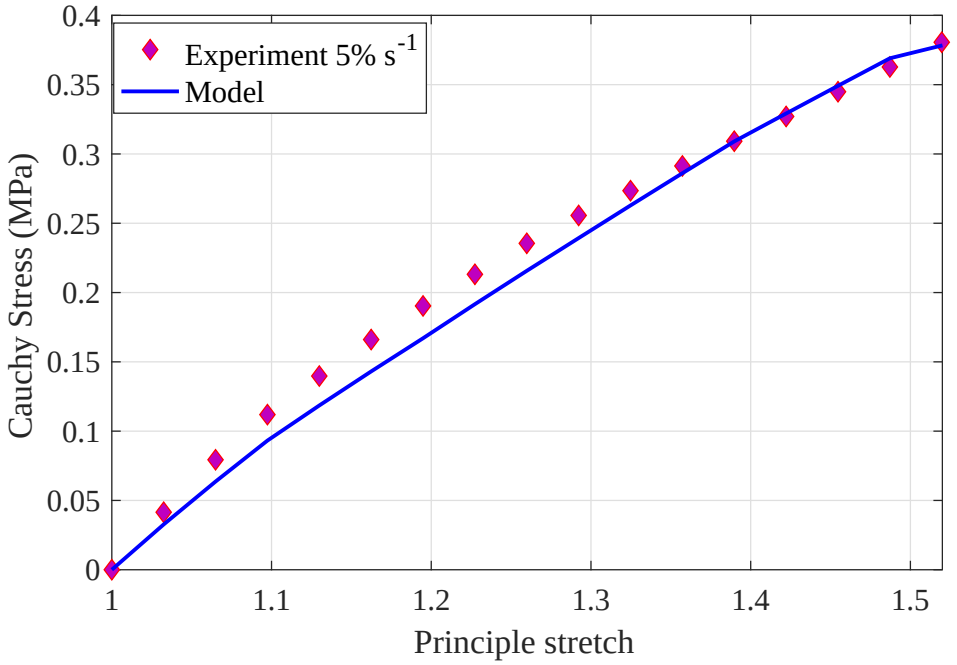

Figure 3.13: Cauchy stress versus principle stretch for pure shear experiment: experimental (diamond) model (solid curve)

3.4 Conclusion

Within this chapter, the identification of several functions involved in the model presented in the second chapter of this Thesis was addressed. Each function's identification procedure turns out to the resolution of a linear or nonlinear system. Moreover, a regularization procedure of Tikhonov was applied in the resolution of the ill-posed problem arising from the identification of the viscoelastic kernel from dynamic data.
This identification procedure was applied to a generated data from a multi-integral viscoelastic model and a static and dynamic experimental characterization of a BIIR rubber. The results of the identification has shown a huge capacity of the model to describe the multi-integral viscoelastic model in the time domain of the behavior within and outside the range of strain rates considered in deriving the model. The results from the experimental characterization has shown a huge capacity to depict the behavior of the material in the time domain for the equilibrium and instantaneous responses.
Our main object was to develop a constitutive equation compatible with the second law of thermodynamics and suitable with the Finite-elements theory. The implementation of the model within Abaqus software is the goal of the next chapter.

CHAPTER 4

NUMERICAL IMPLEMENTATION AND INTEGRATION SCHEME

Contents

In general, the response of a viscoelastic material depends on the excitation history. For an integral based formulation viscoelasticity, the entire excitation history must be stored in order to evaluate the response numerically. Therefore, the memory storage increases in time. The storage problem can be avoided by representing the kernel function as a Prony series. Thanks to the *semigroup* property of the exponential function, the use of Prony series in the kernel function leads to an efficient recursive relation [129]. The incremental representation of the kernel function is combined with an incremental form of the excitation history which describes

the evolution of the excitation history inside the time increment. Several form have been proposed in the literature, which goes from constant proposed by [150], piecewise constant proposed by [61], linear suggested by [137] to exponential form proposed by [1]. These forms have been successfully used in the implementation of the Schapery model by [6], [60] and [53] among others, for the Duvaut-Lions viscoplasticity model in [130] and in finite strain viscoelasticity by [68]. For further details about the integration schemes in viscoelasticity, the reader is directed to the work of [132] and [42].
On the other hand, in addition to the integration scheme of the kernel function, one needs to derive the discrete form of the constitutive equation based on the decomposition of the deformation gradient tensor into volumetric and isochoric parts. To this end, following the formulation of the model, the Cauchy stress tensor is decomposed into an instantaneous hyperelastic and viscoelastic over-stress parts. The discrete representation of each part of the stress tensor is calculated separately.
The aim of this chapter is to presents the numerical implementation of the nonlinear viscoelastic model developed in the previous chapters. First, the integration scheme of the one dimensional viscoelastic model is recalled. In fact, the integration scheme for the one dimensional viscoelastic model was implemented using Matlab software and validated through the comparison with numerical simulations performed with Abaqus software for simple extension with several strain histories. Then, the implementation of the three dimensional viscoelastic model into Abaqus software is performed using an implicit integration scheme in a Umat subroutine. To this end, the discrete form of the nonlinear viscoelatic model was performed following [63] using the objective rate derivative of Jaumann. Finally the fourth order tangent stiffness needed in the coding of the subroutine Umat is calculated accordingly.

4.1 Integration scheme for one dimensional viscoelastic model

In this section, we present the integration scheme of the Simo [131] model implemented in Abaqus software. The constitutive equation for a one dimensional experiment will be implemented in a Matlab code then compared to the numerical simulation performed with Abaqus software. Our starting point is the one dimensional model presented in 2.2 by the constitutive equation of the stress which reads in the absence of the reduced time

ξ i.e. $\xi(t) = t$ as follow

$$\sigma(t) = \int_0^t G\left(t - t'\right) \dot{\varepsilon}\left(t'\right) dt'. \tag{4.1}$$

4.1.1 Integration scheme

The integration scheme of the constitutive equation of the stress is performed in a discrete manner. Hence, let $[0,t], t > 0$ be the time interval of interest. It will be decomposed into sub-intervals as follows:

$$[0,t] = \bigcup_n [t_n, t_{n+1}],\ t_{n+1} = t_n + \Delta t_n. \tag{4.2}$$

Without loss of generality, the time intervals Δt_n are assumed to be equals. Since the model considered is a deformation driven model, the total deformation ε applied in the time interval $[0,t]$ is also subdivided into equal deformation increments $\Delta\varepsilon$ following (4.2). Hence, the convolution integral in (2.8) does not need to be totally evaluated and it is split into an integral over $[0,t_n]$ and an integral over the last time increment $[t_n, t_{n+1}]$ through the following recursive update formula

$$\begin{aligned}
\sigma(t_{n+1}) =& G_\infty \varepsilon(t_{n+1}) + \sum_i \left[G_i \exp\left(-\frac{\Delta t}{\tau_i}\right) \int_0^{t_n} \exp\left(-\frac{t_n - t'}{\tau_i}\right) \dot{\varepsilon}\left(t'\right) dt' + G_i \tau_i \left(1 - \exp\left(-\frac{\Delta t}{\tau_i}\right)\right) \frac{\Delta\varepsilon}{\Delta t} \right] \\
=& G_\infty \varepsilon(t_{n+1}) + \sum_i \left[h_i(t_{n+1}) + G_i p_i \Delta\varepsilon \right], \\
& \text{with } p_i = \frac{\tau_i}{\Delta t}\left(1 - \exp\left(-\frac{\Delta t}{\tau_i}\right)\right),
\end{aligned} \tag{4.3}$$

where h_i are the algorithmic stresses expressed by :

$$h_i(t) = G_i \int_0^t \exp\left(-\frac{t - t'}{\tau_i}\right) \dot{\varepsilon}\left(t'\right) dt'. \tag{4.4}$$

The whole procedure is summarized in the following algorithm: Note that the update

Algorithm 1 Recursive update procedure

1: Database $\sigma(t_n), h_i(t_n),\ \ i = 1..N$ at time t_n
2: Give the strain increment $\Delta\varepsilon$
3: Calculate the elastic stress $\sigma^e(t_{n+1}) = G_\infty \varepsilon(t_{n+1})$
4: Update the algorithmic stresses $h_i(t_{n+1}) = \exp\left(-\frac{\Delta t}{\tau_i}\right) h_i(t_n) + G_i \exp\left(-\frac{\Delta t}{2\tau_i}\right) \Delta\varepsilon$
5: Compute the total stress using (4.3)

formula of the algorithmic stresses h_i expressed in the previous algorithm is not unique and alternative formulas could be found in [129]. With equations (4.3) and (4.4) and the update procedure described above, we have all the quantities needed for the implementation of the one dimensional viscoelastic model which will be performed with Matlab software.

4.1.2 Validation of the integration scheme

The validation of the integration scheme described in the previous section is performed using three strain histories, for each case the total stress σ obtained from the discrete scheme of equation (4.3) is compared to the stress obtained from the Abaqus simulation. The Abaqus model consists of a single brick element undergoing simple extension strain. The three strain histories considered here are defined by the following

$$\varepsilon(t) = \dot{\varepsilon}_o t, \tag{4.5}$$

for monotonic strain history, where $\dot{\varepsilon}_o$ is a positive constant denoting the strain rate and

$$\varepsilon(t) = \begin{cases} 0 & \text{for} \quad t < 0 \\ \varepsilon_o & \text{for} \quad t \geq 0 \end{cases}, \tag{4.6}$$

for the relaxation strain history, where ε_o is the relaxation level and

$$\varepsilon(t) = \varepsilon^A \sin(wt), \tag{4.7}$$

for a sinusoidal strain history in which ε^A is the amplitude of the strain and w is its frequency. Note that the form of the strain history of equation (4.6) can not be applied neither experimentally nor numerically, hence a very fast ramp is applied to shift the strain from 0 to ε_o. The results of the comparison between the discrete stress of equation (4.3) and the one obtained from the Abaqus simulation are reported in figures 4.1, 4.2 and 4.3 in terms of the total stress versus time for monotonic, relaxation and sinusoidal strain histories respectively. The material parameters used in this calculus are those from [110]. From these results, it is concluded that the recurrence update formula of (4.3) gives the same result as the viscoelastic model implemented in Abaqus software. This result establish a big step to the implementation of the three dimensional viscoelastic model since it has the same integration scheme as the Simo's model [131] implemented in Abaqus software. The implementation of the nonlinear viscoelastic model presented in 2 will be presented in the next section of this chapter.

4.2 Implementation of the nonlinear viscoelastic model

In this section we address the implementation of the nonlinear viscoelastic model presented in chapter 2. To this end, we start by recalling the formulation of initial boundary

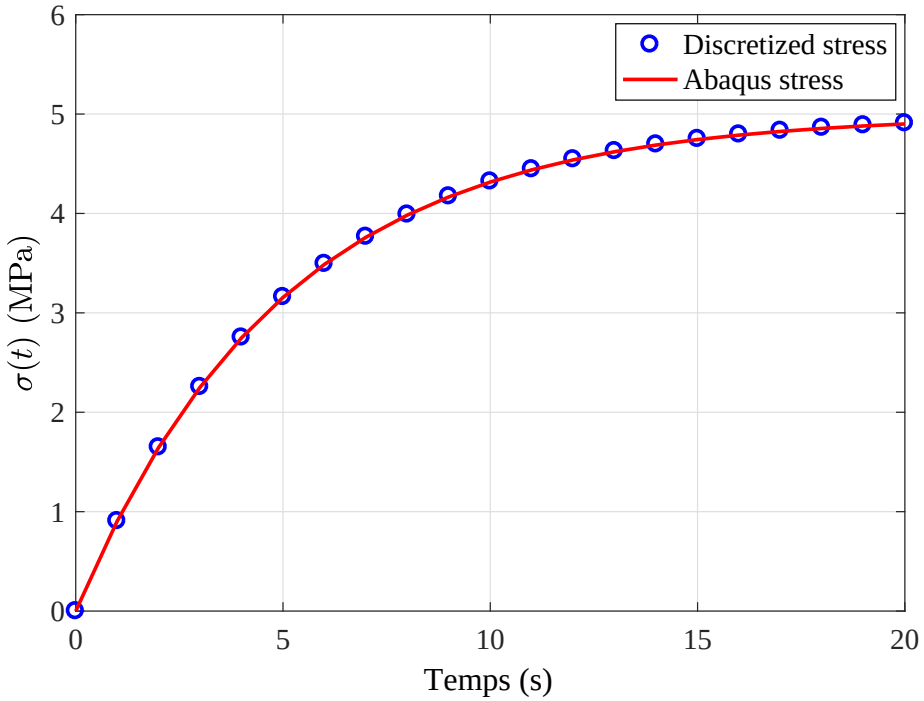

Figure 4.1: Stress versus time for a monotonic strain history

problems for a nonlinear viscoelastic solid. Then, we present the discrete form of the constitutive equations of the model as well as the approximation of the tangent modulus needed in the Umat subroutine.

4.2.1 Finite element method for nonlinear viscoelastic solids

Consider a continuum viscoelastic body occupying the reference placement Ω_0 in the reference configuration C_0. It occupies at the time t the placement Ω in the deformed configuration C_t. Let $\varphi(X,t)$ denote a macroscopic motion between the two configurations, which maps any point X in the reference configuration C_0 to the point x in the deformed configuration characterized by its displacement vector field noted u pointing from the reference configuration to the current configuration. The typical use of the finite element method is to resolve initial boundary value problem. In the absence of body forces, the momentum equation is expressed, in the current configuration, as :

$$div(\boldsymbol{\sigma}) = \rho \ddot{\boldsymbol{u}}, \tag{4.8}$$

where ρ is density and div is the divergence operator with respect to the current configuration. In the following we consider boundary and initial conditions for the motion

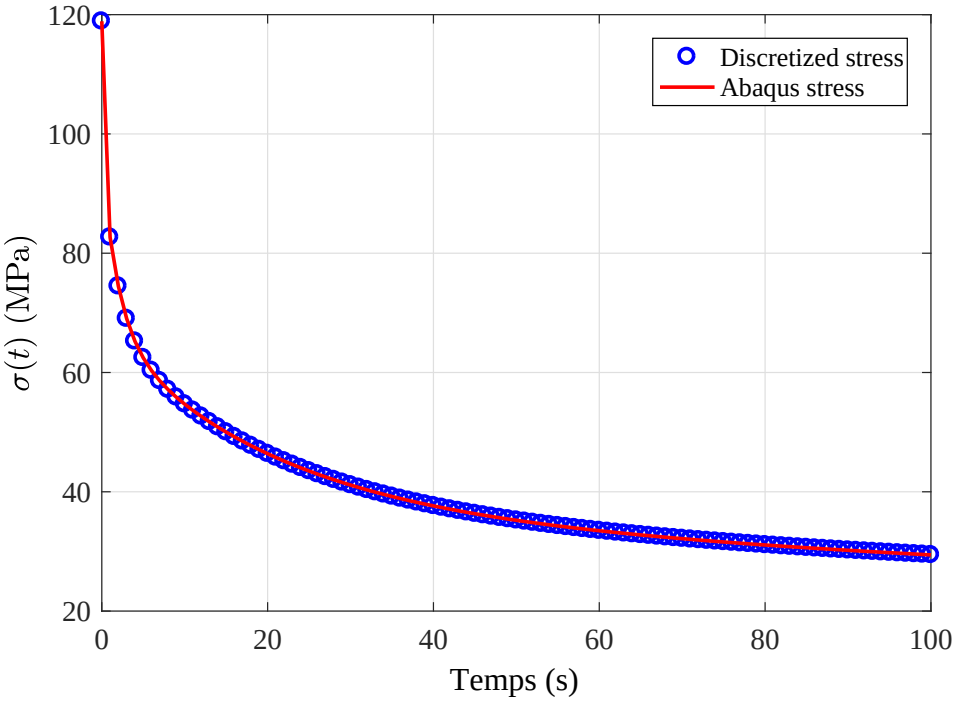

Figure 4.2: Stress versus time for relaxation strain history

$x = \varphi(X,t)$ required to satisfy the momentum equation (4.8). we assume afterwards that the boundary surface $\partial\Omega$ of the continuum occupying Ω is decomposed into disjoint parts so that

$$\partial\Omega = \partial_{\boldsymbol{u}}\Omega \cup \partial_{\boldsymbol{F}}\Omega \quad \text{with } \partial_{\boldsymbol{u}}\Omega \cup \partial_{\boldsymbol{F}}\Omega = \emptyset. \tag{4.9}$$

Figure 4.4 illustrates the decomposition of the boundary surface $\partial\Omega$ at the time t. There are two classes of boundary conditions, namely the **Dirichlet boundary conditions,** which corresponds to the definition of a displacement field $\boldsymbol{u} = \bar{\boldsymbol{u}}(x,t)$ in the displacement boundary surface $\partial_{\boldsymbol{u}}\Omega$, and the **Nuemann boundary conditions,** which are identified with $\boldsymbol{\sigma}.\boldsymbol{n} = \boldsymbol{F}(x,t)$ in the force boundary surface $\partial_{\boldsymbol{F}}\Omega$. The second order differential equations of (4.9) require additional data to be resolved in the form of initial conditions. The displacement field $\boldsymbol{u}$ and the velocity field $\dot{\boldsymbol{u}}$ at the initial time $t = 0$ are specified as

$$\boldsymbol{u}(x,t) = \boldsymbol{u}_0(X)|_{t=0} \quad , \quad \dot{\boldsymbol{u}}(x,t) = \dot{\boldsymbol{u}}_0(X)|_{t=0} \tag{4.10}$$

In order to achieve the compatibility of the boundary conditions, the initial conditions of equation (4.10) are also applied to the prescribed displacement field in the displacement boundary surface $\partial\Omega$. Hence, the problem now is to find a motion that satisfies equation (4.8) with the prescribed initial and boundary conditions of equations (4.9) and (4.10).

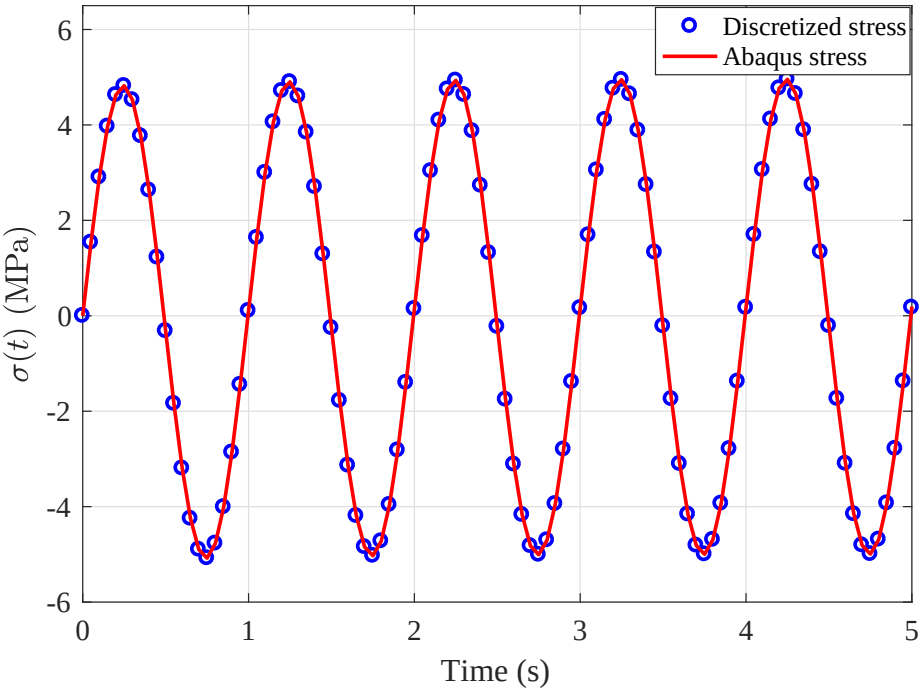

Figure 4.3: Stress versus time for a sinusoidal strain history

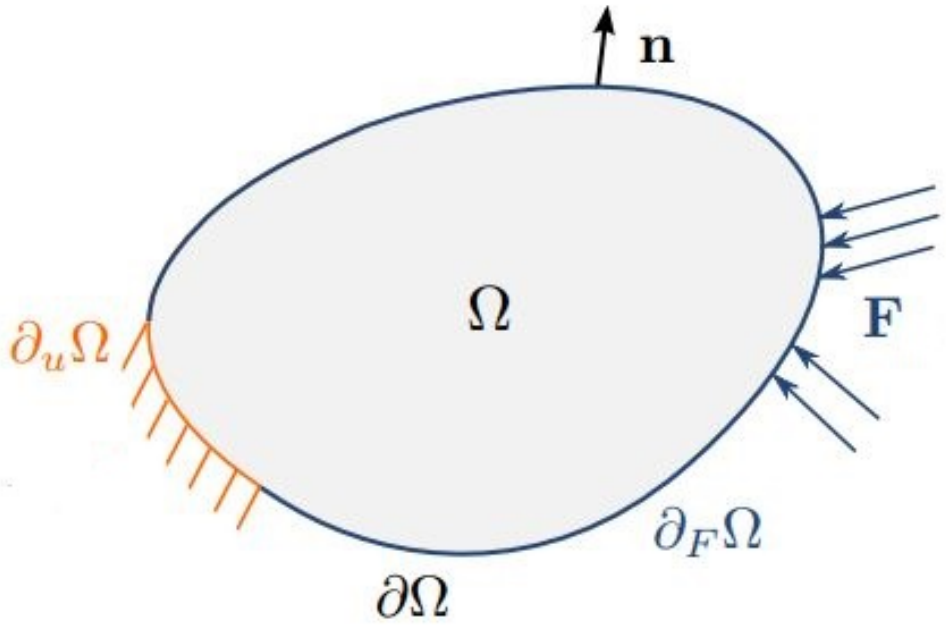

Figure 4.4: Initial boundary value problem considered

This leads to the formulation in the strong form of the initial boundary value problem: find a displacement field $\boldsymbol{u}$ such that

$$\begin{aligned} &div(\boldsymbol{\sigma}) = \rho\ddot{\boldsymbol{u}}, \\ &\boldsymbol{u} = \bar{\boldsymbol{u}} \ \text{ on } \partial_{\boldsymbol{u}}\Omega, \\ &\boldsymbol{\sigma}.\boldsymbol{n} = \boldsymbol{F} \ \text{ on } \partial_{\boldsymbol{F}}\Omega, \\ &\boldsymbol{u}(x,t) = \boldsymbol{u}_0(X)|_{t=0}\ , \\ &\dot{\boldsymbol{u}}(x,t) = \dot{\boldsymbol{u}}_0(X)|_{t=0}, \end{aligned} \tag{4.11}$$

where $\boldsymbol{n}$ is the unit exterior normal vector to the force boundary surface $\partial_{\boldsymbol{F}}\Omega$. The analytic solution of the nonlinear system of the initial boundary value problem of equation (4.11) is only possible for some special cases. Therefore, solutions are often obtained using the finite element method which is based on the variational formulation of (4.11). The variational formulation of the initial boundary value problem reads

$$\int_\Omega div(\boldsymbol{\sigma})\delta\boldsymbol{u}d\Omega - \int_\Omega \rho\ddot{\boldsymbol{u}}.\delta\boldsymbol{u}\,d\Omega = 0, \tag{4.12}$$

where $\delta\boldsymbol{u}$ is a virtual displacement field which has to verify the initial and boundary conditions. In practice, this virtual displacement field is set to be the displacement field $\boldsymbol{u}$ since verifies all the required conditions for the virtual displacement field $\delta\boldsymbol{u}$. Application of the Divergence formula to the first integral in (4.12) yields the following form of the variational formulation of the initial boundary value problem,

$$\int_\Omega \boldsymbol{\sigma} : \boldsymbol{grad}(\delta\boldsymbol{u})d\Omega - \int_\Omega \rho\ddot{\boldsymbol{u}}.\delta\boldsymbol{u}\,d\Omega - \int_{\partial_{\boldsymbol{F}}\Omega} \boldsymbol{F}.\delta\boldsymbol{u}\,d\partial_{\boldsymbol{F}}\Omega = 0. \tag{4.13}$$

The variational formulation of equation (4.13) is also known as the weak formulation of the initial boundary value problem (4.11). The domain Ω will be subdivided into several elements Ω_e, the displacement field for any point M of the element Ω_e is denoted by $\boldsymbol{u}_e$ and given by

$$\boldsymbol{u}_e(M) = \mathbb{N}\boldsymbol{U}_e, \tag{4.14}$$

in which $\mathbb{N}$ are the shape function of the element Ω_e and $\boldsymbol{U}_e$ is its nodal displacement vector. The internal force vector associated with the element Ω_e, $\boldsymbol{f}_e^{int}$ according to [129] is given by

$$\begin{aligned} \boldsymbol{f}_e^{int}(t) &= \int_{\Omega_e} \boldsymbol{B}_e^t\boldsymbol{\sigma}(t)dV \\ &= \int_\square \left[\boldsymbol{B}_e^t\boldsymbol{\sigma}(t)\right] \circ \phi_e j(\boldsymbol{\xi})d\boldsymbol{\xi} \\ &\cong \sum_{l=1}^{n_{Gauss}} \boldsymbol{B}_e^t(x_l)\boldsymbol{\sigma}_l(t)W_l j_l, \end{aligned} \tag{4.15}$$

where $\phi_e : \square \rightarrow \Omega_e$ is the standard isoprametric map with Jacobian determinant $j = det[D\phi_e]$, $\boldsymbol{B}_e$ is the discrete strain-displacement operator and W_l are the quadrature weights corresponding to the quadrature point x_l. In (4.15) the subscript l denotes evaluation at the quadrature point $x_l \in \Omega_e$ with $l = 1, 2, \cdots, n_{Gauss}$. This notation is standard; see [75] and [149] for further development. From (4.15) it is concluded that the evaluation of the internal force vector $\boldsymbol{f}_e^{int}(t)$ requires knowledge of the stress history at the quadrature point $\sigma_l(t)$ for the time interval considered assuming knowledge of the strain at any given time in the time interval considered. Therefore, a discrete representation of the convolution representation of the stress of equation (2.43) is required to complete the resolution of the initial boundary value problem of equation (4.11). Since our model is not existing in any finite element software, it should be implemented into a finite element software (e.g. Abaqus) via a user defined subroutine. The implementation procedure of the model will be presented in the remaining of this chapter.

4.2.2 Discrete representation of the constitutive equations

In this section, the implementation of the nonlinear viscoelastic model at finite strain into Abaqus software is presented via a user defined Umat subroutine. First, the discrete representation of the model is presented in terms of the expression of the update formula of the Cauchy stress (4.11). Then, the fourth order tangent stiffness tensor needed in the writing of the Umat is calculated using the Jaumann objective derivative. Finally, the use of the user defined Umat subroutine is explained.

4.2.2.1 Discrete stress-strain relationship

To investigate the performance of the proposed model in [136] and presented in chapter 2 of this thesis for boundary value problems, it is needful to implement the constitutive equations into a finite element software e.g. Abaqus through a user-defined umat subroutine, which requires an update formulas for the Cauchy stress $\boldsymbol{\sigma}$ and the tangent modulus $\mathbb{C}$. Before we start with the formulation of the discrete form of the constitutive equation of the model, it is necessary to point out that this implementation procedure is done with a compressible viscoelastic model even thought the model proposed in this thesis is an incompressible viscoelastic model. In fact, Abaqus software gives the possibility to do so in the writing of the user defined Umat subroutine. According to [62], to avoid the penalty formulation due to the incompressibility [64], it is sufficient to consider

a bulk modulus about $10^4 - 10^6$ times the shear modulus and use hybrid elements in the mesh module of Abaqus see [63] for further details. First, for numerical reasons [129] with respect to the implementation procedure, it is more convenient to consider the constitutive equation of the stress of equation (2.43) in terms of the Kirchhoff stress tensor $\boldsymbol{\tau} = J\boldsymbol{\sigma}$ namely

$$\boldsymbol{\tau} = \boldsymbol{\tau}_o^d + dev \int_0^{\xi} \frac{\partial g\left(\xi'\right)}{\partial \xi'} \left(\bar{\boldsymbol{F}}_t^{-1}\left(t-t'\right) \boldsymbol{\tau}_o^d \left(t-t'\right) \bar{\boldsymbol{F}}_t^{-t}\left(t-t'\right) \right) d\xi' + Jp\boldsymbol{I}. \tag{4.16}$$

To present the discrete representation of the constitutive model of equations (2.43), different functions of the model need to be defined. We start with the definition of the reduced time function $a(\boldsymbol{C})$. Motivated by the form proposed in [113] to describe the behavior of ligaments, a more general form for the reduced time function is postulated as follows:

$$a(\boldsymbol{C}) = \exp\left(c_1 (I_1 - 3) + c_2 (I_2 - 3)\right), \tag{4.17}$$

where c_1 and c_2 are material parameters. Also, as it is explained in the formulation of the model, the instantaneous stored elastic energy density Ψ is decomposed into volumetric and isochoric parts

$$\Psi = \Psi^{iso}\left(\bar{\boldsymbol{B}}\right) + \Psi^{vol}(J), \tag{4.18}$$

The superscript $\bullet^{iso}$ and $\bullet^{vol}$ denote the isochoric and volumetric parts of the instantaneous stored elastic energy density respectively. $\bar{\boldsymbol{F}}_t\left(t'\right) = J^{-1/3}\partial\varphi\left(X,t'\right)/\partial\varphi(X,t)$ is the relative distortional deformation gradient tensor for the mapping function $\varphi(X,t)$, g is the normalized shear relaxation modulus and it is expressed by a sum of decaying exponential functions of time as

$$g(t) = g_\infty + \sum_r g_r \exp\left(-\frac{t}{\tau_r}\right), \tag{4.19}$$

g_r and τ_r are the coefficients of the Prony series and relaxation times respectively, g_∞ is the equilibrium normalized shear modulus. $p = \partial\Psi^{iso}(J)/\partial J$ is the hydrostatic part of the stress which could be determined in the case of incompressibile behavior through boundary conditions. In equation (4.16), $\boldsymbol{\tau}_o^d$ is the deviatoric part of the instantaneous elastic Kirchhoff tensor which is expressed from the instantaneous stored elastic energy density Ψ by

$$\boldsymbol{\tau}_o = 2\boldsymbol{B}\frac{\partial\Psi(\boldsymbol{B})}{\partial\boldsymbol{B}}. \tag{4.20}$$

Using equation (4.20), the instantaneous elastic Kirchhoff stress $\boldsymbol{\tau}_o$ is decomposed as well into isochoric and volumetric parts

$$\boldsymbol{\tau}_o = \boldsymbol{\tau}_o^h(J) + \boldsymbol{\tau}_o^d(\bar{\boldsymbol{B}}), \tag{4.21a}$$

$$\boldsymbol{\tau}_o^h(J) = 2J\boldsymbol{B}\frac{\partial \Psi^{vol}(J)}{\partial \boldsymbol{B}}, \tag{4.21b}$$

$$\boldsymbol{\tau}_o^d(\bar{\boldsymbol{B}}) = 2\boldsymbol{B}\frac{\partial \Psi^{iso}(\bar{\boldsymbol{B}})}{\partial \boldsymbol{B}}. \tag{4.21c}$$

From equation (4.21b) with $\partial J/\partial \boldsymbol{B} = 0.5J\boldsymbol{B}^{-1}$ it follows

$$\boldsymbol{\tau}_o^h(J) = J\frac{\partial \Psi^{iso}(J)}{\partial J}\boldsymbol{I}, \tag{4.22}$$

and from equation (4.21c) and

$$\frac{\partial \bar{\boldsymbol{B}}}{\partial \boldsymbol{B}} = J^{-2/3}\left(\mathbb{I} - \frac{1}{3}\boldsymbol{B}\otimes\boldsymbol{B}^{-1}\right), \tag{4.23}$$

in which $\mathbb{I}$ denotes the fourth order identity tensor defined by

$$\mathbb{I}_{ijkl} = \frac{1}{2}(\delta_{ik}\delta_{jl} + \delta_{il}\delta_{jk}), \tag{4.24}$$

and $\otimes$ designates the tensorial product operator, it follows

$$\boldsymbol{\tau}_o^d(\bar{\boldsymbol{B}}) = \mathbb{P} : \bar{\boldsymbol{\tau}}. \tag{4.25}$$

$\mathbb{P}$ is the fourth order projection tensor and $\bar{\boldsymbol{\tau}}$ is an algorithmic Kirchhoff stress tensor derived from $\Psi^{iso}(\bar{\boldsymbol{B}})$ with respect to $\bar{\boldsymbol{B}}$. With all needed quantities been defined, we shall now address the discretization of the constitutive equation of the Kirchhoff stress tensor of equation (4.16) and the reduced time of equation (4.17). Let $[0,t]$ be the time interval of interest, this interval is subdivided into n increments as follows

$$[0,t] = \bigcup_n [t_n, t_{n+1}], \quad t_{n+1} = t_n + \Delta t_n. \tag{4.26}$$

The reduced time increment $\Delta\xi_n$ is related to the real time increment Δt_n defined in equation (4.26) and may be expressed as follows

$$\Delta\xi_n = \frac{\Delta t_n}{a(\boldsymbol{C})}. \tag{4.27}$$

Since the implementation is performed in Abaqus software, the discrete form of equation (4.16) is obtained in the same way as in [63] taking into account that all quantities are

known at t_n and all strain quantities are known at t_{n+1}. This discrete form reads

$$\begin{aligned}
&\boldsymbol{\tau}(t_{n+1}) = \boldsymbol{\tau}_o^d(t_{n+1}) - \sum_{i=1}^{r} \boldsymbol{\tau}_i^d(t_{n+1}) + \boldsymbol{\tau}_o^h(t_{n+1}) \\
&\boldsymbol{\tau}_i^d(t_n) = \frac{g_i}{\tau_i} \int_0^{\xi} \bar{\boldsymbol{F}}_t^{-1}(t-t')\, \boldsymbol{\tau}_o^d(t-t')\, \bar{\boldsymbol{F}}_t^{-t}(t-t') \exp\left(-\frac{\xi'}{\tau_i}\right) d\xi' \\
&\boldsymbol{\tau}_i^d(t_{n+1}) = \alpha_i g_i \boldsymbol{\tau}_o^d(t_{n+1}) + \beta_i g_i \hat{\boldsymbol{\tau}}_o^d(t_n) + \gamma_i \hat{\boldsymbol{\tau}}_i^d(t_n) \qquad (4.28) \\
&\text{with} \\
&\gamma_i = \exp\left(-\frac{\Delta\xi_n}{\tau_i}\right);\ \alpha_i = 1 - \frac{\tau_i}{\Delta\xi_n}(1-\gamma_i);\ \beta_i = \frac{\tau_i}{\Delta\xi_n}(1-\gamma_i) - \gamma_i \\
&\hat{\boldsymbol{\tau}}_j^d(t) = \bar{\boldsymbol{F}}_t(t+\Delta t_n)\boldsymbol{\tau}_j^d(t)\bar{\boldsymbol{F}}_t^{\,t}(t+\Delta t_n)\ ;\ j = 0,1,...r.
\end{aligned}$$

In equation (4.28) r is the number of Prony series coefficients.

4.2.2.2 Tangent stiffness

In this section we specify the formula for the tangent modulus $\mathbb{C}$ required in the implementation of the model. To this end, it is essential to derive the stress rate quantities that are objective. First, we start with the so-called Oldroyd stress rate (see [94]) of the elastic part of the model and get,

$$\mathbb{L}_v \boldsymbol{\tau}_o = \dot{\boldsymbol{\tau}}_o - \boldsymbol{L}\boldsymbol{\tau}_o - \boldsymbol{\tau}_o \boldsymbol{L}^t = 4\boldsymbol{B}\frac{\partial^2 \Psi(\boldsymbol{B})}{\partial \boldsymbol{B}^2}\boldsymbol{B} : \boldsymbol{D} := \mathbb{C}^e : \boldsymbol{D}, \qquad (4.29)$$

in which $\boldsymbol{L}$ is the velocity gradient tensor, $\boldsymbol{D} = 0.5(\boldsymbol{L} + \boldsymbol{L}^t)$ is the rate of deformation tensor and $\mathbb{C}^e$ is the elastic tangent modulus. This tangent modulus is decomposed into isochoric and volumetric parts as well

$$\mathbb{C}^e = \mathbb{C}^e{}_{vol}(J) + \mathbb{C}^e{}_{iso}(\bar{\boldsymbol{B}}). \qquad (4.30)$$

Using equations (4.21b) and (4.21c) the isochoric and volumetric parts of the elastic tangent modulus follow

$$\mathbb{C}^e{}_{vol}(J) = 4\boldsymbol{B}\frac{\partial^2 \Psi^{vol}(J)}{\partial \boldsymbol{B}^2}\boldsymbol{B} = \left(\frac{\partial^2 \Psi^{vol}(J)}{\partial J^2} + J\frac{\partial \Psi^{vol}(J)}{\partial J}\right)\boldsymbol{I}\otimes\boldsymbol{I} - 2J\frac{\partial \Psi^{vol}(J)}{\partial J}\mathbb{I}, \qquad (4.31)$$

for the volumetric part and

$$\mathbb{C}^e{}_{iso}(\bar{\boldsymbol{B}}) = 4\boldsymbol{B}\frac{\partial^2 \Psi^{iso}(\bar{\boldsymbol{B}})}{\partial \boldsymbol{B}^2}\boldsymbol{B} = \frac{2}{3}tr(\bar{\boldsymbol{\tau}})\mathbb{P} - \frac{2}{3}\left(\boldsymbol{\tau}_o^d \otimes \boldsymbol{I} + \boldsymbol{I}\otimes\boldsymbol{\tau}_o^d\right) + \mathbb{P} : \bar{\mathbb{C}} : \mathbb{P}, \qquad (4.32)$$

for the isochoric part. In equation (4.32), $tr(\bullet)$ denotes the trace operator and $\bar{\mathbb{C}}$ is an algorithmic tangent modulus following from $\bar{\boldsymbol{\tau}}$ and has the following expression:

$$\bar{\mathbb{C}} = 4\bar{\boldsymbol{B}}\frac{\partial^2 \Psi^{iso}(\bar{\boldsymbol{B}})}{\partial \bar{\boldsymbol{B}}^2}\bar{\boldsymbol{B}}. \qquad (4.33)$$

The viscoelastic isochoric and volumetric moduli, according to [63], could be easily obtained from the elastic moduli through the following relations :

$$\mathbb{C}^v = \mathbb{C}^v{}_{vol}(\boldsymbol{J}) + \mathbb{C}^v{}_{iso}(\bar{\boldsymbol{B}}), \tag{4.34a}$$

$$\mathbb{C}^v{}_{vol}(\boldsymbol{J}) = \mathbb{C}^e{}_{vol}(\boldsymbol{J}), \tag{4.34b}$$

$$\mathbb{C}^v{}_{iso}(\bar{\boldsymbol{B}}) = \left(1 - \sum_{i=1}^{r} \alpha_i g_i\right) \mathbb{C}^e{}_{iso}(\bar{\boldsymbol{B}}), \tag{4.34c}$$

equation (4.34b) follows from the fact that the behavior is considered purely elastic in bulk. α_i are the functions deriving from the discrete form of the stress of equation (4.28) and g_i are the coefficients of the Prony series. Note that the viscoelastic tangent modulus $\mathbb{C}^v$ was derived using Oldroyd objective derivative of equation (4.29) . Hence, to obtain the Jaumann derivative used in Abaqus software we used the following transformation (see [133])

$$\mathbb{C}^J{}_{abcd} = \mathbb{C}^v{}_{abcd} + \frac{1}{2}(\delta_{ac}\tau_{bd} + \tau_{ac}\delta_{bd} + \delta_{ad}\tau_{bc} + \tau_{ad}\delta_{bc}), \tag{4.35}$$

the superscript $\bullet^J$ refers to Jaumann and $\boldsymbol{\delta}$ denotes the Kronecker symbol referring to the second order identity tensor $\boldsymbol{I}$. Finally, the tangent modulus to be implemented in the umat subroutine reads

$$\mathbb{C}^{Abaqus} = \frac{1}{J}\mathbb{C}^J. \tag{4.36}$$

Equations (4.28) and (4.36) with $\boldsymbol{\sigma} = \frac{1}{J}\boldsymbol{\tau}$ describe the implementation of the nonlinear viscoelastic model for a compressible material. In order to investigate incompressible material's behavior using this model, it is sufficient to consider a bulk modulus about $10^4$to 10^6 times the shear modulus with hybrid element, see [62] for details. In this case, p in equations (4.16) became an indeterminate pressure to be obtained from boundary conditions. Henceforth, the behavior is considered incompressible.

4.2.2.3 Flowchart of the Umat subroutine

In figure 4.5, the interaction of the subroutine UMAT with the Abaqus package is illustrated for the Newton-Raphson iterative procedure during a single time increment [62]. The subroutine Umat calculates the components of Cauchy stress and material Jacobian for each Gauss integration point. These quantities are subsequently used by Abaqus to form up the element stiffness matrix. Finally, the global stiffness matrix is assembled by Abaqus using the element stiffness matrices. The user subroutines used in other FE packages to define custom constitutive equations are integrated with the remainder of the program in a similar way and play the same role. These two quantities

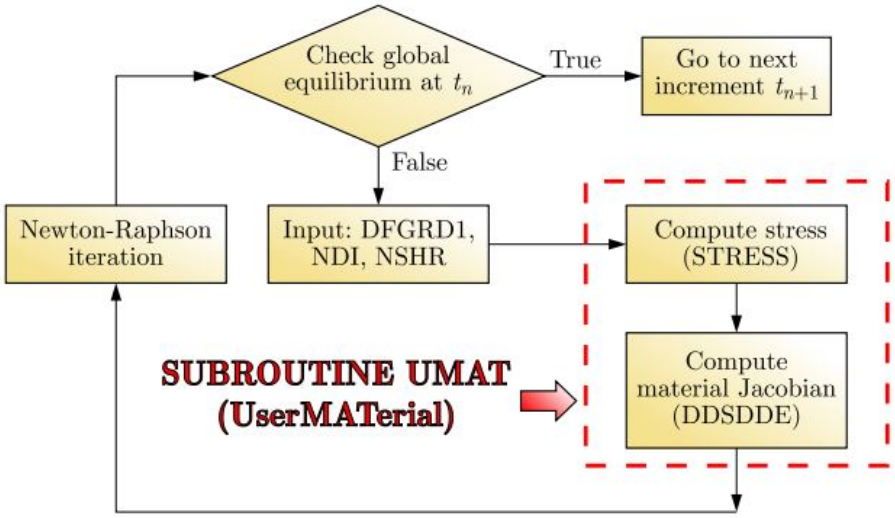

Figure 4.5: Flowchart for the interaction of Abaqus and Umat

are defined in the subroutine Umat by **STRESS** which is a 6×1 vector for the Cauchy stress $\boldsymbol{\sigma}$ and **DDSDDE** which is a 6×6 matrix for the tangent stiffness modulus $\mathbb{C}$. The algorithm of the subroutine Umat is presented by the following algorithm. The subroutine Umat is coded in Fortran 90 and reported in Appendix A

4.3 Conclusions

In this chapter, we presented the implementation of a nonlinear viscoelastic model at finite strain previously proposed in [136] into Abaqus software via a user-defined umat subroutine. The model incorporates a strain dependent relaxation times and based upon the internal state variables approach and the framework of rational thermodynamics and experimental arguments. The decomposition of the deformation gradient tensor into volume-preserving and volumetric parts led to a decomposition in the stress response. The implementation of the model was carried out in two steps. First, the discrete form of the instantaneous stress was calculated from the instantaneous stored elastic energy density. Then, the viscoelastic stress was computed from the instantaneous response following the discretization scheme of Abaqus software. The tangent stiffness necessary for the implementation was computed accordingly using the objective rate derivative of Jaumann.

In the next chapter we present the validation of the implementation procedure outlined in this chapter through the solution of boundary value problems for homogeneous and non homogeneous transformations.

Algorithm 2 Algorithm of the subroutine Umat

1: Calculate Finger tensor $\boldsymbol{B}$
$\boldsymbol{B} = \boldsymbol{F}\boldsymbol{F}^t$
2: Calculate the Jacobian
$J = det[\boldsymbol{B}]^{0.5} = det[\boldsymbol{F}]$
3: Calculate the deviatoric part of $\boldsymbol{B}$
$\bar{\boldsymbol{B}} = J^{\frac{-2}{3}}\boldsymbol{B}$
4: Calculate $tr[\bar{\boldsymbol{B}}]$
5: Calculate $\bar{\boldsymbol{\tau}}$
$\bar{\boldsymbol{\tau}} = 2\bar{\boldsymbol{B}}\frac{\partial\Psi(\bar{\boldsymbol{B}})}{\partial\bar{\boldsymbol{B}}}$
6: Establish unit tensor δ_{ij} and fourth order projection tensor
$\mathbb{P}_{ijkl} = \frac{1}{2}\left(\delta_{ik}\delta_{jl} + \delta_{il}\delta_{jk}\right) - \frac{1}{3}\delta_{ij}\delta_{kl}$
7: Compute $tr[\bar{\boldsymbol{\tau}}]$
8: Calculate isochric contribution $\boldsymbol{\tau}_o^d$
$\boldsymbol{\tau}_o^d{}_{ij} = \bar{\boldsymbol{\tau}}_{ij} - \frac{1}{3}\bar{\boldsymbol{\tau}}_{kk}\delta ij$
9: Calculate volumetric contribution $\boldsymbol{\tau}_o^h$
$\boldsymbol{\tau}_o^h(J) = 2J\boldsymbol{B}\frac{\partial\Psi^{vol}(J)}{\partial\boldsymbol{B}}$
10: Calculate $\bar{\mathbb{C}}$
$\bar{\mathbb{C}} = 4\bar{\boldsymbol{B}}\frac{\partial^2\Psi^{iso}(\bar{\boldsymbol{B}})}{\partial\bar{\boldsymbol{B}}^2}\bar{\boldsymbol{B}}$
11: Calculate isochoric contribution $\mathbb{C}^e{}_{iso}$
$\mathbb{C}^e{}_{iso}(\bar{\boldsymbol{B}}) = 4\boldsymbol{B}\frac{\partial^2\Psi^{iso}(\bar{\boldsymbol{B}})}{\partial\boldsymbol{B}^2}\boldsymbol{B} = \frac{2}{3}tr(\bar{\boldsymbol{\tau}})\mathbb{P} - \frac{2}{3}\left(\boldsymbol{\tau}_o^d\otimes\boldsymbol{I} + \boldsymbol{I}\otimes\boldsymbol{\tau}_o^d\right) + \mathbb{P}:\bar{\mathbb{C}}:\mathbb{P}$
12: Calculate volumetric contribution $\mathbb{C}^e{}_{vol}$
$\mathbb{C}^e{}_{vol}(J) = 4\boldsymbol{B}\frac{\partial^2\Psi^{vol}(J)}{\partial\boldsymbol{B}^2}\boldsymbol{B} = (\frac{\partial^2\Psi^{vol}(J)}{\partial J^2} + J\frac{\partial\Psi^{vol}(J)}{\partial J})\boldsymbol{I}\otimes\boldsymbol{I} - 2J\frac{\partial\Psi^{vol}(J)}{\partial J}\mathbb{I}$
13: Compose elastic tangent stiffness modulus $\mathbb{C}^e$
$\mathbb{C}^e = \mathbb{C}^e{}_{vol}(J) + \mathbb{C}^e{}_{iso}(\bar{\boldsymbol{B}})$
14: Calculate $\mathbb{C}^v{}_{iso}$
$\mathbb{C}^v{}_{iso}(\bar{\boldsymbol{B}}) = \left(1 - \sum_{i=1}^{r}\alpha_i g_i\right)\mathbb{C}^e{}_{iso}(\bar{\boldsymbol{B}})$
15: Compose the viscoelastic tangent stiffness modulus $\mathbb{C}^v$
$\mathbb{C}^v = \mathbb{C}^v{}_{vol}(J) + \mathbb{C}^v{}_{iso}(\bar{\boldsymbol{B}})$
16: Calculate the Jaumann stiffness modulus $\mathbb{C}^J$ and the total stiffness modulus $\mathbb{C}^{Abaqus}$
$\mathbb{C}^J{}_{abcd} = \mathbb{C}^v{}_{abcd} + \frac{1}{2}\left(\boldsymbol{\delta}_{ac}\boldsymbol{\tau}_{bd} + \boldsymbol{\tau}_{ac}\boldsymbol{\delta}_{bd} + \boldsymbol{\delta}_{ad}\boldsymbol{\tau}_{bc} + \boldsymbol{\tau}_{ad}\boldsymbol{\delta}_{bc}\right)$ and $\mathbb{C}^{Abaqus} = \frac{1}{J}\mathbb{C}^J$
17: Calculate the total Kirchhoff stress $\boldsymbol{\tau}$ from (4.28)
18: Calculate the Cauchy stress from the Kirchhoff stress $\boldsymbol{\sigma} = \frac{1}{J}\boldsymbol{\tau}$

CHAPTER 5

VALIDATION OF THE IMPLEMENTATION PROCEDURE WITH HOMOGENEOUS AND NON HOMOGENEOUS TRANSFORMATIONS

Contents

This chapter presents the validation of the implementation of the nonlinear viscoelastic model presented in the previous chapter via the solution of homogeneous and nonhomogeneous initial boundary problems numerically and analytically.

In the literature, several works have been dedicated to the resolution of boundary value problems for nonlinear elastic solids such as the series of papers by Horgan and Saccomandi for simple torsion in [70], pure axial shear in [69], pure azimuthal shear in [71] and helical shear in [72]. For nonlinear viscoelastic materials this subject has been

addressed in many works as well, namely the work of Lee and Wineman for the response of elastomeric bushings in [85] and [84] and the response of viscoelastic cylinder to simple torsion due to [5] and [22].
On the other hand, from a numerical stand point, the definition of the boundary conditions leading to the studied transformation presents a real challenge [32] because an equivalence between the boundary conditions prescribed and the resulting transformation should be ensured. In fact, for a displacement driven study, such as the work presented in this chapter and having the purpose of comparison between analytic and numerical solutions, one needs to carefully define the boundary conditions prescribed in order to obtain the desired transformation.
This chapter is subdivided to three parts. First, the parameters of the instantaneous stored elastic energy density, the relaxation function and the reduced time function involved in the model are specified. Then the validation of the implemented model is addressed via the solution of two boundary value problems for homogeneous transformations which are the simple extension and the simple shear. The equilibrium equations arising from these two transformations allows us to eliminate the indeterminate hydraustatic pressure p accounting for incompressibility. Finally, the problem of simple torsion of hollow cylinder was addressed. Thanks to the axisymmetry of the problem, all the stress components were functions of the radius r only.

5.1 Specification of the parameters of the model

The validation of the implementation procedure presented in the previous chapter is presented in this chapter via the comparison between analytic results and numerical results using the implemented model. To this end, we specify every characteristic function and parameter used in the model. We start by the instantaneous stored elastic energy density which is expressed following the decomposition of the deformation gradient tensor into isochoric and deviatoric parts of equation (2.35) by a Mooney-Rivlin development [123] as

$$\begin{aligned}\Psi(\boldsymbol{B}) =& c_{10}\left(\bar{I}_1-3\right)+c_{20}\left(\bar{I}_1-3\right)^2+c_{11}\left(\bar{I}_1-3\right)\left(\bar{I}_2-3\right)\\ &+c_{01}\left(\bar{I}_2-3\right)+c_{02}\left(\bar{I}_2-3\right)^2+\frac{1}{D_1}(J-1)^2.\end{aligned} \tag{5.1}$$

In which $\bar{I}_1$ and $\bar{I}_2$ are the first two invariants of the deviatoric Finger tensor $\bar{\boldsymbol{B}}$ and $c_{ij}, i,j = 0..2$ and D_1 are material parameters of the Mooney-Rivlin instantaneous elastic stored energy density. Numerical value of these parameters of equation as well as those

of the reduced time function of equation (4.17) are reported in table 5.1. The viscoelastic parameters of the Prony series expansion of equation (4.19) are reported in table 5.2. The initial bulk modulus is given by

$$k_0 = \frac{2}{D_1} = 2.10^5\ MPa, \tag{5.2}$$

and the initial shear modulus is given by

$$\mu_0 = 2(c_{10} + c_{01}) = 0,656\ Mpa. \tag{5.3}$$

From equations (5.2) and (5.3), it is clear that the initial bulk modulus is large enough according to [62] (about 10^4 to 10^6 times the initial shear modulus) to consider the behavior incompressible and hence the $(\bar{\bullet})$ notation for strain tensors and their invariants will be omitted in the reminder of this chapter. Therefore, the Kirchhoff and Cauchy stress tensors are equal.

Parameters	Value (Mpa)
c_{10}	$3.15\ 10^{-1}$
c_{20}	$1.3\ 10^{-2}$
c_{11}	$2.11\ 10^{-2}$
c_{01}	$3.01\ 10^{-2}$
c_{02}	$-1.81\ 10^{-2}$
c_1	$1.62\ 10^{-1}$
c_2	$5.9\ 10^{-3}$
$\frac{1}{D_1}$	$1\ 10^5$

Table 5.1: Model's parameters

g_i	$\tau_i(s)$
0.09	1
0.08	10
0.07	100

Table 5.2: Prony series parameters

As a result of the incompressibility of the material considered, the numerical simulations for the boundary value problems will use hybrid type of element. The material parameters defined in this section will be used in the reminder of this chapter for the solution of homogeneous and non homogeneous boundary value problems.

5.2 Homogeneous transformations

In this section, we validate the implementation of the model using parameters of section 5.1 by solving boundary value problems of simple extension and simple shear.

5.2.1 Simple extension

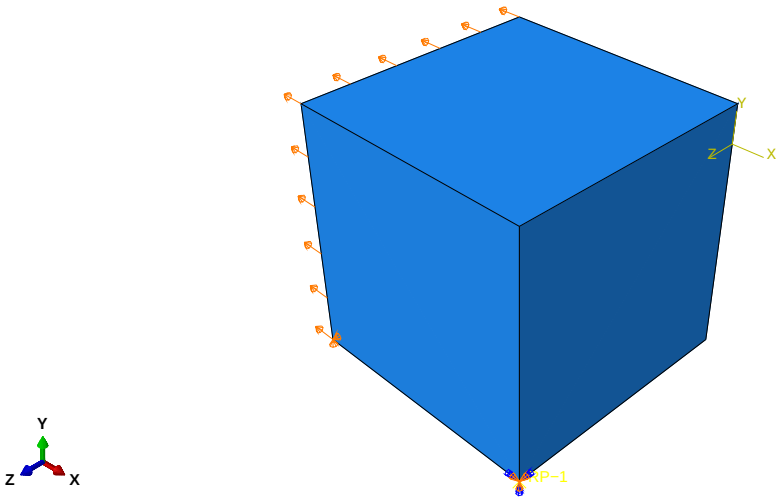

(a) Boundary conditions applied to the cube

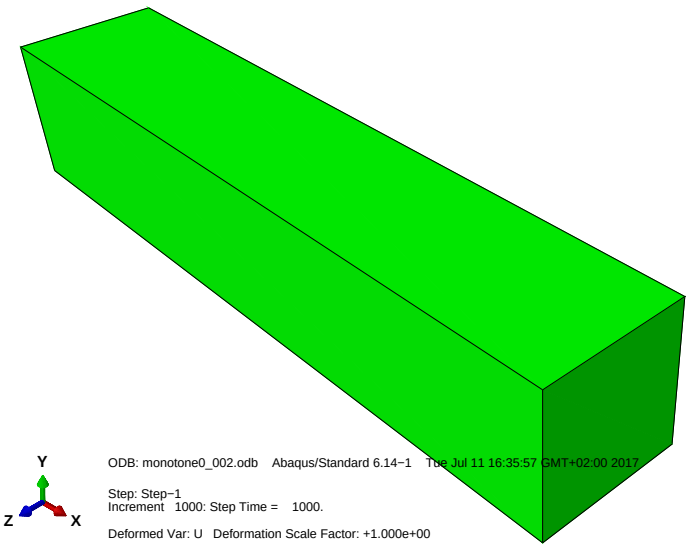

(b) Cube undergoing simple extension deformation

Figure 5.1: Boundary conditions and deformed form of the cube undergoing simple extension deformation

Consider a viscoelastic body undergoing simple extension deformation for which each material point M is referred by its positions X and $x(t)$ in the reference and deformed configurations respectively. Since the transformation is homogeneous, it is sufficient to consider a one cubic element in the simulation with Abaqus software instead of the whole simple extension sample. The boundary conditions applied to the cube guarantees that the transformation is homogeneous and that the Poisson's effect is accepted. The boundary conditions and the deformed form of the cube are reported in figure 5.1. This transformation is defined by

$$x_1(t) = \lambda_1(t)X_1, x_2(t) = \lambda_2(t)X_2 \text{ and } \quad x_3(t) = \lambda_2(t)X_3, \tag{5.4}$$

where λ_1 and λ_2 are the principle stretches. From the constraint of incompressibility $J = 1$, it follows that $\lambda_2 = {\lambda_1}^{-1/2}$. Setting $\lambda_1 = \lambda$, the expression of the deformation gradient tensor $\boldsymbol{F}$ and the left Cauchy-Green strain tensor $\boldsymbol{B}$ using equation (5.4) read

$$\begin{aligned} \boldsymbol{F}(t) =& diag\left(\lambda(t), \lambda^{-1/2}(t), \lambda^{-1/2}(t)\right) \text{and} \\ \boldsymbol{B}(t) =& diag\left(\lambda^2(t), \lambda^{-1}(t), \lambda^{-1}(t)\right), \end{aligned} \tag{5.5}$$

their invariants are

$$I_1 = \lambda^2 + \frac{2}{\lambda}, \;\; I_2 = 2\lambda + \frac{1}{\lambda^2} \text{ and } \; I_3 = 1. \tag{5.6}$$

Note that the only nonzero stress component, assuming free stress lateral surfaces, is

$$\sigma_{11}(t) = \sigma(t) \text{ and } \sigma_{ij} = 0 \; (i \neq 0 \text{ and } \; j \neq 0). \tag{5.7}$$

From equations (4.25), (5.1), (5.6) and (5.7) the nonzero components of the deviatoric part of the instantaneous elastic Cauchy stress tensor are obtained

$$\begin{aligned} \sigma^d_{11} &= 2\left[\frac{1}{3}\left(\left(2\lambda + \frac{1}{\lambda^2}\right)\Psi_2 - \left(\lambda^2 + \frac{2}{\lambda}\right)\Psi_1\right) + \Psi_1\lambda^2 - \frac{\Psi_2}{\lambda^2}\right] \text{and} \\ \sigma^d_{22} &= \sigma^d_{33} = 2\left[\frac{1}{3}\left(\left(2\lambda + \frac{1}{\lambda^2}\right)\Psi_2 - \left(\lambda^2 + \frac{2}{\lambda}\right)\Psi_1\right) + \frac{\Psi_1}{\lambda} - \Psi_2\lambda\right], \end{aligned} \tag{5.8}$$

where Ψ_1 and Ψ_2 denote the derivative of the instantaneous stored elastic energy density Ψ with respect to I_1 and I_2 respectively. Using equation (5.6) these derivative are expressed by

$$\begin{aligned} \Psi_1 &= c_{10} + 2c_{20}\left(\lambda^2 + \frac{2}{\lambda} - 3\right) + c_{11}\left(2\lambda + \frac{1}{\lambda^2} - 3\right) \text{ and} \\ \Psi_2 &= c_{01} + 2c_{02}\left(2\lambda + \frac{1}{\lambda^2} - 3\right) + c_{11}\left(\lambda^2 + \frac{2}{\lambda} - 3\right). \end{aligned} \tag{5.9}$$

Hence, the nonzero Cauchy stress of equation (5.7), using equation (4.16) and (5.8) after eliminating the undetermined pressure p using the second equality of equation (5.7), reads

$$\begin{aligned}\sigma(t) =& \sigma^d_{11}(t) - \sigma^d_{22}(t) - \sum_{i=1}^{3} \frac{g_i}{\tau_i} \int_0^{\xi} \frac{\lambda^2(t-t')}{\lambda^2(t)} \sigma^d_{11}(t-t') \exp\left(-\frac{\xi'}{\tau_i}\right) d\xi' \\ &+ \sum_{i=1}^{3} \frac{g_i}{\tau_i} \int_0^{\xi} \frac{\lambda(t)}{\lambda(t-t')} \sigma^d_{22}(t-t') \exp\left(-\frac{\xi'}{\tau_i}\right) d\xi',\end{aligned} \tag{5.10}$$

using equation (4.28) one leads to the discrete form of the Cauchy stress $\sigma(t)$ in the case of simple extension transformation. With the discrete form of the reduced time of equation (4.27), the discrete form of (5.10) reads

$$\begin{aligned}&\sigma(t_{n+1}) = \sigma^d_{11}(t_{n+1}) - \sigma^d_{22}(t_{n+1}) + \sum_{i=1}^{3} \left(\sigma^i_{22}(t_{n+1}) - \sigma^i_{11}(t_{n+1})\right), \\ &\sigma^i_{22}(0) = \sigma^i_{11}(0) = 0\,; \quad i = 1..3, \\ &\sigma^i_{11}(t_{n+1}) = \frac{\lambda^2(t_{n+1})}{\lambda^2(t_n)} \left(\beta_i g_i \sigma^d_{11}(t_n) + \gamma_i \sigma^i_{11}(t_n)\right) + \alpha_i g_i \sigma^d_{11}(t_{n+1})\,; \quad i = 1..3, \\ &\sigma^i_{22}(t_{n+1}) = \frac{\lambda(t_n)}{\lambda(t_{n+1})} \left(\beta_i g_i \sigma^d_{22}(t_n) + \gamma_i \sigma^i_{22}(t_n)\right) + \alpha_i g_i \sigma^d_{22}(t_{n+1})\,; \quad i = 1..3,\end{aligned} \tag{5.11}$$

where σ^i_{11} and σ^i_{22} are the components of the viscoelastic contribution to the deviatoric part of the Cauchy stress tensor representing the convolution integral in equation (4.16). Equation (5.11) will be used in the comparison to the response of the implemented model for different stretch histories $\lambda(t)$. First, we consider a ramp stretch history defined by

$$\lambda(t) = 1 + \dot{\lambda}\, t \quad ; \quad t \geq 0, \tag{5.12}$$

where $\dot{\lambda}$ is the stretch rate and it is a positive constant. Combining equation (5.11) with the expression of λ in equation (5.12) one leads to the expression of the stress $\sigma(t)$. In figure 5.2 is reported the comparison between the implemented model and the analytic results in terms of the Cauchy stress $\sigma(t)$ and its relative error for the stretch rates of $0.2s^{-1}$, $0.02s^{-1}$ and $0.002s^{-1}$.

Then, a relaxation stretch history is considered for which the stretch is defined by a Heaviside function as

$$\lambda(t) = \begin{cases} 1 & \text{for} \quad t < 0 \\ \lambda_o & \text{for} \quad t > 0 \end{cases}, \tag{5.13}$$

where λ_o is the stretch level of the relaxation process. It should be noted, however, that the stretch history of equation (5.13) is impossible to define. Hence a very brief rise

time (about $10^{-3}s$) to the relaxation level λ_o is employed. Substitution of λ of equation (5.13) in the stress expression of equation (5.11) leads to $\sigma(t)$ in the case of a relaxation process. The analytic result of this stretch history is reported in 5.3 in comparison to the implemented model via the Cauchy stress and its relative error for three values of stretch levels $\lambda = 3$, $\lambda = 2.5$ and $\lambda = 2$.
Finally, a dynamic imposed stretch history is considered for which λ is defined by the following expression

$$\lambda(t) = 1 + A_o \sin \omega t \quad ; \quad t \geq 0, \tag{5.14}$$

where ω is the circular frequency and A_o is the dynamic amplitude of the stretch. Substituting of $\lambda(t)$ of equation (5.14) in equation (5.11) leads to the expression of the stress $\sigma(t)$ for a sinusoidal stretch history. Figure 5.4 shows the result of the comparison between the implemented model and the analytic result in the case of a sinusoidal stretch history for three different circular frequency $\omega = 6.28\ Hz$, $\omega = 3.14\ Hz$ and $\omega = 0.628\ Hz$. From figures 5.2, 5.3 and 5.4 it is concluded that the implementation of the viscoelastic model into Abaqus software is validated since the relative error of the Cauchy stress for the stretch histories considered remain less than 0.7%.

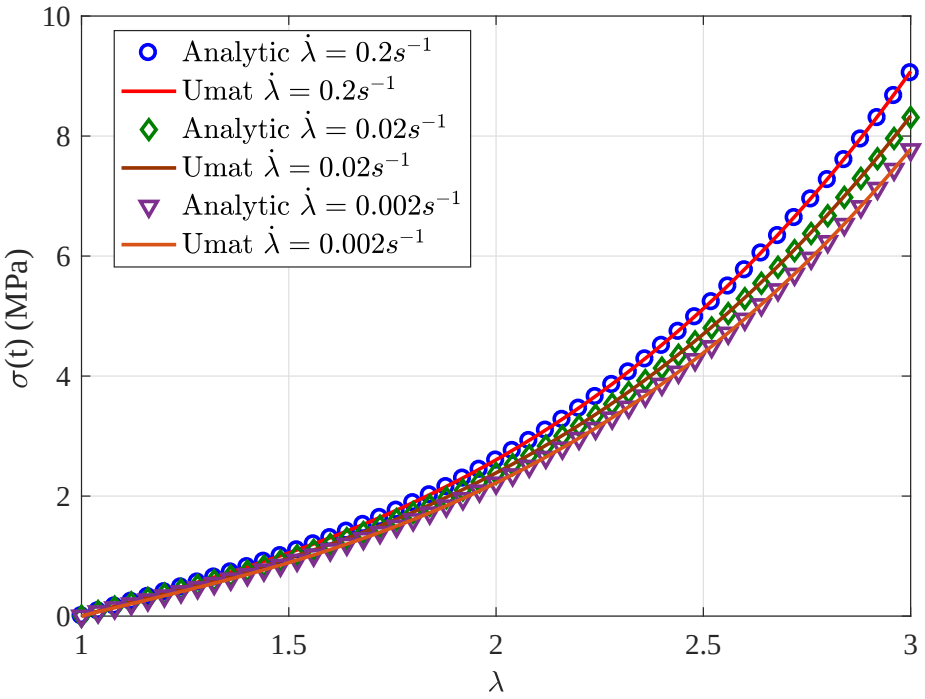

(a) Cauchy stress versus stretch λ for several stretch rates: analytic results (symbol) implemented model (solid curve)

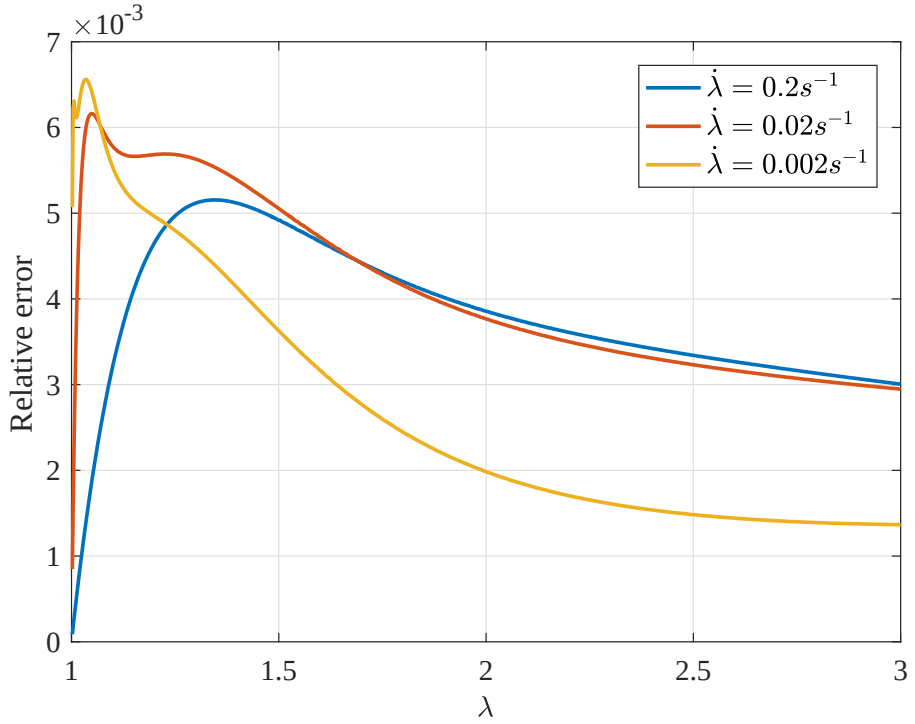

(b) Relative error of Cauchy stress versus stretch λ for several stretch rates

Figure 5.2: Comparison of analytic results with the implemented model in simple extension for a ramp stretch history

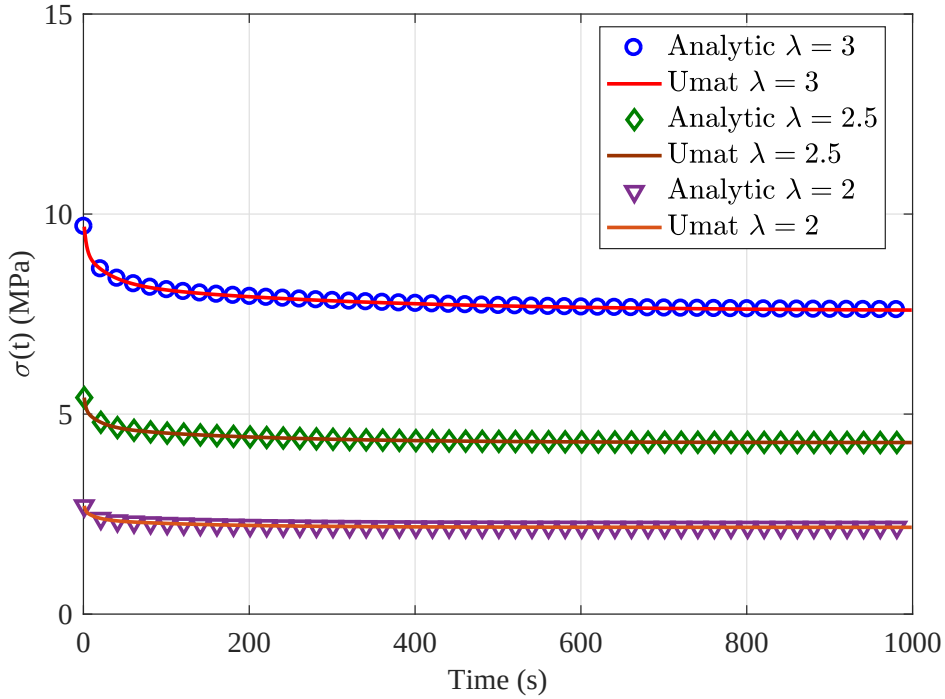

(a) Cauchy stress time for several stretch levels: analytic results (symbol) implemented model (solid curve)

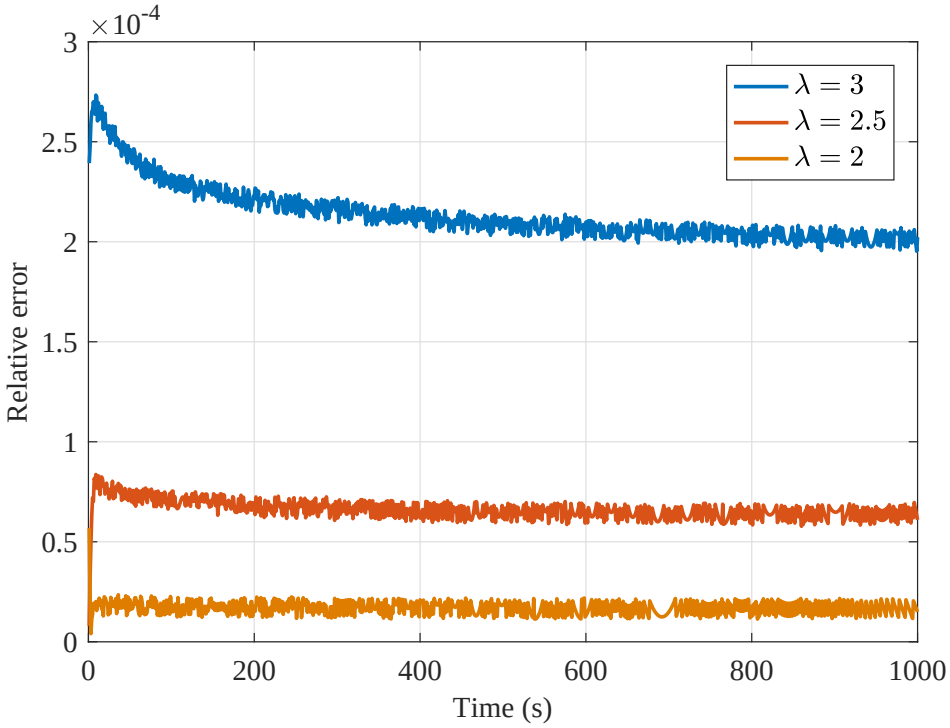

(b) Relative error of Cauchy stress versus time for several stretch levels

Figure 5.3: Comparison of analytic results with the implemented model in simple extension for a relaxation (Heaviside) stretch history

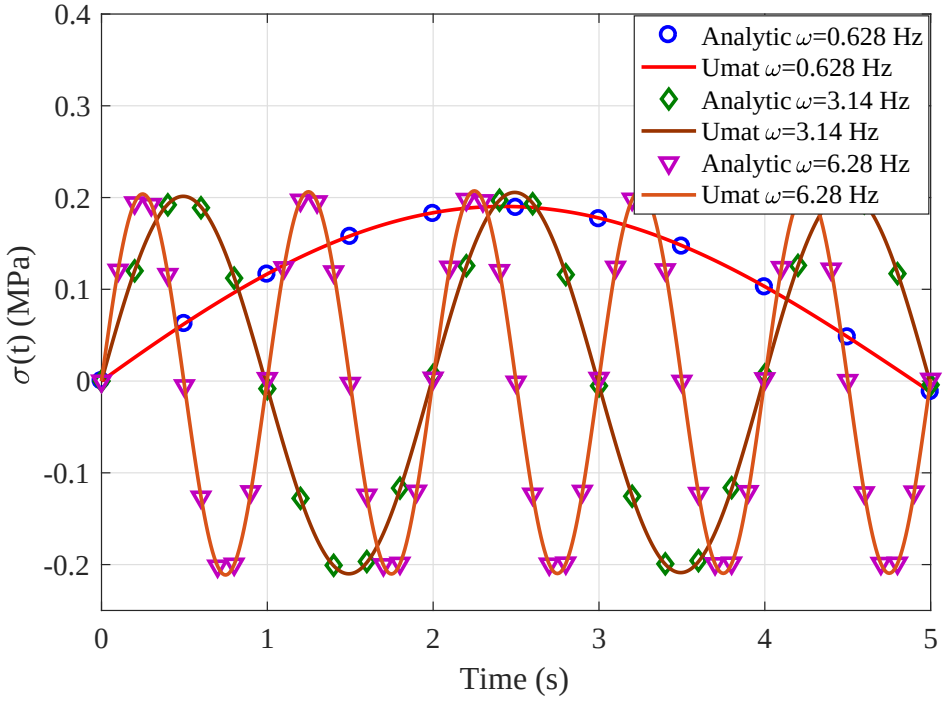

(a) Cauchy stress versus time for several circular frequency ω: analytic results (symbol) implemented model (solid curve)

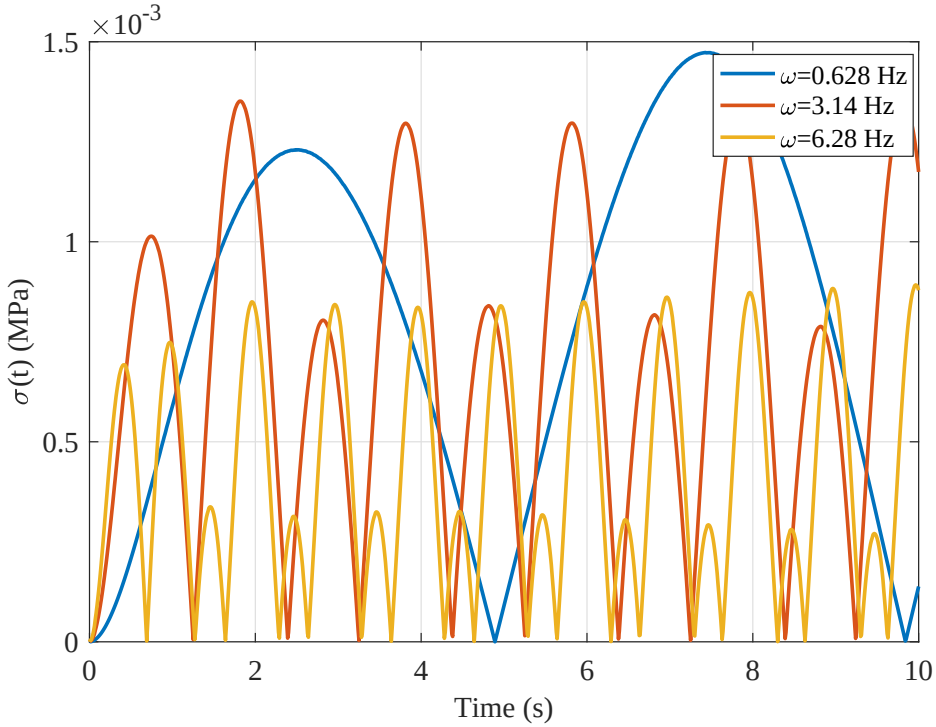

(b) Relative error of Cauchy stress versus time for several circular frequency ω

Figure 5.4: Comparison of analytic results with the implemented model in simple extension for a sinusoidal stretch history

5.2.2 Simple shear

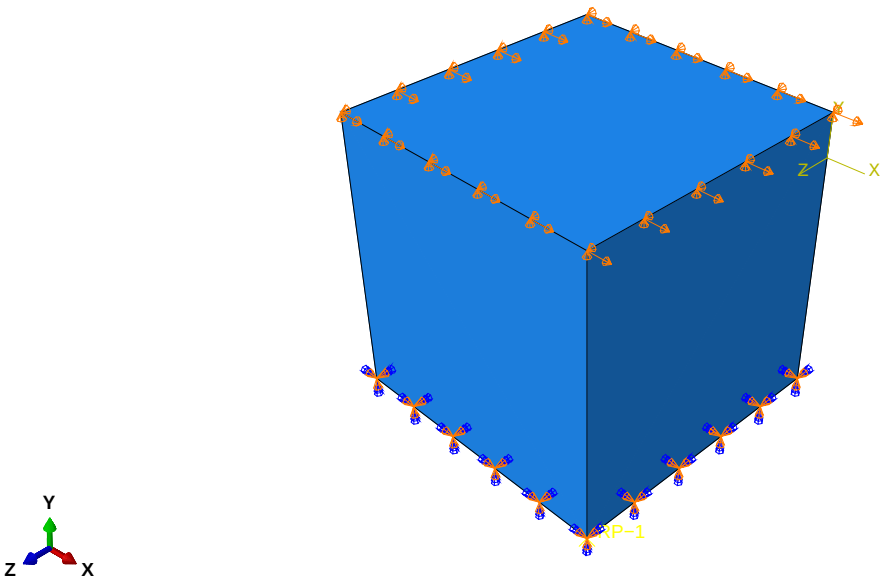

(a) Boundary conditions applied to the cube

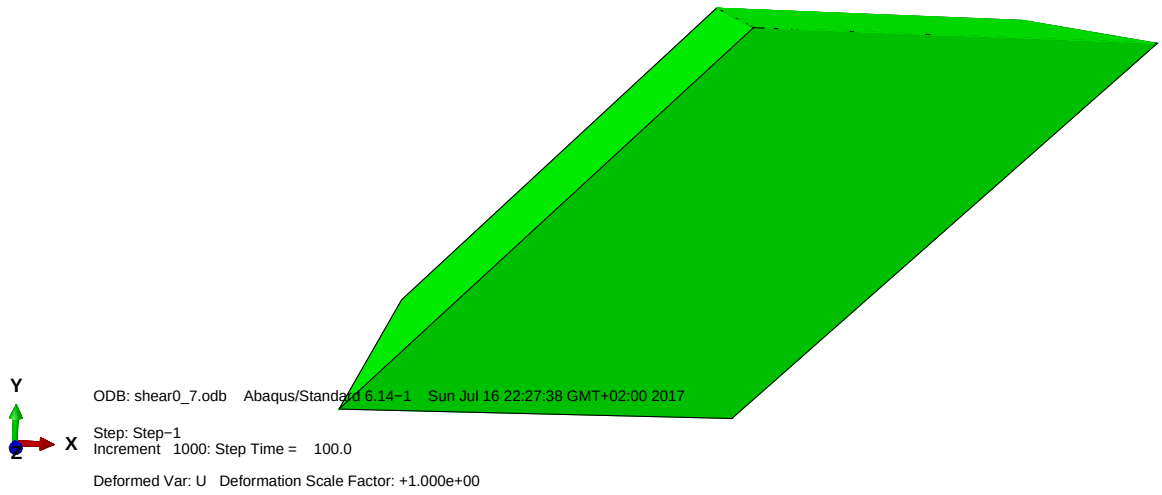

(b) Cube undergoing simple shear deformation

Figure 5.5: Boundary conditions and deformed form of the cube undergoing simple shear deformation

In this section, we investigate the response of the implemented model and analytic results for the homogeneous transformation of simple shear. The model for this transformation is also a single element cube fixed in the bottom face and undergoing a simple shear motion in the top face as it is reported in figure. This transformation is defined by

$$x_1(t) = X_1 + k(t)X_2, x_2(t) = X_2 \text{ and } \quad x_3(t) = X_3, \tag{5.15}$$

where $k(t)$ is the shearing strain. From equation (5.15) the deformation gradient tensor and the left Cauchy-Green strain tensor are obtained

$$\boldsymbol{F} = \begin{pmatrix} 1 & k(t) & 0 \\ 0 & 1 & 0 \\ 0 & 0 & 1 \end{pmatrix}, \quad \boldsymbol{B} = \begin{pmatrix} k^2(t)+1 & k(t) & 0 \\ k(t) & 1 & 0 \\ 0 & 0 & 1 \end{pmatrix}, \tag{5.16}$$

their invariants are

$$I_1 = I_2 = k^2(t) + 3 \text{ and } \; I_3 = 1. \tag{5.17}$$

From equations (4.16), (5.1), (5.16) and (5.17) the nonzero components of the deviatoric part of the elastic instantaneous Cauchy stress tensor are obtained

$$\begin{aligned} \sigma^d_{11} &= 2\left[\tfrac{1}{3}\left(k^2+3\right)(\Psi_2-\Psi_1)+\Psi_1\left(k^2+1\right)-\Psi_2\right] \\ \sigma^d_{22} &= 2\left[\tfrac{1}{3}\left(k^2+3\right)(\Psi_2-\Psi_1)+\Psi_1-\Psi_2\left(k^2+1\right)\right] \\ \sigma^d_{33} &= \tfrac{2}{3}\left(k^2+2\right)(\Psi_2-\Psi_1) \\ \sigma^d_{12} &= \sigma^d_{21} = 2k(\Psi_2+\Psi_1) \end{aligned} \quad . \tag{5.18}$$

where

$$\Psi_1 = c_{10} + (2c_{20} + c_{11})k^2$$
$$\Psi_2 = c_{01} + (2c_{02} + c_{11})k^2$$

Therefore, the nonzero components of the Cauchy stress are obtained from (4.16)

$$\begin{aligned}
\sigma_{11}(t) =& \sigma^d_{11}(t) + p(t) - \sum_{i=1}^{3} \frac{g_i}{\tau_i} \int_0^{\xi} \sigma^d_{11}(t-t') \exp\left(-\frac{\xi'}{\tau_i}\right) d\xi' \\
& - \sum_{i=1}^{3} \frac{g_i}{\tau_i} \int_0^{\xi} 2\left(k(t) - k(t-t')\right) \sigma^d_{12}(t-t') \exp\left(-\frac{\xi'}{\tau_i}\right) d\xi' \\
& - \sum_{i=1}^{3} \frac{g_i}{\tau_i} \int_0^{\xi} \left(k(t) - k(t-t')\right)^2 \sigma^d_{22}(t-t') \exp\left(-\frac{\xi'}{\tau_i}\right) d\xi' \\
\sigma_{22}(t) =& \sigma^d_{22}(t) + p(t) - \sum_{i=1}^{3} \frac{g_i}{\tau_i} \int_0^{\xi} \sigma^d_{22}(t-t') \exp\left(-\frac{\xi'}{\tau_i}\right) d\xi' \qquad . \\
\sigma_{33}(t) =& \sigma^d_{33}(t) + p(t) - \sum_{i=1}^{3} \frac{g_i}{\tau_i} \int_0^{\xi} \sigma^d_{33}(t-t') \exp\left(-\frac{\xi'}{\tau_i}\right) d\xi' \\
\sigma_{12}(t) =& \sigma_{21}(t) = \sigma^d_{12}(t) - \sum_{i=1}^{3} \frac{g_i}{\tau_i} \int_0^{\xi} \sigma^d_{12}(t-t') \exp\left(-\frac{\xi'}{\tau_i}\right) d\xi' \\
& - \sum_{i=1}^{3} \frac{g_i}{\tau_i} \int_0^{\xi} \left(k(t) - k(t-t')\right) \sigma^d_{22}(t-t') \exp\left(-\frac{\xi'}{\tau_i}\right) d\xi'
\end{aligned} \tag{5.19}$$

Our main interest in this work is the shearing stress σ_{12} which will be used in the comparison to the implemented model. The discrete form of this stress reads

$$\begin{aligned}
& \sigma_{12}(t_{n+1}) = \sigma^d_{12}(t_{n+1}) - \sum_{i=1}^{3} \left(\sigma^i_{12}(t_{n+1}) - \sigma^i_{22}(t_{n+1})\right) \\
& \sigma^i_{12}(0) = \sigma^i_{22}(0) = 0 \\
& \sigma^i_{12}(t_{n+1}) = \left(\beta_i g_i \sigma^d_{12}(t_n) + \gamma_i \sigma^i_{12}(t_n)\right) + \alpha_i g_i \sigma^d_{12}(t_{n+1}) \,;\; i = 1..3\text{'} \\
& \sigma^i_{22}(t_{n+1}) = \left(k(t_n) - k(t_{n+1})\right)\left(\beta_i g_i \sigma^d_{22}(t_n) + \gamma_i \sigma^i_{22}(t_n)\right) + \\
& \alpha_i g_i \sigma^d_{22}(t_{n+1}) \,;\; i = 1..3
\end{aligned} \tag{5.20}$$

where σ^i_{12} and σ^i_{22} are the components of the viscoelastic contribution to the deviatoric part of the Cauchy stress tensor representing the convolution integral in equation (4.16). As in the previous section, equation (5.20) will be used in the comparison to the implemented model. Let us consider a monotonic shearing strain of the form

$$k(t) = \dot{k}t \tag{5.21}$$

where $\dot{k}$ is the rate of the shearing strain and it is a positive constant. In figure 5.6 is reported the comparison between the analytic response of equation (5.20) and the implemented model in terms of the shearing Cauchy stress $\sigma_{12}(t)$ and its relative error

for the strain rates of $0.1s^{-1}$, $0.01s^{-1}$ and $0.001s^{-1}$.

The second shearing strain history considered here is the relaxation shearing strain history for which the shearing strain takes the following form :

$$k(t) = \begin{cases} 0 \text{ for } & t < 0 \\ k_o \text{ for } & t > 0 \end{cases}, \tag{5.22}$$

where k_o is the level of the relaxation shearing strain. In figure 5.7 is reported the result of the comparison between the analytic calculation from equations (5.20) and (5.22) and the implemented model for a relaxation shearing strain of $k = 1$, $k = 0.8$ and $k = 0.6$. Note that the difference observed in figure 5.7a is due to the difference in the rise time of the shearing strain which is null for the analytic calculation and can not vanish for the implemented model and is about $10^{-3}s$.

Now we consider a sinusoidal shearing strain history of the form

$$k(t) = k^A \sin(wt), \tag{5.23}$$

where k^A is the amplitude of the shearing strain and w is its circular frequency. The results are reported in figure 5.8 in terms of the shearing Cauchy stress $\sigma_{12}(t)$ and its relative error for three different circular frequencies of $\omega = 0.628\ Hz$, $\omega = 3.14\ Hz$ and $\omega = 6.28\ Hz$. The aim of this section was to further validate the implementation of the model into Abaqus software with another homogeneous transformation of simple shear. It is seen from the relative error of figures 5.6, 5.7 and 5.8 that the response of the implemented model is identical to the analytic calculation since its value for the three shearing strain histories considered remain under 1%.
The aim of this section was to validate the implementation of the nonlinear viscoelastic model presented in chapter 2 for an incompressible isotropic material via homogeneous transformations of simple extension and simple shear. The next section deals with solution of a non homogeneous boundary value problem of simple torsion of a hollow cylinder.

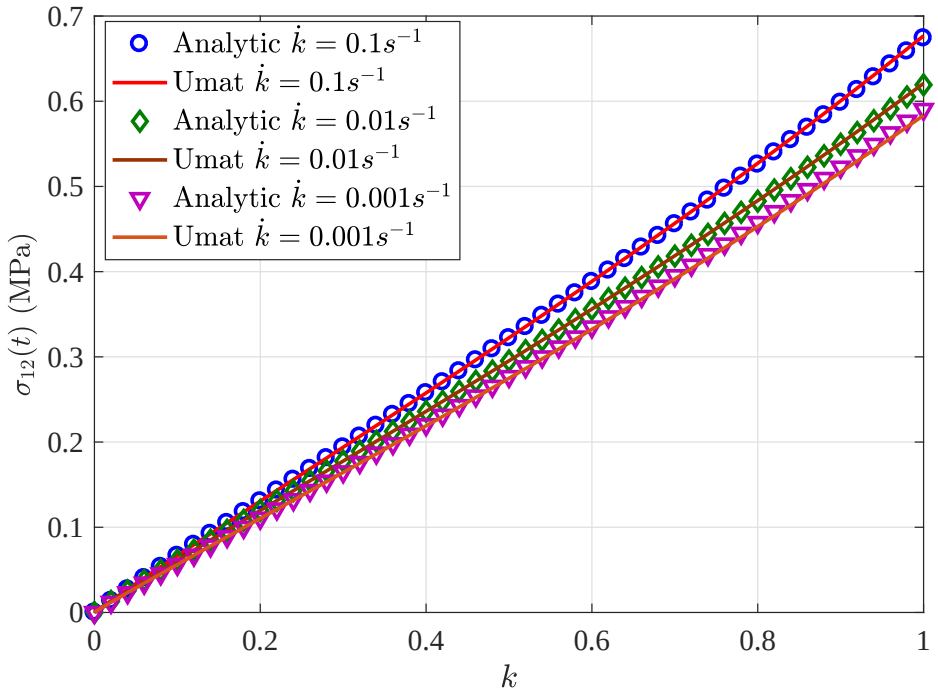

(a) Shearing Cauchy stress versus shearing strain k for several stretch rates: analytic results (symbol) implemented model (solid curve)

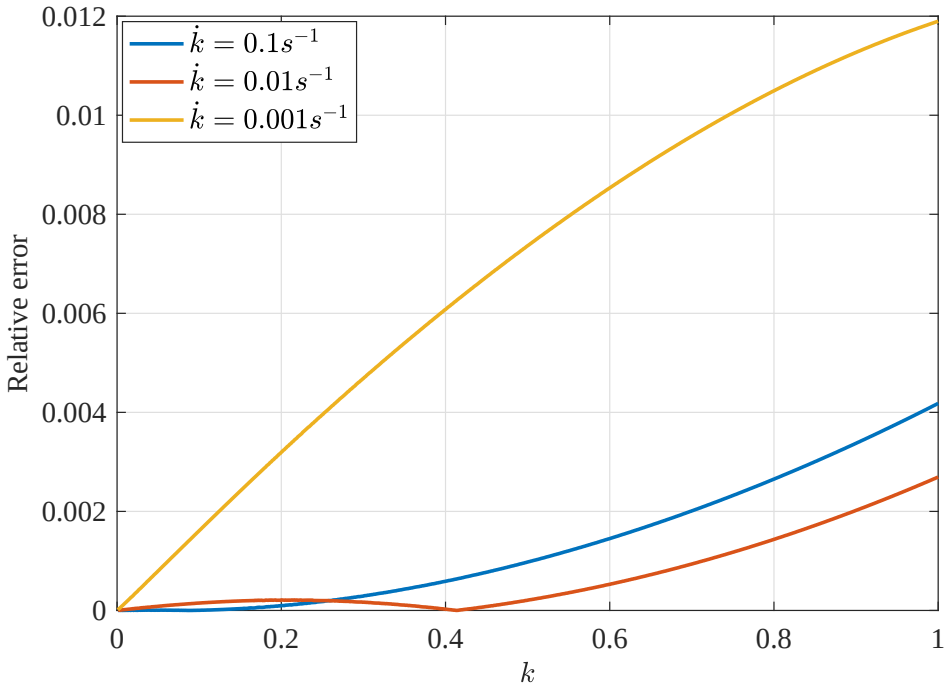

(b) Relative error of Cauchy stress versus shearing strain k for several stretch rates

Figure 5.6: Comparison of analytic results with the implemented model in simple shear for a ramp strain history

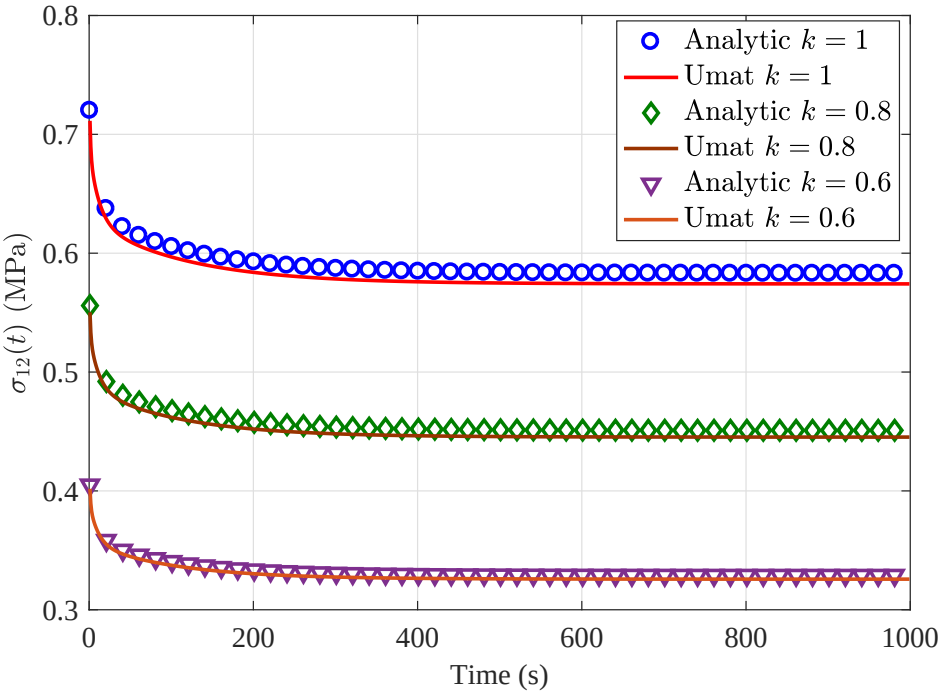

(a) Shearing Cauchy stress versus time for several shearing strain levels: analytic results (symbol) implemented model (solid curve)

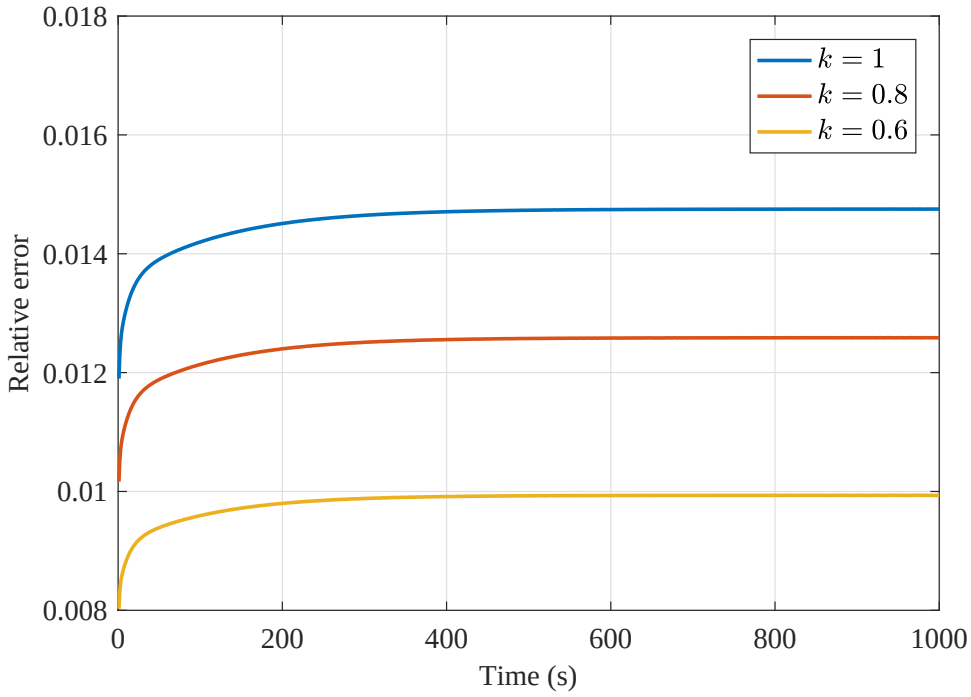

(b) Relative error of shearing Cauchy stress versus time for several shearing strain levels

Figure 5.7: Comparison of analytic results with the implemented model in simple shear for a relaxation (Heaviside) shearing strain history

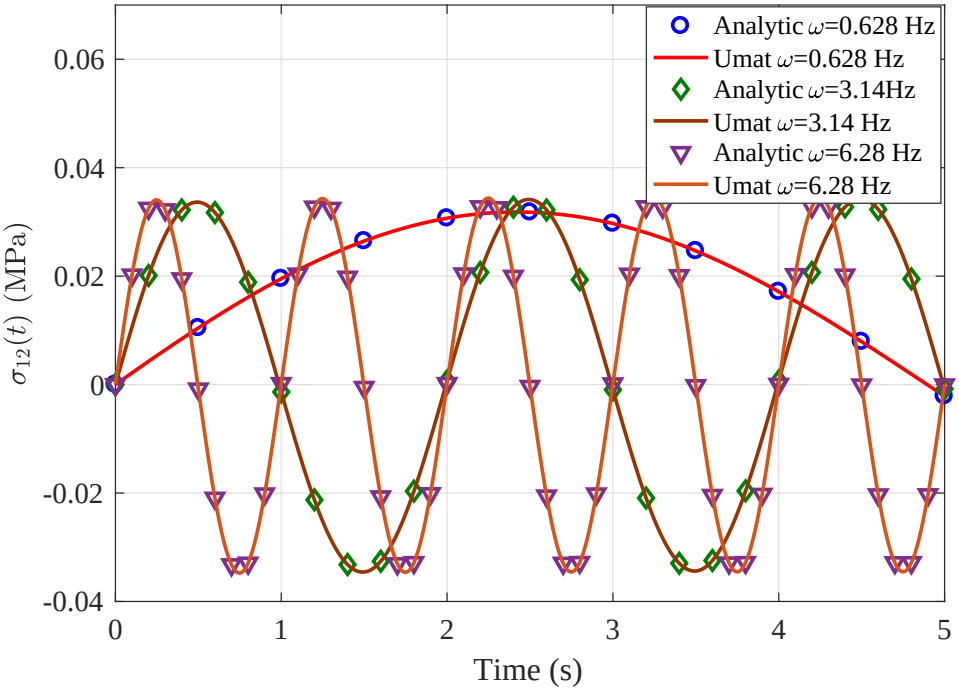

(a) Shearing Cauchy stress versus time for several circular frequency ω: analytic results (symbol) implemented model (solid curve)

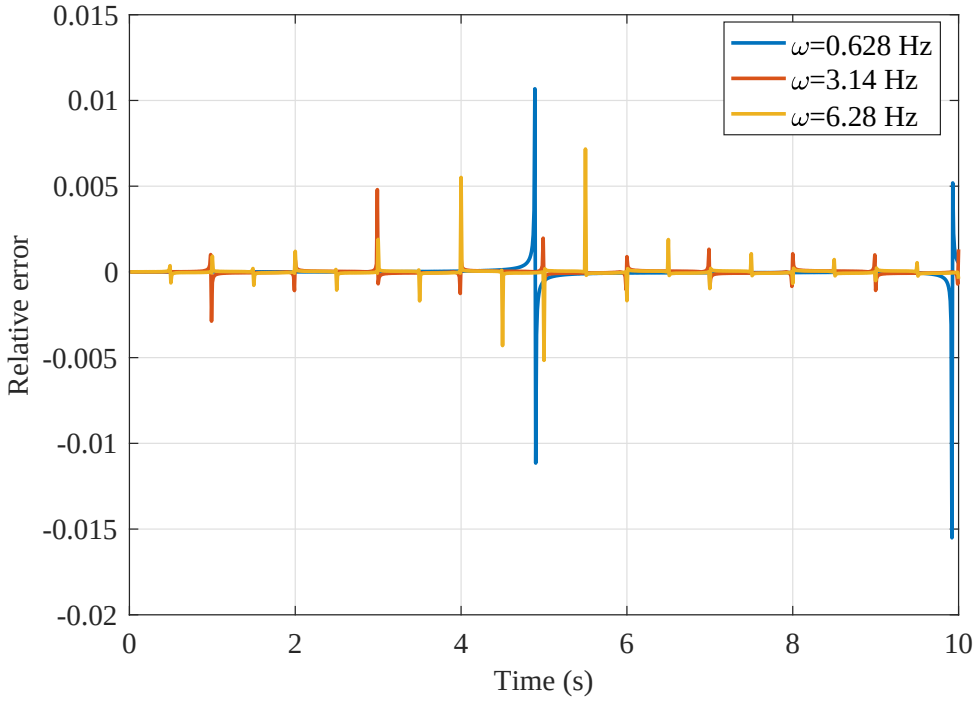

(b) Relative error of shearing Cauchy stress versus time for several circular frequency ω

Figure 5.8: Comparison of analytic results with the implemented model in simple shear for a sinusoidal shearing strain history

5.3 Nonhomogeneous transformation: Simple torsion of hollow cylinder

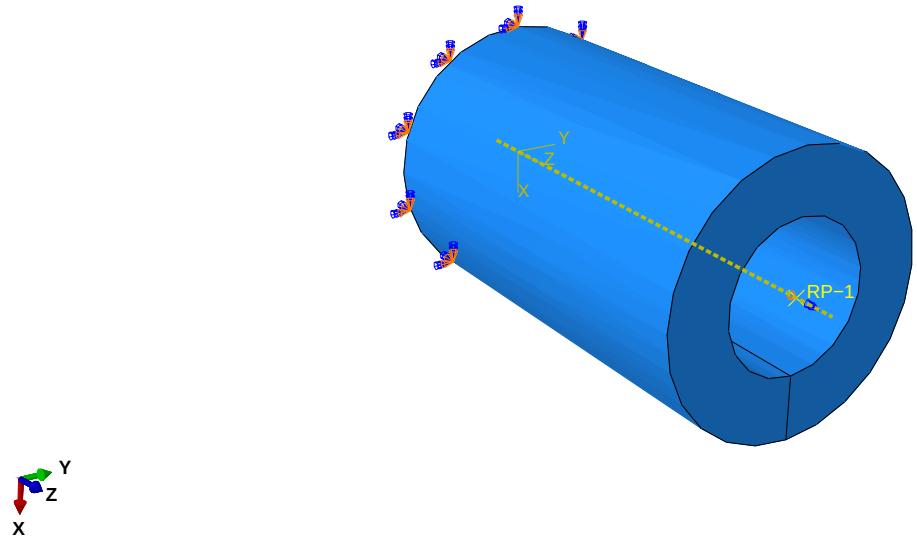

(a) Boundary conditions applied to the cylinder

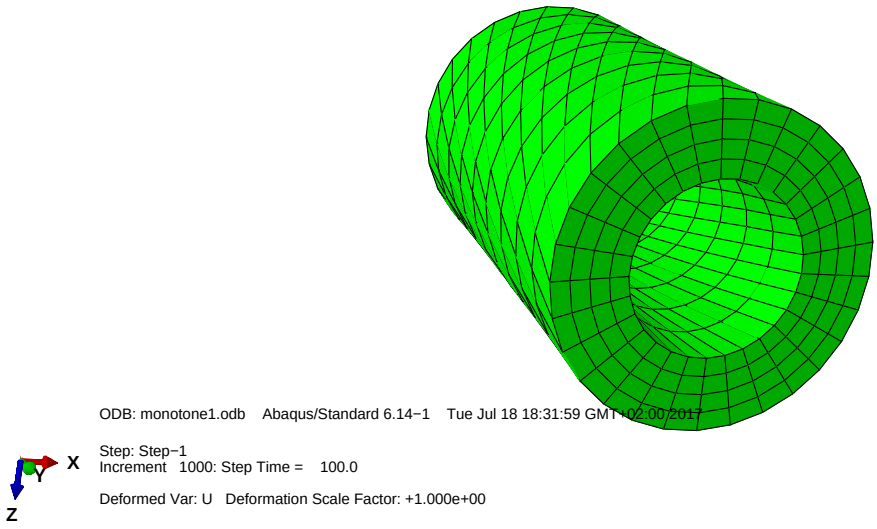

(b) Cylinder undergoing simple torsion

Figure 5.9: Boundary conditions and deformed form of the cylinder undergoing simple torsion deformation

In the previous subsections 5.2.1 and 5.2.2, it has been shown the validation of the implemented model through homogeneous transformations of simple extension and simple shear for several strain histories. In this section, we shall investigate a non-homogeneous transformation of simple torsion of a hollow cylinder. Although, it has been shown in [19] and [38] among others that this problem has a universal solution for elastic and viscoelastic solids. The cylinder has an inner radius of $R_i = 9.85\ mm$ and an outer radius of $R_o = 18.2\ mm$ and a length of $L = 60\ mm$. In cylindrical coordinates, simple torsion of a hollow cylinder is described by $r = R$, $\theta = \Theta + \psi Z$ and $z = Z$, where (r,θ,z) are the cylindrical coordinates of a point in the deformed configuration, (R,Θ,Z) are the cylindrical coordinates of a point in the reference configuration and ψ is the angle of twist per unit length. The finite element model for the simulation of this transformation is presented in figure 5.9 for the deformed and undeformed states. The bottom face of the cylinder is fixed to the referential and an angle of twist is applied to the its top face. The element type for the model is set to be an *8 node linear hybrid brick* **C3D8H**. From this transformation the deformation gradient tensor and the left Cauchy-Green strain tensor read in the orthonormal cylindrical base

$$\boldsymbol{F} = \begin{pmatrix} 1 & 0 & 0 \\ 0 & 1 & \psi r \\ 0 & 0 & 1 \end{pmatrix}, \quad \boldsymbol{B} = \begin{pmatrix} 1 & 0 & 0 \\ 0 & 1+(\psi r)^2 & \psi r \\ 0 & \psi r & 1 \end{pmatrix}, \tag{5.24}$$

their invariants are

$$I_1 = I_2 = (\psi r)^2 + 3,\ I_3 = 1. \tag{5.25}$$

From equations (4.16), (5.1), (5.24) and (5.25) the nonzero components of the deviatoric part of the instantaneous elastic Cauchy stress tensor are obtained

$$\begin{aligned}
\sigma^d_{rr} &= \left[\tfrac{(\psi r)^2+1}{3}(\Psi_2 - \Psi_1) + \Psi_1 - \Psi_2\right] \\
\sigma^d_{\theta\theta} &= \left[\tfrac{(\psi r)^2+1}{3}(\Psi_2 - \Psi_1) + \left((\psi r)^2 + 1\right)\Psi_1 - \Psi_2\right] \\
\sigma^d_{zz} &= \left[\tfrac{(\psi r)^2+1}{3}(\Psi_2 - \Psi_1) + \Psi_1 - \left((\psi r)^2 + 1\right)\Psi_2\right] \\
\sigma^d_{\theta z} &= \sigma^d_{z\theta} = 2\psi r(\Psi_1 + \Psi_2) \\
&\text{where} \\
\Psi_1 &= c_{10} + (2c_{20} + c_{11})(\psi r)^2 \\
\Psi_2 &= c_{01} + (2c_{02} + c_{11})(\psi r)^2
\end{aligned} \tag{5.26}$$

The nonzero Cauchy stress components following from the Constitutive equation (4.16)

in the case of simple torsion of a hollow cylinder are

$$\begin{aligned}
\sigma_{rr}(t) =& \sigma^d_{rr}(t) + p - \sum_{i=1}^{3} \frac{g_i}{\tau_i} \int_0^{\xi} \sigma^d_{rr}(t-t') \exp\left(-\frac{\xi'}{\tau_i}\right) d\xi' - \\
& \sum_{i=1}^{3} \frac{g_i}{3\tau_i} \int_0^{\xi} r\sigma^d_{zz}(t-t') \left(\psi(t) - \psi(t-t')\right)^2 \exp\left(-\frac{\xi'}{\tau_i}\right) d\xi' + \\
& \sum_{i=1}^{3} \frac{2g_i}{3\tau_i} \int_0^{\xi} r\sigma^d_{z\theta}(t-t') \left(\psi(t) - \psi(t-t')\right) \exp\left(-\frac{\xi'}{\tau_i}\right) d\xi' \\
\sigma_{\theta\theta}(t) =& \sigma^d_{\theta\theta}(t) + p - \sum_{i=1}^{3} \frac{g_i}{\tau_i} \int_0^{\xi} \sigma^d_{\theta\theta}(t-t') \exp\left(-\frac{\xi'}{\tau_i}\right) d\xi' + \\
& \sum_{i=1}^{3} \frac{2g_i}{3\tau_i} \int_0^{\xi} r\sigma^d_{zz}(t-t') \left(\psi(t) - \psi(t-t')\right)^2 \exp\left(-\frac{\xi'}{\tau_i}\right) d\xi' - \\
& \sum_{i=1}^{3} \frac{4g_i}{3\tau_i} \int_0^{\xi} r\sigma^d_{z\theta}(t-t') \left(\psi(t) - \psi(t-t')\right) \exp\left(-\frac{\xi'}{\tau_i}\right) d\xi' \quad . \\
\sigma_{zz}(t) =& \sigma^d_{zz}(t) + p - \sum_{i=1}^{3} \frac{g_i}{\tau_i} \int_0^{\xi} \sigma^d_{zz}(t-t') \exp\left(-\frac{\xi'}{\tau_i}\right) d\xi' - \\
& \sum_{i=1}^{3} \frac{g_i}{3\tau_i} \int_0^{\xi} r\sigma^d_{zz}(t-t') \left(\psi(t) - \psi(t-t')\right)^2 \exp\left(-\frac{\xi'}{\tau_i}\right) d\xi' + \\
& \sum_{i=1}^{3} \frac{2g_i}{3\tau_i} \int_0^{\xi} r\sigma^d_{z\theta}(t-t') \left(\psi(t) - \psi(t-t')\right) \exp\left(-\frac{\xi'}{\tau_i}\right) d\xi' \\
\sigma_{z\theta}(t) =& \sigma^d_{z\theta}(t) - \sum_{i=1}^{3} \frac{g_i}{\tau_i} \int_0^{\xi} \sigma^d_{z\theta}(t-t') \exp\left(-\frac{\xi'}{\tau_i}\right) d\xi' - \\
& \sum_{i=1}^{3} \frac{2g_i}{3\tau_i} \int_0^{\xi} r\sigma^d_{z\theta}(t-t') \left(\psi(t) - \psi(t-t')\right) \exp\left(-\frac{\xi'}{\tau_i}\right) d\xi'
\end{aligned} \tag{5.27}$$

The hydrostatic pressure p in equation (5.27) is the most difficult variable to determine. It is determined from the equilibrium equations

$$\frac{\partial \sigma_{rr}}{\partial r} + \frac{\sigma_{rr} - \sigma_{\theta\theta}}{r} = 0 \tag{5.28a}$$

$$\frac{\partial \sigma_{zz}}{\partial z} = 0 \tag{5.28b}$$

$$\frac{\partial \sigma_{zz}}{\partial z} = 0. \tag{5.28c}$$

All stresses are function of r only, from equations (5.28b) and (5.28c) it follows that p is a function of r only

$$p = p(r). \tag{5.29}$$

The hydraustatic pressure is then determined from the first equilibrium equation (5.28a) through

$$\sigma_{rr} = \int_{R_i}^{R_o} \frac{\sigma_{\theta\theta} - \sigma_{rr}}{r}\, dr. \tag{5.30}$$

Replacing σ_{rr} and $\sigma_{\theta\theta}$ by their expressions from (5.27) in equation (5.30) yield the expression of the hydraustatic pressure p. The integral in equation (5.30) is evaluated numerically through a discretization over the radius r using the discrete form of σ_{rr} and $\sigma_{\theta\theta}$ following from equation (4.28). In what follows, a comparison between the numerical simulation of the simple torsion and the analytic results of equation (5.27) will be performed using different histories of the angle of twist ψ. In Abaqus, the cylinder will be built-in from the bottom base and the angle of twist will be applied to the top base of the cylinder. First, we consider a monotonic angle of twist of the form

$$\psi(t) = \dot{\psi} t \tag{5.31}$$

where $\dot{\psi}$ is the rate of the angle of twist. The result of the comparison between the response of the implemented model and equation (5.27) are reported in figure 5.10 in terms of the Von Mises stress for several value of the radius r for a value of the rate of the angle of twist of $1.5\ 10^{-2}\ rad\ s^{-1}$.

For a relaxation process the angle of twist reads

$$\psi(t) = \begin{cases} 0 & \text{for } t < 0 \\ \psi_o & \text{for } t > 0 \end{cases}, \tag{5.32}$$

where $\psi_o = 1.5\ rad$ is the level of the relaxation angle of twist. The components of the Cauchy stress tensor are calculated using equations (5.27) and (5.32). The results are reported in figure 5.11 in terms of the relaxed Von Mises stress for different radii and its distribution along the cylinder.

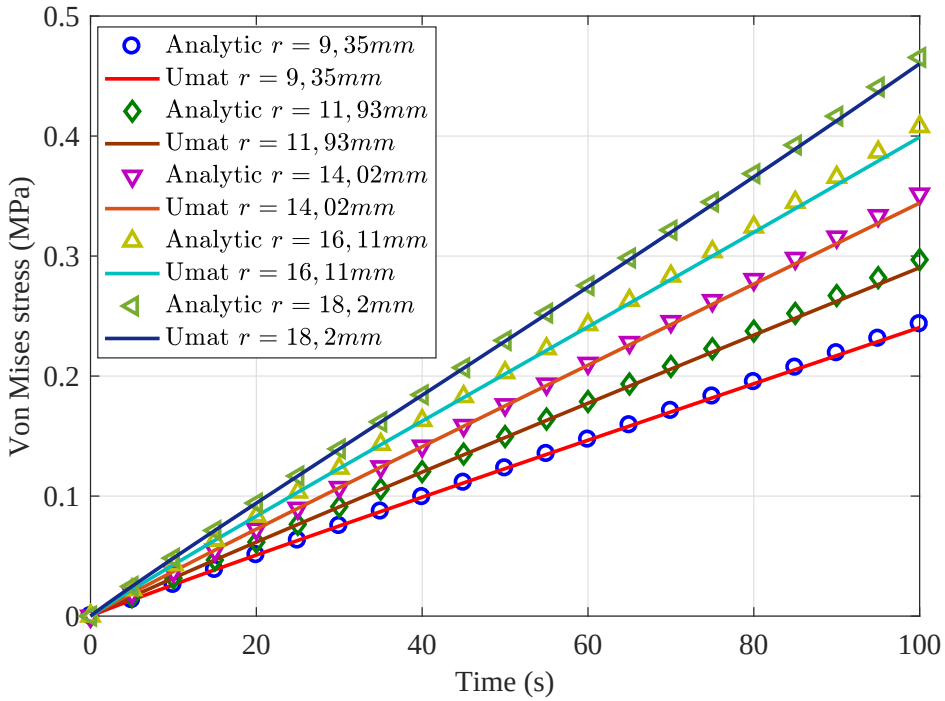

(a) Von Mises stress versus time for several radii: analytic results (symbol) implemented model (solid curve)

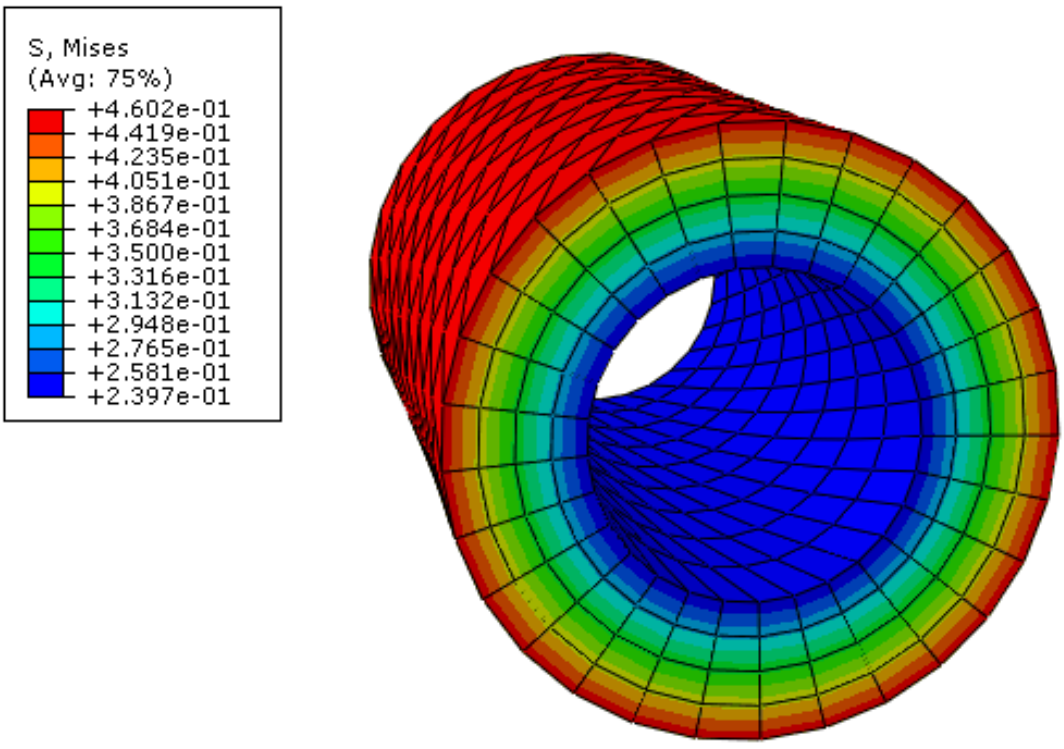

(b) Von Mises stress distribution in the cylinder

Figure 5.10: Comparison of analytic results with the implemented model in simple torsion of hollow cylinder for a ramp angle of twist

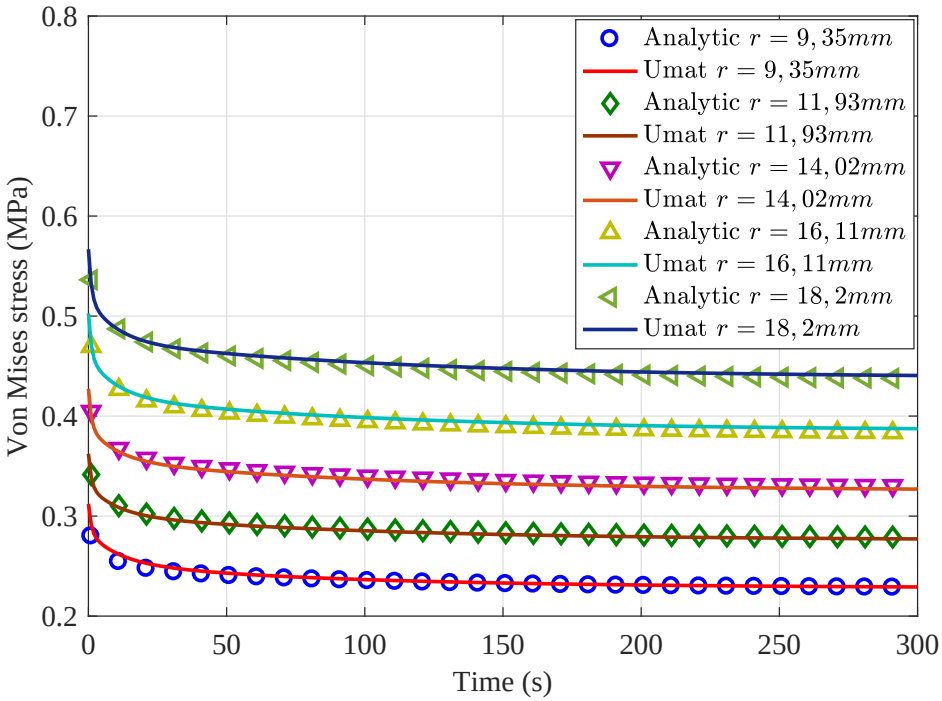

(a) Von Mises stress versus time for several radii: analytic results (symbol) implemented model (solid curve)

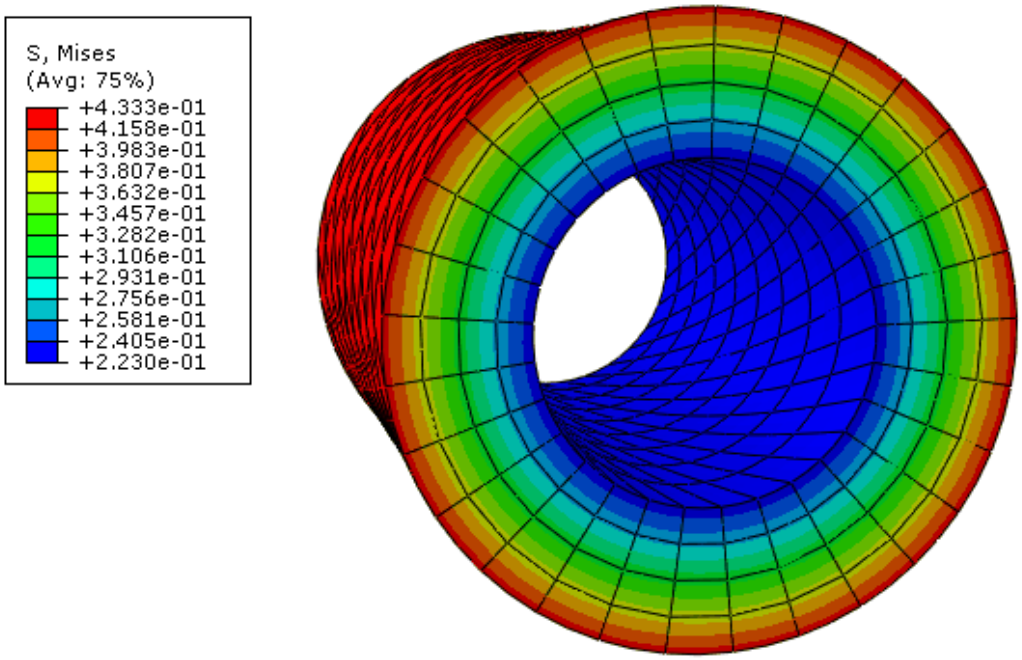

(b) Von Mises stress distribution in the cylinder

Figure 5.11: Comparison of analytic results with the implemented model in simple torsion of hollow cylinder for a relaxed angle of twist

5.4 Conclusions

In this chapter, the implementation procedure explained in chapter 4 was validated through the resolution of several boundary value problems analytically. First, we considered two homogeneous transformations of simple extension and simple shear which led to a total validation of the implemented model. Then, a non-homogeneous transformation was investigated, namely the torsion of a hollow cylinder. The resolution of the equilibrium equations led to the computation of the nonzero stresses for this transformation. A good agreement between the response of the implemented model and analytic results was found for the different strain and strain rates configurations considered. The simulation of real component with complex industrial application such as elastomeric bushings and tires compound is the goal of future work.

Conclusion & Outlooks

This thesis addresses three types of difficulty encountered when dealing with nonlinear materials models

- On the one hand, a behavioral difficulty concerning the choice of the modeling approach to follow in order to build the model capable of predicting experimental results
- On the other hand, a numerical difficulty with respect to the identification of the model's parameters from experimental data arising essentially from the nonlinearity of the model and consequently the minimization problems and from the exactitude of experiments.
- Finally, another numerical difficulty with respect to the implementation of the model into finite element software which needs a special expertise in this area.

In that sense, A three-dimensional viscoelastic model at finite strain that incorporate a strain dependent relaxation times has been proposed to describe nonfactorizable behavior of rubber-like materials. The model is based upon the internal state variables approach and the framework of rational thermodynamics and experimental arguments. Following the decomposition of the deformation gradient tensor, the free energy density was decomposed into a volumetric and deviatoric parts. Motivating by experimental results which show that the relaxation function for the studied material is a function of the strain level, a nonlinear evolution equation for the internal variables,originally postulated from the generalized Maxwell rheological model, was postulated which incorporates a strain dependent relaxation times. This formulation led to the use of the strain dependent reduced time which is analogous to the so-called *thermorheoligically simple behavior*. Therefore, the resulting model is a generalization of the nonlinear viscoelastic model of Simo implemented in Abaqus software. Furthermore, thermodynamic restrictions are fulfilled via a sufficient condition on the model's parameters resulting from the application of the Clausius-Duhem inequality for an arbitrary process. In fact we found

out that the positivity of the reduced time shift function ensures the positivity of the intrinsic dissipation, thereby, the satisfaction of the second law of thermodynamics.
In second place, we made interest to the identification of different parameters involved in the model to experimental data. In fact, a systematic identification of the material parameters for an incompressible nonseparable viscoelastic behavior at finite strain was developed. This procedure relies on the separate identification of hyperelastic potential, viscoelastic kernel and the reduced time function. Considering the form of the constitutive equation of the stress, each characteristic function identification reduces to the solution of a nonlinear optimization problem. The identification of the hyperelastic free energy density was performed using equilibrium experimental data of simple extension and pure shear such that the constraint of stability of the behavior is guaranteed. This constraint is imposed in order to avoid material's parameters leading to non physical responses. Depending on the linearity or nonlinearity of the free energy density with respect to its arguments, the arising minimization problem is linear or nonlinear constrained system respectively. The relaxation function was expressed in terms of a Prony series, its identification is assured using relaxation experiments at low levels of strain typically below 10%. Another way to identify this function is by using dynamic data. From the expression of the dynamic moduli, the Prony series coefficient were identified thanks to a Tikhonov regularization procedure. Finally, the reduced time function was identified numerically thanks to a minimization procedure over the error of the discrete and experimental stresses. At every experimental time the corresponding reduced time is obtained from the minimization of this error and the strain shift function was then obtained numerically. The results of this identification were shown in the third chapter of this thesis and good capacity of the model to depict the behavior of the material was concluded. This identification was also applied to generated data from the multi-integral model of Pipkin and similar results were found.
The second numerical difficulty addressed in this thesis was the implementation of the proposed model into Abaqus software via a user-defined Umat subroutine. To this end, the discrete form of the constitutive equations is computed using the discretization formula used in Abaqus software. First, the instantaneous contribution to the stress is computed by the derivation of the instantaneous stored elastic energy density with respect to the invariants of the Cauchy-Green strain tensors. Then, the total Cauchy stress tensor was computed by introducing the viscoelastic properties following the discretization scheme. Accordingly, the tangent stiffness was calculated from the instantaneous and viscoelastic responses using the objective rate derivative of Jaumann. The

validation of the implemented model was performed through the comparison between analytic solutions of homogeneous boundary value problems of simple extension and simple shear and non-homogeneous one of simple torsion of a hollow cylinder to simulations using the implemented model. Following the formulation of the model, the resolution of the boundary value problems was done with the instantaneous elastic stress, then the total viscoelastic stress is computed according to the constitutive equations. The results reported in the last chapter of this thesis show a total agreement between the analytic and numerical results.

Since the experimental results have shown the relaxation dependency to the level of deformation, it is of huge interest to characterize this link by analytical form which allow a better understanding of such behavior nonlinearity. Furthermore, since the model developed in this work used traditional measure of strain, it is very important to consider logarithmic measure of strain and develop the constitutive equations in this framework and perform the identification of the model's parameters. Also, a very interesting work is to perform the identification of the model's parameters via a minimization procedure over the error between theoretical and experimental energy function like it was performed in [57], which enables us to compare the results obtained from the two identification procedures. Finally, with respect to the implementation of the model one can add the discrete form of the energy function and the dissipation potential in the Umat subroutine since these two quantities are very important especially for viscoelastic materials. Moreover, thanks to the implementation of the model into Abaqus software, one can investigate the response of real elastomeric compounds subjected to real world loading such as bushings, tires and suspension compounds.

APPENDIX A

In this appendix we present the code of the Umat subroutine for the nonlinear viscoelastic model proposed within this work.

```
      subroutine umat(stress,statev,ddsdde,sse,spd,scd,
     1 rpl,ddsddt,drplde,drpldt,
     2 stran,dstran,time,dtime,temp,dtemp,predef,dpred,cmname,
     3 ndi,nshr,ntens,nstatv,props,nprops,coords,drot,pnewdt,
     4 celent,dfgrd0,dfgrd1,noel,npt,layer,kspt,kstep,kinc)
c
      include 'aba_param.inc'
c
      character*80 cmname
      dimension stress(ntens),statev(nstatv),
     1 ddsdde(ntens,ntens),ddsddt(ntens),drplde(ntens),
     2 stran(ntens),dstran(ntens),time(2),predef(1),dpred(1),
     3 props(nprops),coords(3),drot(3,3),dfgrd0(3,3),dfgrd1(3,3)
      double precision :: ib0(3,3),ib1(3,3),bbar0(3,3),bbar1(3,3)
      double precision :: btau0(3,3),bbarcarre0(3,3),fbar0(3,3),fbar1(3,3),tauiso0(3,3)
      double precision :: tauisovis2(3,3,3),tauiso1(3,3),tauvol0(3,3),tauvol1(3,3)
      double precision :: tauisovis1(3,3,3),delta(3,3),tau(3,3),cb(3,3,3,3),A_t(3,3,3)
      double precision :: iip(3,3,3,3),cbar1(3,3,3,3),cisoh(3,3,3,3),cvolh(3,3,3,3)
      double precision :: ic(3,3,3,3),btau1(3,3),gama(3),alfa(3),beta(3),term(3)
      double precision :: invfbar(3,3),deltafbar(3,3),tauisotild0(3,3)!,a(3,3,3)
      double precision :: b(3,3,3),bb(3,3,3),tauvisd(3,3,3),traced(3),tauiso(3,3)
      double precision :: tauvol(3,3),cbar(3,3,3,3),cisovh(3,3,3,3)!,tauvolvis2(3,3,3)
      double precision :: cvolvh(3,3,3,3),bbarcarre1(3,3),cbar11(3,3,3,3),cbar22(3,3,3,3)
    double precision :: invfb1(3,3),tauisotild1(3,3),fb1(3,3),tau1(3,3),fb0(3,3)
    double precision, save :: a(3,3,3),tauvolvis2(3,3,3),tauvolvis1(3,3,3)
      integer :: i,j,k,l,s,t,u,v,ii
      parameter(zero=0.0d0,one=1.0d0,two=2.0d0,three=3.0d0)
      parameter(four=4.0d0,nine=9.0d0,mone=-1.0d0,eight=8.0d0,
```

```
     1 newton=10, toler=1.d-8)
!-----------------------------------------------------------------------
! props of the model
!-----------------------------------------------------------------------
      c10=props(1)
      c01=props(2)
      c02=props(3)
      c20=props(4)
      c11=props(5)
      g1=props(6)
      g2=props(7)
      g3=props(8)
      t1=props(9)
      t2=props(10)
      t3=props(11)
      d1=props(12)
    c1=props(13)
    c2=props(14)
!-----------------------------------------------------------------------
!     rotate deformation gradient tensor
!-----------------------------------------------------------------------
      do i=1,3
    fb0(i,i)=dexp(stran(i)+dstran(i))
    enddo
    fb0(1,2)=stran(4)+dstran(4)
    fb0(1,3)=stran(5)+dstran(5)
    fb0(2,3)=stran(6)+dstran(6)
    do i=1,3
    do j=1,3
    fb0(j,i)=fb0(i,j)
    enddo
    enddo
    fb1=matmul(drot,fb0)
!-----------------------------------------------------------------------
!  finger tensor at the begining of the step
!     fill ib0(i,j)
!-----------------------------------------------------------------------
       do i=1,3
        do j=1,3
        ib0(i,j)=zero
        do k=1,3
!   if ((dfgrd0(i,k) .gt. 1.d-8) .and. ((dfgrd0(j,k) .gt. 1.d-8))) then
        ib0(i,j)=ib0(i,j)+dfgrd0(i,k)*dfgrd0(j,k)
!   endif
        enddo
        enddo
       enddo
!-----------------------------------------------------------------------
! jacobian aj0=dte[b0]^-.5
!-----------------------------------------------------------------------
      aj0=dfgrd0(1, 1)*dfgrd0(2, 2)*dfgrd0(3, 3)+
```

```
     1 dfgrd0(2, 1)*dfgrd0(3, 2)*dfgrd0(1, 3)+
     2 dfgrd0(3, 1)*dfgrd0(1, 2)*dfgrd0(2, 3)-
     3 dfgrd0(3, 1)*dfgrd0(2, 2)*dfgrd0(1, 3)-
     4 dfgrd0(1, 1)*dfgrd0(3,2)*dfgrd0(2, 3)-
     5 dfgrd0(2, 1)*dfgrd0(1, 2)*dfgrd0(3, 3)
!-----------------------------------------------------------------------
!     bbar0
!-----------------------------------------------------------------------
       do i=1,3
        do j=1,3
        bbar0(i,j)=zero
        bbar0(i,j)=ib0(i,j)/(aj0**(two/three))
        enddo
       enddo
!-----------------------------------------------------------------------
!     fbar0
!-----------------------------------------------------------------------
       do i=1,3
        do j=1,3
        fbar0(i,j)=zero
!   if (dfgrd0(i,j) .gt. 1.d-8) then
        fbar0(i,j)=dfgrd0(i,j)/(aj0**(one/three))
!   endif
        enddo
       enddo
!-----------------------------------------------------------------------
!   calcul of the inverse of fbar0 : invfbar
!-----------------------------------------------------------------------

!     calculate the inverse of the matrix
      invfbar(1,1) =(fbar0(2,2)*fbar0(3,3)-
     1 fbar0(2,3)*fbar0(3,2))
      invfbar(2,1) = mone*(fbar0(2,1)*fbar0(3,3)-
     1 fbar0(2,3)*fbar0(3,1))
      invfbar(3,1) = (fbar0(2,1)*fbar0(3,2)-
     1 fbar0(2,2)*fbar0(3,1))
      invfbar(1,2) = mone*(fbar0(1,2)*fbar0(3,3)-
     1 fbar0(1,3)*fbar0(3,2))
      invfbar(2,2) =(fbar0(1,1)*fbar0(3,3)-
     1 fbar0(1,3)*fbar0(3,1))
      invfbar(3,2) = mone*(fbar0(1,1)*fbar0(3,2)-
     1 fbar0(1,2)*fbar0(3,1))
      invfbar(1,3) =(fbar0(1,2)*fbar0(2,3)-
     1 fbar0(1,3)*fbar0(2,2))
      invfbar(2,3) = mone*(fbar0(1,1)*fbar0(2,3)-
     1 fbar0(1,3)*fbar0(2,1))
      invfbar(3,3) =(fbar0(1,1)*fbar0(2,2)-
     1 fbar0(1,2)*fbar0(2,1))
!-----------------------------------------------------------------------
!   bbarcarre0
!-----------------------------------------------------------------------
```

```
       do i=1,3
        do j=1,3
        bbarcarre0(i,j)=zero
        do k=1,3
        bbarcarre0(i,j)=bbarcarre0(i,j)+bbar0(i,k)*bbar0(k,j)
        enddo
        enddo
       enddo
       trb0=bbarcarre0(1,1)+bbarcarre0(2,2)+bbarcarre0(3,3)
!-----------------------------------------------------------------------
!      invariants bi10 and bi20 at the begining of the step
!-----------------------------------------------------------------------
      bi10=zero
      do i=1,3
      bi10=bi10+bbar0(i,i)
      enddo
      bi20=zero
      bi20=(one/two)*(bi10*bi10-trb0)
!-----------------------------------------------------------------------
!   second order identity tensor
!-----------------------------------------------------------------------
       do i=1,3
        do j=1,3
         delta(i,j)=zero
        enddo
       enddo
       do i=1,3
       delta(i,i)=one
       enddo
!-----------------------------------------------------------------------
!    tensor btau0
!-----------------------------------------------------------------------
      do i=1,3
      do j=1,3
      btau0(i,j)=zero
      btau0(i,j)=two*c10*bbar0(i,j)+
     1 two*c01*(bi10*bbar0(i,j)-bbarcarre0(i,j))+
     2 four*c20*(bi10-three)*bbar0(i,j)+
     3 four*c02*(bi20-three)*(bi10*bbar0(i,j)-bbarcarre0(i,j))+
     4 two*c11*(bi20-three)*bbar0(i,j)+
     5 two*c11*(bi10-three)*(bi10*bbar0(i,j)-bbarcarre0(i,j))
      enddo
      enddo
!-----------------------------------------------------------------------
!       tauiso0: hyperelastic deviator of kirrcchoff stress the
!              begining of the step
!-----------------------------------------------------------------------
      tracebtau0=btau0(1,1) + btau0(2,2) + btau0(3,3)
      tauiso0(1,1)=btau0(1,1) - (one/three)*tracebtau0
      tauiso0(2,2)=btau0(2,2) - (one/three)*tracebtau0
      tauiso0(3,3)=btau0(3,3) - (one/three)*tracebtau0
```

```
      tauiso0(1,2)=btau0(1,2)
      tauiso0(1,3)=btau0(1,3)
      tauiso0(2,3)=btau0(2,3)
      tauiso0(2,1)=btau0(2,1)
      tauiso0(3,1)=btau0(3,1)
      tauiso0(3,2)=btau0(3,2)
!-----------------------------------------------------------------------
!      tauvol0: hyperelastic volumetric kirchhoff stress at the
!               begining of the step
!-----------------------------------------------------------------------
      p=((two*aj0)*(aj0-one))/d1
      do i=1,3
       do j=1,3
       tauvol0(i,j)=zero
       tauvol0(i,j)=p*delta(i,j)
       enddo
      enddo

!-----------------------------------------------------------------------
!  finger tensor at the end of the step
!-----------------------------------------------------------------------
!    set ib1(i,j) to zero
!-----------------------------------------------------------------------
       do i=1,3
        do j=1,3
        ib1(i,j)=zero
        enddo
       enddo
!-----------------------------------------------------------------------
!     fill ib1(i,j)
!-----------------------------------------------------------------------
       do i=1,3
        do j=1,3
        ib1(i,j)=zero
        do k=1,3
!   if ((dfgrd1(i,k) .gt. 1.d-8) .and. ((dfgrd1(j,k) .gt. 1.d-8))) then
        ib1(i,j)=ib1(i,j)+dfgrd1(i,k)*dfgrd1(j,k)
!   endif
        enddo
        enddo
       enddo
!-----------------------------------------------------------------------
! jacobian aj1=dte[b1]^-.5, at the end of the time increment
!-----------------------------------------------------------------------
      aj1=dfgrd1(1, 1)*dfgrd1(2, 2)*dfgrd1(3, 3)+
     1 dfgrd1(2, 1)*dfgrd1(3, 2)*dfgrd1(1, 3)+
     2 dfgrd1(3, 1)*dfgrd1(1, 2)*dfgrd1(2, 3)-
     3 dfgrd1(3, 1)*dfgrd1(2, 2)*dfgrd1(1, 3)-
     4 dfgrd1(1, 1)*dfgrd1(3, 2)*dfgrd1(2, 3)-
     5 dfgrd1(2, 1)*dfgrd1(1, 2)*dfgrd1(3, 3)
    aj11=fb1(1, 1)*fb1(2, 2)*fb1(3, 3)+
```

```
     1 fb1(2, 1)*fb1(3, 2)*fb1(1, 3)+
     2 fb1(3, 1)*fb1(1, 2)*fb1(2, 3)-
     3 fb1(3, 1)*fb1(2, 2)*fb1(1, 3)-
     4 fb1(1, 1)*fb1(3, 2)*fb1(2, 3)-
     5 fb1(2, 1)*fb1(1, 2)*fb1(3, 3)
!-----------------------------------------------------------------------
!     bbar1: at the end of the increment
!-----------------------------------------------------------------------
       do i=1,3
        do j=1,3
        bbar1(i,j)=zero
        bbar1(i,j)=ib1(i,j)/(aj1**(two/three))
        enddo
       enddo
!-----------------------------------------------------------------------
!     fbar1: at the end of the increment
!-----------------------------------------------------------------------
       do i=1,3
        do j=1,3
        fbar1(i,j)=zero
!   if (dfgrd1(i,j) .gt. 1.d-8) then
        fbar1(i,j)=dfgrd1(i,j)/(aj1**(one/three))
!   endif
        enddo
       enddo
!-----------------------------------------------------------------------
!   calcul of the inverse of fbar1 : invfb1
!-----------------------------------------------------------------------
    invfb1(1,1) =(fbar1(2,2)*fbar1(3,3)-
     1 fbar1(2,3)*fbar1(3,2))
      invfb1(2,1) = mone*(fbar1(2,1)*fbar1(3,3)-
     1 fbar1(2,3)*fbar1(3,1))
      invfb1(3,1) = (fbar1(2,1)*fbar1(3,2)-
     1 fbar1(2,2)*fbar1(3,1))
      invfb1(1,2) = mone*(fbar1(1,2)*fbar1(3,3)-
     1 fbar1(1,3)*fbar1(3,2))
      invfb1(2,2) =(fbar1(1,1)*fbar1(3,3)-
     1 fbar1(1,3)*fbar1(3,1))
      invfb1(3,2) = mone*(fbar1(1,1)*fbar1(3,2)-
     1 fbar1(1,2)*fbar1(3,1))
      invfb1(1,3) =(fbar1(1,2)*fbar1(2,3)-
     1 fbar1(1,3)*fbar1(2,2))
      invfb1(2,3) = mone*(fbar1(1,1)*fbar1(2,3)-
     1 fbar1(1,3)*fbar1(2,1))
      invfb1(3,3) =(fbar1(1,1)*fbar1(2,2)-
     1 fbar1(1,2)*fbar1(2,1))
!-----------------------------------------------------------------------
! calcul of the tensor deltafbar=fbar1*fbar0^-1
!-----------------------------------------------------------------------
      do i=1,3
       do j=1,3
```

```
       deltafbar(i,j)=zero
        do k=1,3
        deltafbar(i,j)=deltafbar(i,j)+fbar1(i,k)*invfbar(k,j)
        enddo
       enddo
      enddo
!-----------------------------------------------------------------------
!   bbarcarre1: b^2 at the end of the increment
!-----------------------------------------------------------------------
      do i=1,3
      do j=1,3
      bbarcarre1(i,j)=zero
      do k=1,3
      bbarcarre1(i,j)=bbarcarre1(i,j)+bbar1(i,k)*bbar1(k,j)
      enddo
      enddo
      enddo
      trb1=bbarcarre1(1,1)+bbarcarre1(2,2)+bbarcarre1(3,3)

!-----------------------------------------------------------------------
!      invariants bi11 and bi21 at the end of the increment
!-----------------------------------------------------------------------
      bi11=zero
      do i=1,3
      bi11=bi11+bbar1(i,i)
      enddo
      bi21=zero
      bi21=(one/two)*(bi11*bi11-trb1)
!-----------------------------------------------------------------------
!    tensor btau1 at the end of the increment
!-----------------------------------------------------------------------
      do i=1,3
      do j=1,3
      btau1(i,j)=zero
      btau1(i,j)=two*c10*bbar1(i,j)+
     1 two*c01*(bi11*bbar1(i,j) - bbarcarre1(i,j))+
     2 four*c20*(bi11-three)*bbar1(i,j)+
     3 four*c02*(bi21-three)*(bi11*bbar1(i,j) - bbarcarre1(i,j))+
     4 two*c11*(bi21-three)*bbar1(i,j)+
     5 two*c11*(bi11-three)*(bi11*bbar1(i,j) - bbarcarre1(i,j))
      enddo
      enddo
!-----------------------------------------------------------------------
!       tauiso1:deviatoric hyperelastic kirchhoff stress at the
!              end of the increment
!-----------------------------------------------------------------------
      tracebtau1=btau1(1,1) + btau1(2,2) + btau1(3,3)
      tauiso1(1,1)=btau1(1,1) - (one/three)*tracebtau1
      tauiso1(2,2)=btau1(2,2) - (one/three)*tracebtau1
      tauiso1(3,3)=btau1(3,3) - (one/three)*tracebtau1
      tauiso1(1,2)=btau1(1,2)
```

```
      tauiso1(1,3)=btau1(1,3)
      tauiso1(2,3)=btau1(2,3)
      tauiso1(2,1)=btau1(2,1)
      tauiso1(3,1)=btau1(3,1)
      tauiso1(3,2)=btau1(3,2)
!-----------------------------------------------------------------------
!      tauvol1: volumetric hyperelastic kirchhoff stress at the
!               end of the encrement
!-----------------------------------------------------------------------
      p1=((two*aj1)*(aj1-one))/d1
      do i=1,3
       do j=1,3
       tauvol1(i,j)=zero
       tauvol1(i,j)=p1*delta(i,j)
       enddo
      enddo
    if((kinc.le.1).and.(kstep.eq.1)) then
         !
         ! this is the first increment, of the first step.
         !  Give initial conditions.
         !
         do i=1,3
            A_t(i,:,:) = zero
         enddo
         !
      else
         !
         ! this is not the first increment, read old values
         !
         do i=1,3
            ii = (i-1)*6
            A_t(i,1,1) = statev(1+ii)
            A_t(i,2,2) = statev(2+ii)
            A_t(i,3,3) = statev(3+ii)
            A_t(i,2,3) = statev(4+ii)
            A_t(i,3,2) = A_t(i,2,3)
            A_t(i,1,3) = statev(5+ii)
            A_t(i,3,1) = A_t(i,1,3)
            A_t(i,1,2) = statev(6+ii)
            A_t(i,2,1) = A_t(i,1,2)
         enddo
         !
      endif
!   pnewdt=two/three!dexp(mone*c01*(bi11-three))
!-----------------------------------------------------------------------
! calcul of viscoelastic functions: alfa, beta and gama
!-----------------------------------------------------------------------
      dt1=dexp(mone*c1*(bi11-three)-c2*(bi21-three))*dtime
      do i=1,3
      gama(i)=dexp(mone*(dt1/props(8+i)))
      enddo
```

```
      do i=1,3
      term(i)=props(8+i)/dt1
      alfa(i)=one-term(i)+term(i)*gama(i)
      enddo
      do i=1,3
      beta(i)=term(i)-term(i)*gama(i)-gama(i)
      enddo
!-----------------------------------------------------------------------
!    calcul of tauisotild0=deltafbar*tauiso0*deltafbar^t
!-----------------------------------------------------------------------
      do i=1,3
       do j=1,3
       tauisotild0(i,j)=zero
       enddo
      enddo

      tauisotild0=matmul(matmul(invfbar,tauiso0),transpose(invfbar))
    tauisotild1=matmul(matmul(invfb1,tauiso1),transpose(invfb1))


!-----------------------------------------------------------------------
!  calcul of viscoelastic stresses tauisovis1 and tauvolvis1
!     a(i,j,k), b(i,j,k) : variables de passage
!-----------------------------------------------------------------------
      do k=1,3
      tauisovis2(k,:,:)=(beta(k)*props(k+5)*tauisotild0)+
     1 (alfa(k)*props(k+5)*tauisotild1)+gama(k)*A_t(k,:,:)

    enddo
    do i=1,3
         ii = (i-1)*6
         statev(1+ii) = tauisovis2(i,1,1)
         statev(2+ii) = tauisovis2(i,2,2)
         statev(3+ii) = tauisovis2(i,3,3)
         statev(4+ii) = tauisovis2(i,2,3)
         statev(5+ii) = tauisovis2(i,1,3)
         statev(6+ii) = tauisovis2(i,1,2)
      enddo
    do k=1,3
      tauisovis1(k,:,:)=matmul(matmul(fbar1,tauisovis2(k,:,:)),transpose(fbar1))
    enddo

      do k=1,3
      do i=1,3
      do j=1,3
      tauvolvis1(k,i,j)=zero

      tauvolvis1(k,i,j)=alfa(k)*props(k+5)*tauvol1(i,j)

      b(k,i,j)=tauvolvis1(k,i,j)
      enddo
```

```
      enddo
      enddo
!-----------------------------------------------------------------------
!      calcul of the deviator of tauisovis1: tauvisd,
!              traced=trace(tauisovis1)
!-----------------------------------------------------------------------
      traced(1)=tauisovis1(1,1,1)+tauisovis1(1,2,2)+tauisovis1(1,3,3)
      tauvisd(1,1,1)=tauisovis1(1,1,1) - (one/three)*traced(1)
      tauvisd(1,2,2)=tauisovis1(1,2,2) - (one/three)*traced(1)
      tauvisd(1,3,3)=tauisovis1(1,3,3) - (one/three)*traced(1)
      tauvisd(1,1,2)=tauisovis1(1,1,2)
      tauvisd(1,1,3)=tauisovis1(1,1,3)
      tauvisd(1,2,3)=tauisovis1(1,2,3)
      tauvisd(1,2,1)=tauisovis1(1,2,1)
      tauvisd(1,3,1)=tauisovis1(1,3,1)
      tauvisd(1,3,2)=tauisovis1(1,3,2)
      traced(2)=tauisovis1(2,1,1)+tauisovis1(2,2,2)+tauisovis1(2,3,3)
      tauvisd(2,1,1)=tauisovis1(2,1,1) - (one/three)*traced(2)
      tauvisd(2,2,2)=tauisovis1(2,2,2) - (one/three)*traced(2)
      tauvisd(2,3,3)=tauisovis1(2,3,3) - (one/three)*traced(2)
      tauvisd(2,1,2)=tauisovis1(2,1,2)
      tauvisd(2,1,3)=tauisovis1(2,1,3)
      tauvisd(2,2,3)=tauisovis1(2,2,3)
      tauvisd(2,2,1)=tauisovis1(2,2,1)
      tauvisd(2,3,1)=tauisovis1(2,3,1)
      tauvisd(2,3,2)=tauisovis1(2,3,2)
      traced(3)=tauisovis1(3,1,1)+tauisovis1(3,2,2)+tauisovis1(3,3,3)
      tauvisd(3,1,1)=tauisovis1(3,1,1) - (one/three)*traced(3)
      tauvisd(3,2,2)=tauisovis1(3,2,2) - (one/three)*traced(3)
      tauvisd(3,3,3)=tauisovis1(3,3,3) - (one/three)*traced(3)
      tauvisd(3,1,2)=tauisovis1(3,1,2)
      tauvisd(3,1,3)=tauisovis1(3,1,3)
      tauvisd(3,2,3)=tauisovis1(3,2,3)
      tauvisd(3,2,1)=tauisovis1(3,2,1)
      tauvisd(3,3,1)=tauisovis1(3,3,1)
      tauvisd(3,3,2)=tauisovis1(3,3,2)

!-----------------------------------------------------------------------
!    calcul of the deviator of the hyper-viscoelastic kirchhoff
!       stress: tauiso(i,j)
!-----------------------------------------------------------------------
      do i=1,3
       do j=1,3
       tauiso(i,j)=zero
        tauiso(i,j)=tauiso1(i,j)-tauvisd(1,i,j)-tauvisd(2,i,j)-
     1  tauvisd(3,i,j)
       enddo
      enddo
!-----------------------------------------------------------------------
!    calcul of the volumetric part of hyper-viscoelastic kirchhoff
!             stress: tauvol(i,j)
```

```
!-----------------------------------------------------------------------
      do i=1,3
       do j=1,3
       tauvol(i,j)=zero
        tauvol(i,j)=tauvol1(i,j)!-tauvolvis1(1,i,j)
       -tauvolvis1(2,i,j)-tauvolvis1(3,i,j)
       enddo
      enddo

!-----------------------------------------------------------------------
!     calcul of the total kirchhoff hyper-viscoelastic stress
!-----------------------------------------------------------------------
      do i=1,3
       do j=1,3
       tau(i,j)=zero
       tau(i,j)=tauiso(i,j) + tauvol(i,j)
       enddo
      enddo
    tau1=matmul(matmul(transpose(drot),tau),drot)
!-----------------------------------------------------------------------
!                return stress(i) and statev
!-----------------------------------------------------------------------
      do i=1,3
      stress(i)=tau(i,i)/aj1
      enddo
      stress(4)=tau(1,2)/aj1
      stress(5)=tau(1,3)/aj1
      stress(6)=tau(2,3)/aj1
    statev(19)=dexp(mone*c1*(bi11-three)-c2*(bi21-three))

!-----------------------------------------------------------------------
! fourth order projection tensor
!-----------------------------------------------------------------------
       do i=1,3
        do j=1,3
         do k=1,3
          do l=1,3
          iip(i,j,k,l)=zero
          iip(i,j,k,l)=mone*(one/three)*delta(i,j)*delta(k,l)+
     1     (one/two)*(delta(i,k)*delta(j,l)+delta(i,l)*delta(j,k))
          enddo
         enddo
        enddo
       enddo
!-----------------------------------------------------------------------
!     calcul of the algorithmic tangent modulus cbar1
!-----------------------------------------------------------------------
      do i=1,3
      do j=1,3
      do k=1,3
      do l=1,3
```

```
      cbar1(i,j,k,l)=zero
      do s=1,3
      cbar1(i,j,k,l)=four*bbar1(i,j)*bbar1(k,l)-
     1 two*(bbar1(i,k)*bbar1(j,l)+bbar1(i,s)*bbar1(s,l)*delta(j,k))
      enddo
      enddo
      enddo
      enddo
      enddo
!-----------------------------------------------------------------------
!   calcul of the algorithmic tangent modulus cbar
!-----------------------------------------------------------------------
      do i=1,3
      do j=1,3
      do k=1,3
      do l=1,3
      cbar11(i,j,k,l)=zero
      cbar22(i,j,k,l)=zero
      cbar11(i,j,k,l)=c01*cbar1(i,j,k,l)+
     1 two*c02*(bi21-three)*cbar1(i,j,k,l)+
     2 c11*(bi11-three)*cbar1(i,j,k,l)+
     3 8.0d0*c20*bbar1(i,j)*bbar1(k,l)+
     4 8.0d0*c11*bi11*bbar1(i,j)*bbar1(k,l)
      do s=1,3
      do t=1,3
      cbar22(i,j,k,l)=mone*four*c11*bbar1(i,s)*bbar1(s,j)*bbar1(k,l)-
     1 four*c11*bbar1(i,j)*bbar1(k,s)*bbar1(s,l)+
     2 8.0d0*c02*bi11*bi11*bbar1(i,j)*bbar1(k,l)-
     3 8.0d0*c02*bi11*bbar1(i,j)*bbar1(k,s)*bbar1(s,l)-
     4 8.0d0*c02*bi11*bbar1(i,s)*bbar1(s,j)*bbar1(k,l)+
     5 8.0d0*c02*bbar1(i,s)*bbar1(s,j)*bbar1(k,t)*bbar1(t,l)
      enddo
      enddo
      enddo
      enddo
      enddo
      enddo
      do i=1,3
      do j=1,3
      do k=1,3
      do l=1,3
      cbar(i,j,k,l)=zero
      cbar(i,j,k,l)=cbar11(i,j,k,l)+cbar22(i,j,k,l)
      enddo
      enddo
      enddo
      enddo
!-----------------------------------------------------------------------
!  calcul of the deviatoric hyperelastic tangent modulus cisoh
!-----------------------------------------------------------------------
      do i=1,3
```

```
      do j=1,3
       do k=1,3
       do l=1,3
       cisoh(i,j,k,l)=zero
       do s=1,3
       do t=1,3
       do u=1,3
       do v=1,3
       cisoh(i,j,k,l)=(two/three)*tracebtau1*iip(i,j,k,l)-
     1                 (two/three)*(tauiso1(i,j)*delta(k,l)+
     2                 delta(i,j)*tauiso1(k,l))+
     3                iip(i,j,s,t)*cbar(s,t,u,v)*iip(u,v,k,l)
      enddo
      enddo
      enddo
      enddo
      enddo
      enddo
      enddo
      enddo
!-----------------------------------------------------------------------
!   calcul of the volumetric hyperelastic tangent modulus cvolh
!-----------------------------------------------------------------------
      cs=two*aj1*aj1/d1
      do i=1,3
       do j=1,3
        do k=1,3
         do l=1,3
         cvolh(i,j,k,l)=zero
         cvolh(i,j,k,l)=(p1+cs)*delta(i,j)*delta(k,l)
     1   -p1*(delta(i,k)*delta(j,l)+delta(i,l)*delta(j,k))
         enddo
        enddo
       enddo
      enddo
!-----------------------------------------------------------------------
!   calcul of the deviatoric hyperviscoelastic tangent modulus cisovh
!-----------------------------------------------------------------------
      const1=zero
      const2=zero

      const1=alfa(1)*g1+alfa(2)*g2+alfa(3)*g3
      const2=alfa(1)*g1+alfa(2)*g2+alfa(3)*g3
    do i=1,3
      do j=1,3
      do k=1,3
      do l=1,3
    cb(i,j,k,l)=zero
    cb(i,j,k,l)=delta(i,k)*tau(j,l)+delta(j,l)*tau(i,k)+
    delta(i,l)*tau(j,k)+delta(j,k)*tau(i,l)
    enddo
```

```
    enddo
    enddo
    enddo

      do i=1,3
      do j=1,3
      do k=1,3
      do l=1,3
      cisovh(i,j,k,l)=zero
      cisovh(i,j,k,l)=(one-const1)*cisoh(i,j,k,l)!+(one/(aj1*two))*cb(i,j,k,l)
      enddo
      enddo
      enddo
      enddo
!-----------------------------------------------------------------------
!   calcul of the volumetric hyperviscoelastic tangent modulus cvolvh
!-----------------------------------------------------------------------
      do i=1,3
      do j=1,3
      do k=1,3
      do l=1,3
      cvolvh(i,j,k,l)=zero
      cvolvh(i,j,k,l)=cvolh(i,j,k,l)
      enddo
      enddo
      enddo
      enddo
!-----------------------------------------------------------------------
!            total tangent modulus ic
!-----------------------------------------------------------------------
    do i=1,3
    do j=1,3
    do k=1,3
    do l=1,3
    ic(i,j,k,l)=zero
    ic(i,j,k,l)=cvolvh(i,j,k,l)/aj1+ cisovh(i,j,k,l)/aj1+(one/(aj1*two))*cb(i,j,k,l)
    enddo
    enddo
    enddo
    enddo
!-----------------------------------------------------------------------
!      return ddsdde(i,j)=ic(i,j,k,l)
!-----------------------------------------------------------------------
      do i=1,6
      do j=1,6
      ddsdde(i,j)=zero
      enddo
      enddo
      ddsdde(1,1)=ic(1,1,1,1)
      ddsdde(1,2)=ic(1,1,2,2)
      ddsdde(1,3)=ic(1,1,3,3)
```

```
      ddsdde(1,4)=ic(1,1,1,2)
      ddsdde(1,5)=ic(1,1,1,3)
      ddsdde(1,6)=ic(1,1,2,3)
      ddsdde(2,2)=ic(2,2,2,2)
      ddsdde(2,3)=ic(2,2,3,3)
      ddsdde(2,4)=ic(2,2,1,2)
      ddsdde(2,5)=ic(2,2,1,3)
      ddsdde(2,6)=ic(2,2,2,3)
      ddsdde(3,3)=ic(3,3,3,3)
      ddsdde(3,4)=ic(3,3,1,2)
      ddsdde(3,5)=ic(3,3,1,3)
      ddsdde(3,6)=ic(3,3,2,3)
      ddsdde(4,4)=ic(1,2,1,2)
      ddsdde(4,5)=ic(1,2,1,3)
      ddsdde(4,6)=ic(1,2,2,3)
      ddsdde(5,5)=ic(1,3,1,3)
      ddsdde(5,6)=ic(1,3,2,3)
      ddsdde(6,6)=ic(2,3,2,3)
      do i=1,6
      do j=1,6
      ddsdde(j,i)=ddsdde(i,j)
      enddo
      enddo
    print* , stress(1)
      return
      end
```

BIBLIOGRAPHY

[1] J. Argyris and I. S. Doltsinis. Constitutive modelling and computation of non-linear viscoelastic solids. part i: Rheological models and numerical integration techniques. *Computer Methods in Applied Mechanics and Engineering*, 88(2):135–163, 1991.

[2] G. Astarita and G. Marrucci. *Principles of non-Newtonian fluid mechanics*. McGraw-Hill Companies, 1974.

[3] B.Y. Ballal and R.S. Rivlin. Flow of a viscoelastic fluid between eccentric cylinders. *Rheologica Acta*, 18(3):311–322, 1979.

[4] R.C. Batra and J.H. Yu. Linear constitutive relations in isotropic finite viscoelasticity. *Journal of elasticity*, 55(1):73–77, 1999.

[5] R.C. Batra and J.H. Yu. Torsion of a viscoelastic cylinder. *journal of applied mechanics-the american society of mechanical engineers*, 67(2):424–426, 2000.

[6] J.G.J. Beijer and J.L. Spoormaker. Solution strategies for fem analysis with nonlinear viscoelastic polymers. *Computers & structures*, 80(14):1213–1229, 2002.

[7] M. A. Biot. Theory of stress-strain relations in anisotropic viscoelasticity and relaxation phenomena. *Journal of Applied Physics*, 25(11):1385–1391, 1954.

[8] J. E. Bischoff, E. M. Arruda, and K. Grosh. A new constitutive model for the compressibility of elastomers at finite deformations. *Rubber chemistry and technology*, 74(4):541–559, 2001.

[9] A. V. Boiko, V. M. Kulik, B. M. Seoudi, H.H. Chun, and I. Lee. Measurement method of complex viscoelastic material properties. *International Journal of Solids and Structures*, 47(3):374–382, 2010.

[10] L. Boltzmann. Zur theorie der elastischen nachwirkung. *Annalen der Physik*, 241(11):430–432, 1878.

[11] J. Bonet. Large strain viscoelastic constitutive models. *International Journal of Solids and Structures*, 38(17):2953–2968, 2001.

[12] H. Bouasse and Z. Carrière. Sur les courbes de traction du caoutchouc vulcanisé. In *Annales de la Faculté des sciences de Toulouse: Mathématiques*, volume 5, pages 257–283. GAUTHIER-VILLARS, IMPRIMEUR-EDITEUR; ED. PRIVAT, IMPRIMEUR-LIBRAIRE, 1903.

[13] A. Boukamel. *Modélisation mécaniques et numériques des matériaux et structures en élastomères*. Habilitation à diriger des recherches, Université de la Méditerranée - Aix-Marseille II, October 2006. URL: https://tel.archives-ouvertes.fr/tel-00517997.

[14] C.P. Buckley and D.C. Jones. Glass-rubber constitutive model for amorphous polymers near the glass transition. *Polymer*, 36(17):3301–3312, 1995.

[15] F. Bueche. Molecular basis for the mullins effect. *Journal of Applied Polymer Science*, 4(10):107–114, 1960.

[16] F. Bueche. Mullins effect and rubber–filler interaction. *Journal of applied polymer Science*, 5(15):271–281, 1961.

[17] W. D. Callister and D. G. Rethwisch. *Materials science and engineering*, volume 5. John Wiley & Sons NY, 2011.

[18] D. Calvetti, S. Morigi, L. Reichel, and F. Sgallari. Tikhonov regularization and the l-curve for large discrete ill-posed problems. *Journal of Computational and Applied Mathematics*, 123(1–2):423 – 446, 2000.

[19] M.M. Carroll. Controllable deformations of incompressible simple materials. *International Journal of Engineering Science*, 5(6):515–525, 1967.

[20] L. Chazeau, J.D. Brown, L.C. Yanyo, and S.S. Sternstein. Modulus recovery kinetics and other insights into the payne effect for filled elastomers. *Polymer composites*, 21(2):202–222, 2000.

[21] J. Chen, H. Hu, S. Li, and K. Zhang. Quantitative relation between the relaxation time and the strain rate for polymeric solids under quasi-static conditions. *Journal of Applied Polymer Science*, 133(42), 2016.

[22] R. Christensen. *Theory of viscoelasticity: an introduction*. Elsevier, 2012.

[23] J. Ciambella, A. Paolone, and S. Vidoli. A comparison of nonlinear integral-based viscoelastic models through compression tests on filled rubber. *Mechanics of Materials*, 42(10):932–944, 2010.

[24] B. D. Coleman. Thermodynamics of materials with memory. *Archive for Rational Mechanics and Analysis*, 17(1):1–46, 1964.

[25] B. D. Coleman and M. E. Gurtin. Thermodynamics with internal state variables. *The Journal of Chemical Physics*, 47(2):597–613, 1967.

[26] B. D. Coleman, H. Markovitz, and W. Noll. *Viscometric flows of non-Newtonian fluids: theory and experiment*, volume 5. Springer Science & Business Media, 2012.

[27] B. D. Coleman and W. Noll. Foundations of linear viscoelasticity. *Reviews of Modern Physics*, 33(2):239, 1961.

[28] B. D. Coleman and W. Noll. The thermodynamics of elastic materials with heat conduction and viscosity. *Archive for Rational Mechanics and Analysis*, 13(1):167–178, 1963.

[29] V. A. Coveney. *Elastomers and Components: Service Life Prediction-Progress and Challenges*. Woodhead Publishing, 2006.

[30] R. De Pascalis, I. D. Abrahams, and W. J. Parnell. On nonlinear viscoelastic deformations: a reappraisal of fung's quasi-linear viscoelastic model. In *Proc. R. Soc. A*, volume 470, page 20140058. The Royal Society, 2014.

[31] G. Del Piero and L. Deseri. On the concepts of state and free energy in linear viscoelasticity. *Archive for Rational Mechanics and Analysis*, 138(1):1–35, 1997.

[32] Michel Destrade, Jerry G Murphy, and Giuseppe Saccomandi. Simple shear is not so simple. *International Journal of Non-Linear Mechanics*, 47(2):210–214, 2012.

[33] A. D. Drozdov and A. Dorfmann. Finite viscoelasticity of filled rubber: experiments and numerical simulation. *Archive of Applied Mechanics*, 72(9):651–672, 2003.

[34] A.D. Drozdov. *Viscoelastic structures: mechanics of growth and aging*. Academic Press, 1998.

[35] A.D. Drozdov. Constitutive equations in finite elasticity of rubbers. *International Journal of Solids and Structures*, 44(1):272–297, 2007.

[36] W. Ehlers and G. Eipper. The simple tension problem at large volumetric strains computed from finite hyperelastic material laws. *Acta Mechanica*, 130(1):17–27, 1998.

[37] C. Elster, J. Honerkamp, and J. Weese. Using regularization methods for the determination of relaxation and retardation spectra of polymeric liquids. *Rheologica acta*, 31(2):161–174, 1992.

[38] J.L. Ericksen. Deformations possible in every compressible, isotropic, perfectly elastic material. *Studies in Applied Mathematics*, 34(1-4):126–128, 1955.

[39] M. Fabrizio and A. Morro. *Mathematical problems in linear viscoelasticity*. SIAM, 1992.

[40] E.A. Fancello, J.P. Ponthot, and L. Stainier. A variational framework for nonlinear viscoelastic models in finite deformation regime. *Journal of Computational and Applied Mathematics*, 215(2):400–408, 2008.

[41] M.S.H. Fatt and A.A. Al-Quraishi. High strain rate constitutive modeling for natural rubber. In *CONSTITUTIVE MODELS FOR RUBBER-PROCEEDINGS-*, volume 5, page 53. Balkema, 2008.

[42] W. W. Feng. A recurrence formula for viscoelastic constitutive equations. *International journal of non-linear mechanics*, 27(4):675–678, 1992.

[43] J. D. Ferry. *Viscoelastic properties of polymers*. John Wiley & Sons, 1980.

[44] W. N. Findley and F.A. Davis. *Creep and relaxation of nonlinear viscoelastic materials*. Courier Corporation, 2013.

[45] W.N. Findley and F.A. Davis. *Creep and relaxation of nonlinear viscoelastic materials*. Courier Corporation, 2013.

[46] P. J. Flory. Thermodynamic relations for high elastic materials. *Transactions of the Faraday Society*, 57:829–838, 1961.

[47] R. L. Fosdick and J.H. Yu. Thermodynamics, stability and non-linear oscillations of viscoelastic solids—i. differential type solids of second grade. *International journal of non-linear mechanics*, 31(4):495–516, 1996.

[48] Y.C. B. Fung. Stress-strain-history relations of soft tissues in simple elongation. *Biomechanics its foundations and objectives*, pages 181–208, 1972.

[49] J. Golden. A proposal concerning the physical rate of dissipation in materials with memory. *Quarterly of applied mathematics*, 63(1):117–155, 2005.

[50] S. Govindjee and J. Simo. A micro-mechanically based continuum damage model for carbon black-filled rubbers incorporating mullins' effect. *Journal of the Mechanics and Physics of Solids*, 39(1):87–112, 1991.

[51] S. Govindjee and J.C. Simo. Mullins' effect and the strain amplitude dependence of the storage modulus. *International journal of solids and structures*, 29(14-15):1737–1751, 1992.

[52] A. E. Green and R. S. Rivlin. The mechanics of non-linear materials with memory. *Archive for Rational Mechanics and Analysis*, 1(1):1–21, 1957.

[53] R.M. Haj-Ali and A.H. Muliana. Numerical finite element formulation of the schapery non-linear viscoelastic material model. *International Journal for Numerical Methods in Engineering*, 59(1):25–45, 2004.

[54] J. O. Hallquist et al. Ls-dyna theory manual. *Livermore software technology corporation*, 3:25–31, 2006.

[55] J.A.C. Harwood, L. Mullins, and A.R. Payne. Stress softening in rubbers: a review. *Journal of the IRI*, 1:17–27, 1967.

[56] K. Hasanpour, S. Ziaei-Rad, and M. Mahzoon. A large deformation framework for compressible viscoelastic materials: Constitutive equations and finite element implementation. *International Journal of Plasticity*, 25(6):1154–1176, 2009.

[57] S. Hassani, A. A. Soulimani, and A. Ehrlacher. A nonlinear viscoelastic model: the pseudo-linear model. *European Journal of Mechanics-A/Solids*, 17(4):567–598, 1998.

[58] P. Haupt and A. Lion. On finite linear viscoelasticity of incompressible isotropic materials. *Acta Mechanica*, 159(1):87–124, 2002.

[59] R.N. Haward and G. Thackray. The use of a mathematical model to describe isothermal stress-strain curves in glassy thermoplastics. In *Proceedings of the*

Royal Society of London A: Mathematical, Physical and Engineering Sciences, volume 302, pages 453–472. The Royal Society, 1968.

[60] M. Henriksen. Nonlinear viscoelastic stress analysis—a finite element approach. *Computers & structures*, 18(1):133–139, 1984.

[61] L.R. Herrmann and F.E. Peterson. A numerical procedure for viscoelastic stress analysis. In *Seventh meeting of ICRPG mechanical behavior working group, Orlando, FL, CPIA Publication*, number 177, pages 60–69, 1968.

[62] D. Hibbit, B. Karlsson, and P. Sorensen. *Abaqus User Subroutine Reference Manual*, volume 6. Rhode Island, 2007.

[63] D. Hibbit, B. Karlsson, and P. Sorensen. Abaqus/theory manual. *Rhode Island*, 6(7), 2007.

[64] A. G. Holzapfel. Nonlinear solid mechanics ii. 2000.

[65] G. Holzapfel and R. A. Simo. A new viscoelastic constitutive model for continuous media at finite thermomechanical changes. *International Journal of Solids and Structures*, 33:3019–3034, 1996.

[66] G. A. Holzapfel and T. C. Gasser. A viscoelastic model for fiber-reinforced composites at finite strains: Continuum basis, computational aspects and applications. *Computer methods in applied mechanics and engineering*, 190(34):4379–4403, 2001.

[67] G. A. Holzapfel and J. C. Simo. A new viscoelastic constitutive model for continuous media at finite thermomechanical changes. *International Journal of Solids and Structures*, 33(20):3019–3034, 1996.

[68] G.A. Holzapfel. On large strain viscoelasticity: continuum formulation and finite element applications to elastomeric structures. *International Journal for Numerical Methods in Engineering*, 39(22):3903–3926, 1996.

[69] C.O. Horgan and G. Saccomandi. Pure axial shear of isotropic, incompressible nonlinearly elastic materials with limiting chain extensibility. *Journal of elasticity*, 57(3):307–319, 1999.

[70] C.O. Horgan and G. Saccomandi. Simple torsion of isotropic, hyperelastic, incompressible materials with limiting chain extensibility. *Journal of elasticity*, 56(2):159–170, 1999.

[71] C.O. Horgan and G. Saccomandi. Pure azimuthal shear of isotropic, incompressible hyperelastic materials with limiting chain extensibility. *International journal of non-linear mechanics*, 36(3):465–475, 2001.

[72] C.O. Horgan and G. Saccomandi. Helical shear for hardening generalized neo-hookean elastic materials. *Mathematics and Mechanics of Solids*, 8(5):539–559, 2003.

[73] G. Huber, T. A. Vilgis, and G. Heinrich. Universal properties in the dynamical deformation of filled rubbers. *Journal of Physics: Condensed Matter*, 8(29):L409, 1996.

[74] N. Huber and C. Tsakmakis. Finite deformation viscoelasticity laws. *Mechanics of materials*, 32(1):1–18, 2000.

[75] T.J.R. Hughes. *The finite element method: linear static and dynamic finite element analysis*. Courier Corporation, 2012.

[76] R.R. Huilgol. Viscoelastic fluid theories based on the left cauchy-green tensor history. *Rheologica Acta*, 18(4):451–455, 1979.

[77] M.A. Johnson and M.F. Beatty. The mullins effect in uniaxial extension and its influence on the transverse vibration of a rubber string. *Continuum Mechanics and Thermodynamics*, 5(2):83–115, 1993.

[78] H. Khajehsaeid, J. Arghavani, R. Naghdabadi, and S. Sohrabpour. A visco-hyperelastic constitutive model for rubber-like materials: A rate-dependent relaxation time scheme. *International Journal of Engineering Science*, 79:44–58, 2014.

[79] A. S. Khan, O. Lopez-Pamies, and R. Kazmi. Thermo-mechanical large deformation response and constitutive modeling of viscoelastic polymers over a wide range of strain rates and temperatures. *International Journal of Plasticity*, 22(4):581–601, 2006.

[80] W. G. Knauss and J. Zhao. Improved relaxation time coverage in ramp-strain histories. *Mechanics of Time-Dependent Materials*, 11(3-4):199–216, 2007.

[81] G. Kraus. Mechanical losses in carbon-black-filled rubbers. In *Journal of Applied Polymer Science: Applied Polymer Symposium*, volume 39, pages 75–92, 1984.

[82] F. Laraba-Abbes, P. Ienny, and R. Piques. A new 'tailor-made'methodology for the mechanical behaviour analysis of rubber-like materials: Ii. application to the hyperelastic behaviour characterization of a carbon-black filled natural rubber vulcanizate. *Polymer*, 44(3):821–840, 2003.

[83] J.H. Lee and K.J. Kim. Characterization of complex modulus of viscoelastic materials subject to static compression. *Mechanics of Time-Dependent Materials*, 5(3):255–271, 2001.

[84] S.B. Lee and A. Wineman. A model for nonlinear viscoelastic torsional response of an elastomeric bushing. *Acta mechanica*, 135(3-4):199–218, 1999.

[85] S.B. Lee and A. Wineman. A model for non-linear viscoelastic coupled mode response of an elastomeric bushing. *International journal of non-linear mechanics*, 35(2):177–199, 2000.

[86] S. Lejeunes, A. Boukamel, and S. Méo. Finite element implementation of nearly-incompressible rheological models based on multiplicative decompositions. *Computers & structures*, 89(3):411–421, 2011.

[87] C. Lewitzke and P. Lee. Application of elastomeric components for noise and vibration isolation in the automotive industry. Technical report, SAE Technical Paper, 2001.

[88] A. Lion. A physically based method to represent the thermo-mechanical behaviour of elastomers. *Acta Mechanica*, 123(1):1–25, 1997.

[89] A. Lion and C. Kardelky. The payne effect in finite viscoelasticity: constitutive modelling based on fractional derivatives and intrinsic time scales. *International Journal of Plasticity*, 20(7):1313–1345, 2004.

[90] J. Lubliner. A model of rubber viscoelasticity. *Mechanics Research Communications*, 12(2):93–99, 1985.

[91] W. J. MacKnight. Volume changes accompanying the extension of rubber-like materials. *Journal of Applied Physics*, 37(12):4587–4587, 1966.

[92] A. I. Malkin. *Rheology fundamentals*. ChemTec Publishing, 1994.

[93] G. Marckmann. *Contribution à l'étude des élastomères et des membranes soufflées*. PhD thesis, Ecole Centrale de Nantes (ECN)(ECN)(ECN)(ECN); Université de Nantes, 2004.

[94] J. E. Marsden and T. J.R. Hughes. *Mathematical foundations of elasticity*. Courier Corporation, 1994.

[95] S. Matsuoka, C. J. Aloisio, and H. E. Bair. Interpretation of shift of relaxation time with deformation in glassy polymers in terms of excess enthalpy. *Journal of Applied Physics*, 44(10):4265–4268, 1973.

[96] C. Miehe. Discontinuous and continuous damage evolution in ogden-type large-strain elastic materials. *European journal of mechanics. A. Solids*, 14(5):697–720, 1995.

[97] K. N. Morman Jr and T. Y. Pan. Application of finite-element analysis in the design of automotive elastomeric components. *Rubber chemistry and technology*, 61(3):503–533, 1988.

[98] A. Muliana, K.R. Rajagopal, and D. Tscharnuter. A nonlinear integral model for describing responses of viscoelastic solids. *International Journal of Solids and Structures*, 58:146–156, 2015.

[99] A. Muliana, K.R. Rajagopal, and A.S. Wineman. A new class of quasi-linear models for describing the nonlinear viscoelastic response of materials. *Acta Mechanica*, 224(9):2169–2183, 2013.

[100] L. Mullins. Effect of stretching on the properties of rubber. *Rubber Chemistry and Technology*, 21(2):281–300, 1948.

[101] L. Mullins. Softening of rubber by deformation. *Rubber chemistry and technology*, 42(1):339–362, 1969.

[102] M.Z. Nashed. The theory of tikhonov regularization for fredholm equations of the first kind (cw groetsch). *SIAM Review*, 28(1):116–118, 1986.

[103] J. Nidhal, S. Michelle, H. Adel, B. Olivier, A. Makrem, I. Mohamed, and B. Jalel. Predeformation and frequency-dependence : Experiment and fe analysis. *Proceeding of international conference on dynamics of composite structure*, pages 105–112, 2015.

[104] P.A. Oconnell and G.B. McKenna. Large deformation response of polycarbonate: Time-temperature, time-aging time, and time-strain superposition. *Polymer Engineering and Science*, 37(9):1485–1495, 1997.

[105] R. W. Ogden, G. Saccomandi, and I. Sgura. Fitting hyperelastic models to experimental data. *Computational Mechanics*, 34(10):484–502, August 2004.

[106] R.W. Ogden. Volume changes associated with the deformation of rubber-like solids. *Journal of the Mechanics and Physics of Solids*, 24(6):323–338, 1976.

[107] R.W. Ogden. Nearly isochoric elastic deformations: application to rubberlike solids. *Journal of the Mechanics and Physics of Solids*, 26(1):37–57, 1978.

[108] R.W. Ogden and D.G. Roxburgh. A pseudo–elastic model for the mullins effect in filled rubber. In *Proceedings of the Royal Society of London A: Mathematical, Physical and Engineering Sciences*, volume 455, pages 2861–2877. The Royal Society, 1999.

[109] R.W. Ogden, G. Saccomandi, and I. Sgura. Fitting hyperelastic models to experimental data. *Computational Mechanics*, 34(6):484–502, 2004.

[110] S. W. Park and R. A. Schapery. Methods of interconversion between linear viscoelastic material functions. part i—a numerical method based on prony series. *International Journal of Solids and Structures*, 36(11):1653–1675, 1999.

[111] C. Patrick and E. Isabelle. Physique des polymères tome i structure, fabrication, emploi. *Hermann Editeurs des Sciences et des Arts: Paris*, page 42, 2005.

[112] A. R. Payne. The dynamic properties of carbon black loaded natural rubber vulcanizates. part ii. *Journal of Applied Polymer Science*, 6(21):368–372, 1962.

[113] E. Peña, J. A. Peña, and M. Doblaré. On modelling nonlinear viscoelastic effects in ligaments. *Journal of Biomechanics*, 41:2659–2666, 2008.

[114] R. W. Penn. Volume changes accompanying the extension of rubber. *Transactions of the Society of Rheology*, 14(4):509–517, 1970.

[115] A. C. Pipkin. Small finite deformations of viscoelastic solids. *Reviews of Modern Physics*, 36(4):1034–1041, 1964.

[116] A. C. Pipkin. *Lectures on viscoelasticity theory*, volume 7. Springer Science & Business Media, 2012.

[117] A.C. Pipkin and T.G. Rogers. A non-linear integral representation for viscoelastic behaviour. *Journal of the Mechanics and Physics of Solids*, 16(1):59–72, 1968.

[118] P.A. Przybylo and E.M. Arruda. Experimental investigations and numerical modeling of incompressible elastomers during non-homogeneous deformations. *Rubber Chemistry and Technology*, 71(4):730–749, 1998.

[119] E. Pucci and G. Saccomandi. A note on the gent model for rubber-like materials. *Rubber chemistry and technology*, 75(5):839–852, 2002.

[120] S. Reese and S. Govindjee. A theory of viscoelasticity and numerical applications. *International Journal of Solids and Structures*, 35:3455–3482, 1998.

[121] W.F. Reichert, M.K. Hopfenmüller, and D. Göritz. Volume change and gas transport at uniaxial deformation of filled natural rubber. *Journal of materials science*, 22(10):3470–3476, 1987.

[122] R. S. Rivlin and J. L. Ericksen. Stress-deformation relations for isotropic materials. *Journal of Rational Mechanics and Analysis*, 4:323–425, 1955.

[123] R.S. Rivlin. Large elastic deformations of isotropic materials. iv. further developments of the general theory. *Philosophical Transactions of the Royal Society of London A: Mathematical, Physical and Engineering Sciences*, 241(835):379–397, 1948.

[124] P. Saad. *Modélisation et identification du comportement non linéaire des cales en caoutchouc*. PhD thesis, École Centrale de Lyon, 2003.

[125] R. A. Schapery. On the characterization of nonlinear viscoelastic materials. *Polymer Engineering & Science*, 9(4):295–310, 1969.

[126] R. A. Schapery. Nonlinear viscoelastic and viscoplastic constitutive equations based on thermodynamics. *Mechanics of Time-Dependent Materials*, 1(2):209–240, 1997.

[127] V.P.W. Shim, L.M. Yang, C.T. Lim, and P.H. Law. A visco-hyperelastic constitutive model to characterize both tensile and compressive behavior of rubber. *Journal of Applied Polymer Science*, 92(1):523–531, 2004.

[128] F. Sidoroff. Nonlinear viscoelastic model with intermediate configuration. *JOURNAL DE MECANIQUE*, 13(4):679–713, 1974.

[129] J. C. Simo and T. J. R. Hughes. *Computational inelasticity*, volume 7. Springer Science & Business Media, 2006.

[130] J.C. Simo, J.G. Kennedy, and S. Govindjee. Non-smooth multisurface plasticity and viscoplasticity. loading/unloading conditions and numerical algorithms. *International Journal for Numerical Methods in Engineering*, 26(10):2161–2185, 1988.

[131] R. A. Simo. On a fully three-dimensional finite-strain viscoelastic damage model: Formulation and computational aspects. *Computer Methods in Applied Mechanics and Engineering*, 60:153–173, 1987.

[132] J. Sorvari and J. Hämäläinen. Time integration in linear viscoelasticity—a comparative study. *Mechanics of Time-Dependent Materials*, 14(3):307–328, 2010.

[133] E. Stein and G. Sagar. Convergence behavior of 3d finite elements for neo-hookean material. *Engineering Computations*, 25(3):220–232, 2008.

[134] J.L. Sullivan. A nonlinear viscoelastic model for representing nonfactorizable time-dependent behavior in cured rubber. *Journal of Rheology (1978-present)*, 31(3):271–295, 1987.

[135] TA. *Instruments Training Courses*. Woodlands, 2010.

[136] A. Tayeb, M. Arfaoui, A.M. Zine, A. Hamdi, J. Benabdallah, and M. Ichchou. On the nonlinear viscoelastic behavior of rubber-like materials: Constitutive description and identification. *International journal of mechanical sciences*, 130:437 – 447, 2017.

[137] R. L. Taylor, K. S. Pister, and G. L. Goudreau. Thermomechanical analysis of viscoelastic solids. *International Journal for Numerical Methods in Engineering*, 2(1):45–59, 1970.

[138] L. R. G. Treloar. *The physics of rubber elasticity*. Oxford University Press, USA, 1975.

[139] C. Truesdell and W. Noll. *The non-linear field theories of mechanics*, volume 3. Springer, 2004.

[140] N. W. Tschoegl. Time dependence in material properties: An overview. *Mechanics of Time-Dependent Materials*, 1(1):3–31, 1997.

[141] N. W. Tschoegl, W. G. Knauss, and I. Emri. The effect of temperature and pressure on the mechanical properties of thermo-and/or piezorheologically simple polymeric materials in thermodynamic equilibrium–a critical review. *Mechanics of Time-Dependent Materials*, 6(1):53–99, 2002.

[142] N.W. Tschoegl and I. Emri. Generating line spectra from experimental responses. part ii: Storage and loss functions. *Rheologica Acta*, 32(3):322–327, 1993.

[143] B. Tvedt. Quasilinear equations for viscoelasticity of strain-rate type. *Archive for Rational Mechanics and Analysis*, 189(2):237–281, 2008.

[144] K.C. Valanis and R. F. Landel. The strain-energy function of a hyperelastic material in terms of the extension ratios. *Journal of Applied Physics*, 38(7):2997–3002, 1967.

[145] J.L. White and A.B. Metzner. Development of constitutive equations for polymeric melts and solutions. *Journal of Applied Polymer Science*, 7(5):1867–1889, 1963.

[146] M. L. Williams, R. F. Landel, and J. D. Ferry. The temperature dependence of relaxation mechanisms in amorphous polymers and other glass-forming liquids. *Journal of the American Chemical society*, 77(14):3701–3707, 1955.

[147] L.M. Yang, V.P.W. Shim, and C.T. Lim. A visco-hyperelastic approach to modelling the constitutive behaviour of rubber. *International Journal of Impact Engineering*, 24(6):545–560, 2000.

[148] J. Yoshida, M. Abe, and Y. Fujino. Constitutive model of high-damping rubber materials. *Journal of Engineering Mechanics*, 130(2):129–141, 2004.

[149] O. C. Zienkiewicz and R. L. Taylor. *The finite element method*, volume 3. McGraw-hill London, 1977.

[150] O.C. Zienkiewicz, M. Watson, and I.P. King. A numerical method of visco-elastic stress analysis. *International Journal of Mechanical Sciences*, 10(10):807–827, 1968.